(2)

REPORT NO. NADC-87145-60

FRACTURE MECHANICS ANALYSIS OF SOME FATIGUE AND FRACTURE TEST SPECIMENS USING FINITE ELEMENTS

Gary Delserro

Air Vehicle and Crew Systems Technology Department
NAVAL AIR DEVELOPMENT CENTER
Warmisnter, PA 18974

24 AUGUST 1987

FINAL REPORT

Approved for Public Release; Distribution is Unlimited

Prepared for
NAVAL AIR SYSTEMS COMMAND
Department of the Navy
Washington, D.C. 20361

NOTICES

REPORT NUMBERING SYSTEM - The numbering of technical project reports issued by the Naval Air Development Center is arranged for specific identification purposes. Each number consists of the Center acronym, the calendar year in which the number was assigned, the sequence number of the report within the specific calendar year, and the official 2-digit correspondence code of the Command Office or the Functional Department responsible for the report. For example: Report No. NADC-86015-70 indicates the fifteenth Center report for the year 1986 and prepared by the Systems and Software Technology Department. The numerical codes are as follows:

CODE	OFFICE OR DEPARTMENT
00	Commander, Naval Air Development Center
01	Technical Director, Naval Air Development Center
02	Comptroller
05	Computer Department
07	Planning Assessment Resources Department
10	Anti-Submarine Warfare Systems Department
20	Tactical Air Systems Department
30	Battle Force Systems Department
40	Communication & Navigation Technology Department
50	Mission Avionics Technology Department
60	Air Vehicle & Crew Systems Technology Department
70	Systems & Software Technology Department
80	Engineering Support Group

PRODUCT ENDORSEMENT - The discussion or instructions concerning commercial products herein do not constitute an endorsement by the Government nor do they convey or imply the license or right to use such products.

APPROVED BY: W. F. Moroney DATE: 21 July 1988

W. F. MORONEY
CAPT, MSC, U.S. NAVY

SECURITY CLASSIFICATION OF THIS PAGE

REPORT DOCUMENTATION PAGE

1a. REPORT SECURITY CLASSIFICATION UNCLASSIFIED	1b RESTRICTIVE MARKINGS N/A
2a. SECURITY CLASSIFICATION AUTHORITY N/A	3 DISTRIBUTION / AVAILABILITY OF REPORT Approved for Public Release; Distribution is Unlimited
2b DECLASSIFICATION / DOWNGRADING SCHEDULE N/A	
4 PERFORMING ORGANIZATION REPORT NUMBER(S) NADC-87145-60	5 MONITORING ORGANIZATION REPORT NUMBER(S) N/A
6a NAME OF PERFORMING ORGANIZATION Naval Air Development Center 6b OFFICE SYMBOL (If applicable) Code 6042	7a NAME OF MONITORING ORGANIZATION N/A
6c. ADDRESS (City, State, and ZIP Code) Warminster, PA 18974-5000	7b ADDRESS (City, State, and ZIP Code) N/A
8a NAME OF FUNDING / SPONSORING ORGANIZATION Naval Air Systems Command 8b OFFICE SYMBOL (If applicable) N/A	9 PROCUREMENT INSTRUMENT IDENTIFICATION NUMBER N/A
8c. ADDRESS (City, State, and ZIP Code) Department of the Navy Washington, DC 20361	10 SOURCE OF FUNDING NUMBERS PROGRAM ELEMENT NO: 62122N PROJECT NO: TASK NO: R41423000 WORK UNIT ACCESSION NO: 681080

11 TITLE (Include Security Classification)

(U) Fracture Mechanics Analysis of Some Fatigue and Fracture Test Specimens Using Finite Elements

12 PERSONAL AUTHOR(S) Gary Delserro

13a TYPE OF REPORT	13b TIME COVERED	14 DATE OF REPORT (Year, Month, Day)	15 PAGE COUNT
FINAL	FROM N/A TO N/A	87/09/24	132

16 SUPPLEMENTARY NOTATION

17 COSATI CODES			18 SUBJECT TERMS (Continue on reverse if necessary and identify by block number)
FIELD	GROUP	SUB-GROUP	Fatigue (Mechanics); Fracture (Mechanics); Finite Element Analysis; Test Specimens

19 ABSTRACT (Continue on reverse if necessary and identify by block number)

The NASTRAN finite element computer program was used to analyze the Mode I problems of a thin strip fatigue specimen with a cracked central hole in tension, and a single edge cracked specimen in tension and bending. A regular eight node isoparametric quadrilateral element was degenerated into a quarter point triangular element which approximates the stress singularity at the crack tip. Accurate values of the Mode I stress intensity factors were computed using this element.

The normalized stress intensity factors, $K_1/\sigma_0(\pi a)^{1/2}$, for cracks of various lengths were computed for the thin strip fatigue specimen with a cracked central hole in tension. The normalized stress intensity factor increased near the hole.

(continued on reverse)

20 DISTRIBUTION / AVAILABILITY OF ABSTRACT	21 ABSTRACT SECURITY CLASSIFICATION
☐ UNCLASSIFIED/UNLIMITED ☐ SAME AS RPT ☐ DTIC USERS	UNCLASSIFIED
22a NAME OF RESPONSIBLE INDIVIDUAL Gary P. Delserro	22b TELEPHONE (Include Area Code) 215-441-2986 22c. OFFICE SYMBOL 6042

DD FORM 1473, 84 MAR 83 APR edition may be used until exhausted
All other editions are obsolete

SECURITY CLASSIFICATION OF THIS PAGE

19. ABSTRACT (continued)

A boundary condition comparison between a point load, a uniformly distributed load, and a fixed grip-displacement controlled condition was made on the normalized stress intensity factors for the single edge cracked specimen in tension. The stress intensity factors for the point load condition and the uniformly distributed load condition were equal except for very short specimen lengths. The stress intensity factors for the fixed grip condition were significantly different from the point load and uniformly distributed load condtions, except for very long specimens.

The normalized stress intensity factors for the single edge cracked test specimen subjected to a pure bending moment, four point bending, and three point bending were also compared. The normalized stress intensity factors for the four point bend specimen and the pure bend specimen were equal except for very short specimen lengths, however the three point bend specimen had slightly different results.

NADC-87145-60

FRACTURE MECHANICS ANALYSIS OF SOME FATIGUE AND FRACTURE TEST SPECIMENS USING FINITE ELEMENTS

by

G.P. DELSERRO

A Thesis
Presented to the Graduate Committee
of Lehigh University
in Candidacy for the Degree of
Master of Science
in
Mechanical Engineering

Lehigh University
May 1987

TABLE OF CONTENTS

FOREWARD:

This report was submitted to the Graduate Committee of Lehigh University as a thesis for the degree of Master Of Science in Mechanical Enginering.

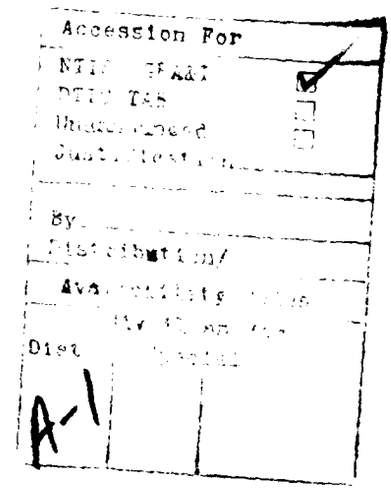

ABSTRACT:

The NASTRAN finite element computer program was used to analyze the Mode I problems of a thin strip fatigue specimen with a cracked central hole in tension, and a single edge cracked specimen in tension and bending. A regular eight node isoparametric quadrilateral element was degenerated into a quarter point triangular element which approximates the stress singularity at the crack tip. Accurate values of the Mode I stress intensity factors were computed using this element.

The normalized stress intensity factors, $K_1/\sigma_o(\pi a)^{1/2}$, for cracks of various lengths were computed for the thin strip fatigue specimen with a cracked central hole in tension. The normalized stress intensity factor increased near the hole.

A boundary condition comparison between a point load, a uniformly distributed load, and a fixed grip-displacement controlled condition was made on the normalized stress intensity factors for the single edge cracked specimen in tension. The stress intensity factors for the point load condition and the uniformly distributed

load condition were equal except for very short specimen lengths. The stress intensity factors for the fixed grip condition were significantly different from the point load and uniformly distributed load conditions, except for very long specimens.

The normalized stress intensity factors for the single edge cracked test specimen subjected to a pure bending moment, four point bending, and three point bending were also compared. The normalized stress intensity factors for the four point bend specimen and the pure bend specimen were equal except for very short specimen lengths, however the three point bend specimen had slightly different results.

1. INTRODUCTION

The finite element method is useful for calculating stress intensity factors for complex geometries where handbook solutions do not exist. This is especially important in aircraft applications where the geometry and loading are usually complicated. Conventional finite elements cannot adequately model the stress singularity at the crack tip[1][1]. Therefore, special methods must be employed to calculate accurate stress intensity values. Since 1970 a number of methods have been developed to compute stress intensity factors with relatively low computer costs[1-12]. The most popular approaches for computing stress intensity factors fall generally into three categories, namely the direct methods, the indirect methods, and the hybrid or cracked element method.

In the direct method, the stress intensity factors are calculated directly by fitting the finite element values of the stresses or the displacements into the asymptotic elasticity relations for stress and displacement around the crack tip. Usually special elements[2-4] are used around the crack tip which

[1] Numbers in brackets designate References at end of paper.

approximate the inverse square root stress singularity. The advantage to this method is its relative simplicity.

The most popular crack tip finite elements are that of Tracey[2], Barsoum[3], Henshell and Shaw[4]. Both elements approximate the stress singularity at the crack tip. Tracey's element must be implemented into the finite element program, however the element in [3] and [4] is obtained by degenerating a standard isoparametric quadrilateral element into a triangle, and moving the midside nodes to the quarter position.

In the indirect method, the stress intensity factor is computed through its relation to other quantities, such as energy release rate. The most commonly used approaches are the line integral method, energy release method, and the crack closure integral method.

The line integral (energy) method employs the J-integral developed by Rice[13],

$$J = \int_c \left(W dy - \hat{T} \cdot \frac{\partial \hat{u}}{\partial x} ds \right) \qquad (1)$$

where c is an arbitrary contour surrounding the crack tip, $\hat{T}$ is the stress vector acting on the contour, $\hat{u}$ is

the displacement vector, and W is the strain energy density,

$$W = \int \sigma_{ij} \, d\epsilon_{ij}.$$

The line integral J is related to the stress intensity factors by

$$J = \frac{[K_1^2 + K_2^2]}{E'} \qquad (2)$$

where $E' = E$ (plane stress)

$E' = E/(1-\nu^2)$ (plane strain)

Linear displacement finite elements can be used with this method resulting in lower computer costs, however multiple analyses with the same mesh and different boundary conditions must be performed to uncouple K_1 and K_2 in a mixed mode analysis[5].

In the energy-release approach [6,7,8], the stress intensity factors are computed from the change in energy resulting from successive crack tip positions along the mesh. The energy release rate, G, is related to the change in

the total potential energy, Π_p , with respect to an increase of crack length, da, by

$$G = -\frac{d\Pi_p}{da} \simeq \frac{\Delta\Pi_p}{\Delta a} \quad . \qquad (3)$$

The total potential energy of the finite element model is

$$\Pi_p = (1/2)\{u\}^T [K] \{u\} - \{u\}^T \{f\} \qquad (4)$$

where {u} is the displacement vector, [K] is the stiffness matrix, and {f} is the force vector. The energy release rate can be computed by incrementing the crack length by a small amount Δa, then

$$\Delta\Pi_p = (\Pi_p + \Delta\Pi_p) - \Pi_p = (1/2)\{u\}^T [\Delta K] \{u\} \qquad (5)$$

Extending the crack by Δa affects the elements around the crack tip only, therefore $[\Delta K]$ need only to be evaluated for those elements.

The energy release rate, G , is computed from equation (3) and the stress intensity factors are related to G by

$$G = \frac{[K_1^2 + K_2^2]}{E'} \qquad (6)$$

where $E' = E$ (plane stress)

$E' = E/(1-\nu^2)$ (plane strain).

The crack closure integral method permits both K_1 and K_2 to be computed from a single analysis [9]. This method is based on Irwin's concept that if a crack extends by a small amount Δa, then the energy absorbed in the process is equal to the work required to close the crack to its original length. The energy release rate equations for mode I and II loading are:

$$G_1 = \lim_{\Delta a \to 0} 1/(2\Delta a) \int_0^{\Delta a} \sigma_{yy}(\Delta a - r, 0) v(r, \pi) dr,$$

$$G_2 = \lim_{\Delta a \to o} 1/(2\,\Delta a) \int_o^{\Delta a} \sigma_{xy}(\,\Delta a - r, 0)u(r, \pi)dr. \qquad (7a,b)$$

The integrals physically represent the amount of work required to close the crack by a small amount Δa. In terms of the finite element representation, this work is equal to one-half the product of the forces at nodes c and d (Figure 1) and the distance $(v_c - v_d)$ required to close the nodes. The equations for G_1 and G_2 become

$$G_1 = \lim_{\Delta a \to 0} \frac{1}{2\Delta a} \bar{F}_c \cdot (v_c - v_d) \qquad (8a,b)$$

$$G_2 = \lim_{\Delta a \to 0} \frac{1}{2\Delta a} \bar{T}_c \cdot (u_c - u_d)$$

where $\bar{F}c$ and $\bar{T}c$ are the X and Y forces, respectively, required to hold nodes c and d together. This approach works best with linear displacement elements.

The Hybrid element approach utilizes cracked elements containing an exact mathematical solution to the stress

singularity within them [10,11]. The stress intensity factors are determined from nodal point displacements along the periphery of the cracked element. These elements are either incorporated into the finite element mesh or are solved separately using the finite element results. Hybrid elements yield highly accurate solutions with very coarse grids.

The objective was to choose a simple method for two-dimensional analysis that can be used with the NASTRAN Finite Element Computer Program, without requiring any computer programing. For this purpose, the degenerated isoparametric element introduced by Barsoum and Henshaw et al. is the most attractive approach. This element used with the direct method can calculate both K_1 and K_2 in a single analysis.

2. THEORY

2.1 Linear Elastic Fracture Mechanics

Consider a flat crack in a two dimensional linearly elastic solid under in-plane loading shown in Figure 2a. The stress and displacement states at a small distance P from the crack tip described by the polar coordinates r, θ are (Figure 2b) given by [14]

$$\sigma_{xx}(r,\theta) = \frac{K_1}{(2\pi r)^{1/2}}\cos(\theta/2)\left[1 - \sin(\theta/2)\sin(3\theta/2)\right] - \frac{K_2}{(2\pi r)^{1/2}}\sin(\theta/2)\left[2 + \cos(\theta/2)\cos(3\theta/2)\right]$$

$$\sigma_{yy}(r,\theta) = \frac{K_1}{(2\pi r)^{1/2}}\cos(\theta/2)\left[1 + \sin(\theta/2)\sin(3\theta/2)\right] + \frac{K_2}{(2\pi r)^{1/2}}\sin(\theta/2)\cos(\theta/2)\cos(3\theta/2)$$

$$\sigma_{xy}(r,\theta) = \frac{K_1}{(2\pi r)^{1/2}}\sin(\theta/2)\cos(\theta/2)\cos(3\theta/2)$$

$$+\frac{K_2}{(2\pi r)^{1/2}} \cos(\theta/2)\left[1 - \sin(\theta/2)\sin(3\theta/2)\right]$$

(9a-d)

$$\sigma_{zz} = 0 \quad \text{(plane stress)}$$

$$\sigma_{zz} = \nu(\sigma_{xx} + \sigma_{yy}) \quad \text{(plane strain)}$$

$$u(r,\theta) = \frac{K_1}{2G}(r/2\pi)^{1/2}\cos(\theta/2)\left[\kappa - 1 + 2\sin^2(\theta/2)\right]$$

$$+\frac{K_2}{2G}(r/2\pi)^{1/2}\sin(\theta/2)\left[\kappa + 1 + 2\cos^2(\theta/2)\right]$$

$$v(r,\theta) = \frac{K_1}{2G}(r/2\pi)^{1/2}\sin(\theta/2)\left[\kappa + 1 - 2\cos^2(\theta/2)\right]$$

$$+\frac{K_2}{2G}(r/2\pi)^{1/2}\cos(\theta/2)\left[1 - \kappa + 2\sin^2(\theta/2)\right]$$

(10a-b)

where G is the shear modulus, ν is Poisson's ratio and

$\kappa = (3-4\nu)$ (plane strain)

$\kappa = (3-\nu)/(1+\nu)$ (plane stress)

The constants K_1 and K_2 are the stress intensity factors associated with the loading modes shown in Figure 3.

2.2 Isoparametric Finite Element

The essential idea behind the 8-node isoparametric element is that a simple square element defined in a local coordinate system may be transformed into a curve-sided element in the global Cartesian Coordinate System, Figure 4. For an element to be isoparametric the interpolation functions defining the geometry and the displacement field are the same.

The interpolation functions of the 8-node quadratic isoparametric element (Serendipity Type) in the local $\xi - \eta$ coordinate system are [15]:

$$N_1 = (1/4)(1 - \xi)(1 - \eta) - (1/2)(N_5 + N_8)$$

$$N_2 = (1/4)(1 + \xi)(1 - \eta) - (1/2)(N_5 + N_6)$$

$$N_3 = (1/4)(1 + \xi)(1 + \eta) - (1/2)(N_6 + N_7)$$

$$N_4 = (1/4)(1 - \xi)(1 + \eta) - (1/2)(N_7 + N_8)$$

$$N_5 = (1/2)(1 - \xi^2)(1 - \eta)$$

$$N_6 = (1/2)(1 - \eta^2)(1 + \xi)$$

$$N_7 = (1/2)(1 - \xi^2)(1 + \eta)$$

$$N_8 = (1/2)(1 - \eta^2)(1 - \xi) \qquad \text{(11a-h)}$$

where the interpolation functions have the property,

$N_i = 1$ at node i,

$N_i = 0$ at every other node.

The mapping which transforms the square element from local coordinates to global X-Y coordinates is:

$$X = \sum_{i=1}^{8} N_i(\xi, \eta) x_i \qquad (12a,b)$$

$$Y = \sum_{i=1}^{8} N_i(\xi, \eta) y_i$$

where i corresponds to the node i whose coordinates are (X_i, Y_i) in the X-Y system and (ξ_i, η_i) in the $\xi - \eta$ system.

The displacements are represented through the interpolating functions by:

$$u(\xi, \eta) = \sum_{i=1}^{8} N_i(\xi, \eta) u_i = [N_i]\{u_i\}$$

$$v(\xi, \eta) = \sum_{i=1}^{8} N_i(\xi, \eta) v_i = [N_i]\{v_i\}$$

or

$$\begin{Bmatrix} u \\ v \end{Bmatrix} = [N_i] \begin{Bmatrix} u_i \\ v_i \end{Bmatrix} \qquad (13a,b,c)$$

where u_i and v_i are the calculated displacements at node i.

The strains can be calculated from the elasticity strain-displacement relationship and equations (13a-c). The strain-displacement relationship is

$$\{\epsilon\} = \begin{Bmatrix} \epsilon_{xx} \\ \epsilon_{yy} \\ 2\epsilon_{xy} \end{Bmatrix} = [D] \begin{Bmatrix} u \\ v \end{Bmatrix}, \qquad [D] = \begin{bmatrix} \partial/\partial x & 0 \\ 0 & \partial/\partial y \\ \partial/\partial y & \partial/\partial x \end{bmatrix} \qquad (14)$$

Substituting equation (13c) into equation (14), the strains can be represented through the interpolation functions and the nodal displacements by

$$\{\epsilon\} = [D][N_i]\begin{Bmatrix} u_i \\ v_i \end{Bmatrix} = [B]\begin{Bmatrix} u_i \\ v_i \end{Bmatrix}$$

$$[B] = \begin{bmatrix} \partial N_i/\partial x & 0 \\ 0 & \partial N_i/\partial y \\ \partial N_i/\partial y & \partial N_i/\partial x \end{bmatrix} \qquad (15)$$

Equation (15) requires differentiation of the interpolation functions with respect to X and Y. Since the interpolation functions $N_i(\xi, \eta)$ are functions of ξ and η the differentiation may be accomplished through the chain rule,

$$\begin{Bmatrix} \partial N_i/\partial \xi \\ \partial N_i/\partial \eta \end{Bmatrix} - \begin{bmatrix} \partial x/\partial \xi & \partial y/\partial \xi \\ \partial x/\partial \eta & \partial y/\partial \eta \end{bmatrix} \begin{Bmatrix} \partial N_i/\partial x \\ \partial N_i/\partial y \end{Bmatrix} = [J] \begin{Bmatrix} \partial N_i/\partial x \\ \partial N_i/\partial y \end{Bmatrix} \tag{16}$$

where [J] is the Jacobian matrix.

Thus,

$$\begin{Bmatrix} \partial N_i/\partial x \\ \partial N_i/\partial y \end{Bmatrix} = [J]^{-1} \begin{Bmatrix} \partial N_i/\partial \xi \\ \partial N_i/\partial \eta \end{Bmatrix} \tag{17}$$

Equation (17) can be used to evaluate the terms in equation (15).

For a homogeneous, isotropic linear elastic body in plane stress, the stresses are calculated from the strains using Hooke's Law.

$$\{\sigma\} = \begin{Bmatrix} \sigma_{xx} \\ \sigma_{yy} \\ \sigma_{xy} \end{Bmatrix} = [C]\{\epsilon\}, \quad [C] = E/(1-\nu^2)\begin{bmatrix} 1 & \nu & 0 \\ \nu & 1 & 0 \\ 0 & 0 & (1/2)(1-\nu) \end{bmatrix} \tag{18}$$

E = Young's Modulus

ν = Poisson's Ratio

The stiffness matrix [K] is defined as[15]:

$$[K] = \int_{-1}^{1}\int_{-1}^{1} [B]^T [C] [B] \det|J| d\xi \, d\eta \tag{19}$$

and the displacements can be solved from the equation

$$[K]\begin{Bmatrix} u_i \\ v_i \end{Bmatrix} = \begin{Bmatrix} F_i \end{Bmatrix} \tag{20}$$

where F_i are the nodal forces at node i.

2.3 Quarter-Point Triangular Crack Tip Element[3,4]

Figure 5 shows a triangular element generated by collapsing side 1-4 of the quadrilateral element in Figure 4 and moving the mid-side nodes adjacent to the crack to the quarter position. Side 1-4 was arbitrarily chosen to be the collapsed side. The crack runs along the negative X-axis.

Along side 1-2 of the triangle, $\eta = -1$ and the interpolation functions are:

$$N_3 = N_4 = N_6 = N_7 = N_8 = 0$$

$$N_1 = (-1/2)\,\xi(1 - \xi)$$

$$N_2 = (1/2)\,\xi(1 + \xi)$$

$$N_5 = (1 - \xi^2) \qquad (21)$$

From equation (12)

$$X = (-1/2)\xi(1 - \xi)x_1 + (1/2)\xi(1 + \xi)x_2 + (1 - \xi^2)x_5 \qquad (22)$$

Choosing $X_1 = 0$, $X_2 = L$, and $X_5 = L/4$, then

$$X = (1/2)\xi(1 + \xi)L + (1 - \xi^2)(L/4) \tag{23}$$

Thus,

$$\xi = (-1 + 2(x/L)^{1/2}) \tag{24}$$

From equation (13), the displacement along side 1-2 is,

$$u = (-1/2)\xi(1-\xi)u_1 + (1/2)\xi(1+\xi)u_2 + (1-\xi^2)u_5 \tag{25}$$

or in terms of X is,

$$\begin{aligned} u = {} & (-1/2)(-1 + 2(x/L)^{1/2})\left[2 - 2(x/L)^{1/2}\right]u_1 \\ & + (1/2)(-1 + 2(x/L)^{1/2})\left[2(x/L)^{1/2}\right]u_2 \\ & + (4(x/L)^{1/2} - 4(x/L))u_5 \end{aligned} \tag{26}$$

The displacement relation in equation (26) approximates the $r^{1/2}$ behavior near the crack tip as equation (10a).

The strains in the X-direction are,

$$\epsilon_{xx} = \partial u/\partial x = (-1/2)\left[3/(xL)^{1/2} - 4/L\right]u_1 + (1/2)\left[-1/(xL)^{1/2} + 4/L\right]u_2 + \left[2/(xL)^{1/2} - 4/L\right]u_5 \quad (27)$$

Equation (27) has the inverse square root singularity at the crack tip as equation (9). Therefore, the Linear Elastic Fracture Mechanics Equations are approximated in the quarter-point crack tip element.

3. NUMERICAL ANALYSIS

The NASTRAN Finite Element Computer Program was used to analyze the following problems: (1) a central cracked plate test case used to study the accuracy of the crack tip elements, (2) a thin strip fatigue specimen with a cracked central hole, (3) a boundary condition comparison on a single edge cracked specimen, and (4) a comparison of single edge cracked bending specimens. In all problems, the following assumptions are applied:

1. the specimens are made of 7075-T6 Aluminum which is homogeneous, isotropic, and linear elastic,
2. the specimens are thin plates under in-plane Mode I loading conditions,
3. the problems are in the plane stress condition.

Collapsed quarter point quadrilateral elements were used around the crack tip while the 8-node isoparametric quadrilateral elements were used in the rest of the mesh.

3.1 The Centrally Cracked Plate Test Case

The crack tip elements were initially tested on a uniformly loaded center cracked plate, shown in Figure 6, to study their accuracy. Only one quarter of the problem was analyzed because of symmetry. The following boundary conditions apply (Figure 6a):

1. $\sigma_{xx}(b,y) = \sigma_{xy}(b,y) = 0,$
2. $\sigma_{xy}(x,h) = 0, \quad \sigma_{yy}(x,h) = \sigma_o$
3. $\sigma_{xy}(0,y) = 0, \quad u(0,y) = 0,$
4. $\sigma_{xy}(x,0) = 0, \quad 0 < x < b,$
   $\sigma_{yy}(x,0) = 0, \quad 0 < x < a,$
   $v(x,0) = 0, \quad a < x < b.$

A total of 66 elements and 229 grid points were used in the mesh shown in Figure 7. The quarter-point element side length to half crack length ratio, L/a was $L/a \approx .10$. The normalized Mode I stress intensity factor $K_1/\sigma_o(\pi a)^{\frac{1}{2}}$ calculated from the finite element results, was 1.146 which is 1.1 percent different from the theoretical value of 1.159 obtained from [16],

$$K_1/\sigma_o(\pi a)^{1/2} = [\sec(\pi a/2b)]^{1/2} \qquad (28)$$

An accurate value of the Mode I stress intensity factor was computed with a relatively coarse mesh.

The following guidelines should be applied when using the collapsed quarter point quadrilateral elements for fracture mechanics analyses:

1. the grid points at the crack tip (on the collapsed side) must be rigidly constrained,
2. the sides of these crack tip elements must be kept straight to avoid error [17],
3. the L/a ratio should be kept small, $L/a \leq .2$, based on this test case and on the results from [18],
4. the finite element displacement results should be used to calculate the stress intensity factors (direct method) since they are more accurate than the stresses,
5. the crack opening displacements $v(r, \pi)$ should be used to compute K_1 and $u(r, \pi)$ should be used for K_2, (equations (10a,b)).

3.2 Thin Strip Fatigue Specimen With A Cracked Central Hole

The thin strip fatigue specimen, Figure 8, was used to study a hole-crack interaction problem. The particular dimensions in Figure 8 represent the lower front spar region of the A-4F Blue Angel aircraft where fatigue cracks have occurred. The specimen was gripped at the short ends and displaced in the Y-direction. The problem was analyzed in two parts: (1) fatigue specimen without a crack and (2) fatigue specimen with a cracked central hole.

3.2.1. Fatigue Specimen Without A Crack

A static stress analysis was performed on the specimen using finite elements to determine regions of high stress and the elastic stress concentration factor, K_t. Due to symmetry, only one quarter of the problem was considered. The following boundary conditions, shown in Figure 9, apply:

1. $\sigma_{xx}(b,y) = \sigma_{xy}(b,y) = 0,$
2. $\sigma_{xy}(0,y) = 0,$
   $u(0,y) = 0,$
3. $\sigma_{xy}(x,0) = 0,$
   $v(x,0) = 0,$

and at the fixed grip end,

4. $u(x,d) = 0,\ v(x,d) = v_o.$

The nominal stress along the fixed grip edge, σ_o, was calculated by

$$\sigma_o = \frac{\sum P_i}{A} \tag{29}$$

where P_i are the nodal reaction forces (at y=d) in the Y-direction from the fixed grip, and A is the cross-sectional area at the fixed grip end.

The finite element mesh, Figure 10, consisted of 162 elements and 557 grid points. The maximum stress occurred at the corner of the large central hole on the X-axis and the elastic stress concentration factor based on gross area, K_{tg}, is 3.99. The tangential stress distribution, $\sigma_{\theta\theta}$ is provided in Table 1, Figure 11 for the central hole and in Table 2, Figure 12 for the small hole.

3.2.2 Fatigue Specimen With A Cracked Central Hole

The effect of a crack of various lengths in the large central hole of Figure 8 was considered. The crack is located along the positive and negative X-axis. The boundary conditions for this problem, Figure 13, are:

1. $\sigma_{xx}(b,y) = \sigma_{xy}(b,y) = 0,$
2. $\sigma_{xy}(0,y) = 0,$
   $u(0,y) = 0,$
3. $\sigma_{xy}(x,0) = 0, \quad 0 < x < b,$
   $\sigma_{yy}(x,0) = 0, \quad 0 < x < a,$
   $v(x,0)=0, \quad a < x < b,$

and at the fixed grip end,

6. $u(x,d) = 0$
   $v(x,d) = v_0.$

The nominal stress along the fixed grip edge was calculated from equation (29).

Figures 14a,b,c show a typical mesh used in the cracked specimen analysis. A refined mesh was used in the region containing the crack. The number of elements ranged from 228 to 287, and the number of grid points ranged from 765 to 956, more elements were used as the crack length increased.

Figure 14c shows an enlarged view of the crack tip region. The L/a ratio was kept smaller than L/a $\leq$ .15. This crack tip region remained the same and was moved along the positive X-axis as the crack length increased.

The normalized stress intensity factors for various lengths are provided in Figures 15,16 and Table 3. A crack length of .375 inches corresponds to (c+a)-b when the crack reaches the side, hence the normalized stress intensity factors increase toward infinity. Even though the normalized stress intensity factor decreases before starting to increase with the increasing crack length (Figure 15), the absolute value of the stress intensity factor is, as expected, a monotonically increasing function of the crack length(Figure 16).

The limit of the normalized stress intensity factor as the crack length approaches zero in Figure 15 should approach the theoretical solution to the semi-infinite plate with an edge crack. As the crack length becomes infinitesimal, the radius of curvature of the hole, and the length and width of the plate appear to be infinitely large. The stresses around the infinitesimal crack are no longer affected by the finite geometry. The stress intensity factors for a uniformly loaded semi-infinite plate with an crack is [16]:

$$K_1 = 1.1215\,\sigma_{max}(\pi a)^{1/2}, \quad K_2 = 0. \tag{30}$$

where σ_{max} is the stress applied normal to the crack.

On the fatigue test specimen, the stress in the corner of the hole where the crack is located is:

$$\sigma_{max} = 3.99\,\sigma_o \tag{31}$$

Substituting equation (31) into equation (30), the stress intensity factor becomes,

$$K_1 = 4.4748\,\sigma_o(\pi a)^{1/2}. \tag{32}$$

Normalizing the stress intensity factor in equation (32),

$$K_1/\sigma_o\,(\pi a)^{1/2} = 4.4748, \tag{33}$$

hence the curve in Figure 15 should approach the value of 4.4748 near a = 0. As seen from the dashed line, the curve is accurate.

The normalized stress intensity factor, (K_1/σ_o) curve in Figure 16 should go to zero as the crack length approaches zero. The stress intensity factor in equation (30) can be written in the form,

$$K_1/\sigma_o = \text{constant} \cdot (a)^{1/2} \qquad (34)$$

Equation (34) has a parabolic shape and as the crack length approaches zero, K_1/σ_o goes to zero. The finite element results do agree with equation (34) near a = 0, and therefore the normalized stress intensity factor curve should follow the dashed line in Figure 16.

3.3 An Applied Load Boundary Condition Comparison On A Single Edge Cracked Test Specimen

The object of this problem was to determine the effect of different loading conditions on the stress intensity factor for a single edge cracked test specimen shown in Figure 17. Three types of tensile loading were considered: (1) a point load assumed to be equivalent to a pin loaded experiment, (2) a uniformly distributed load,(3) an external load applied through a rigid or fixed grip. The length of the specimen was varied to determine at what length (invoking the St. Venant's principle) statically equivalent loads applied in different ways would produce the same K_I values.

Only half of the problem was analyzed due to symmetry. The boundary conditions for the specimen with a point load, P, (Figure 18a) are:

1. $\sigma_{xx}(w,y) = \sigma_{xy}(w,y) = 0,$
2. $\sigma_{xx}(0,y) = \sigma_{xy}(0,y) = 0,$
3. $\sigma_{xy}(x,0) = 0, \quad 0 < x < w,$
   $\sigma_{yy}(x,0) = 0, \quad 0 < x < a,$
   $v(x,0) = 0, \quad a < x < w,$
4. $\sigma_{yy}(x,h) = P\delta(x - w/2), \quad \sigma_{xy}(x,h) = 0.$

and the nominal stress at the loaded end (y=h), σ_o, is given by

$$\sigma_o = P/A \tag{35}$$

where A is the cross sectional area.

Boundary conditions 1-3 apply for the specimen with a uniformly distributed load (Figure 18b), along with the condition,

4. $\sigma_{yy}(x,h) = \sigma_o$, $\sigma_{xy}(x,h) = 0$.

In the finite element analysis, σ_o was calculated from,

$$\sigma_o = \frac{\sum P_i}{A} \tag{36}$$

where Pi are the node point forces in the Y-direction.

For the fixed grip-displacement controlled problem (Figure 18c), boundary conditions 1-3 apply, along with

the condition,

$$4.\ u(x,h) = 0,\ v(x,h) = Vo,\quad 0 < x < w,$$

and σ_o is calculated from equation (29).

Typical finite element meshes for this analysis are shown in Figures 19a,b,c. The crack length, a, and specimen width, w, were constant with a/w = .5, while the specimen length, h, was varied between h/w = .1 and h/w = 100. The ASTM[19] dimensions for this specimen are a/w = .5 and h/w = 1.5.

The normalized stress intensity factor, $K_1/\sigma_o(\pi a)^{1/2}$, is shown for different half-length to width ratios (h/w) in Figures 20a,b and Table 4. The normalized stress intensity factor of 2.836 from Table 4 is 0.2 percent different than the theoretical value of 2.830 for the uniformly loaded strip with an edge crack [16]. For h/w < 1.25, the point and distributed loading conditions have different normalized stress intensity values, but for h/w $\geq$ 1.25 they are exactly the same. The fixed grip condition produces very different results from the point and distributed load conditions for h/w < 20. For very small h/w ratios, the normalized stress intensity factors for the point and distributed loading conditions significantly

increase, while the normalized stress intensity factor for fixed grip condition continues to decrease.

Deformed plots of the single edged cracked specimen under the different applied loading conditions are provided in Figures 21a,b,c,d,e,f for two different specimen lengths. The deformed plots in Figures 21a,b,c show that the specimen rotates for the point and distributed load cases, however the rigid fixed grip prevents rotation. Also, the crack opening displacements, $v(r, \pi)$ are larger for the point and distributed load conditions, than for the fixed grip conditions which is why the stress intensity factor is lower for the fixed grip in Figures 20a,b. The crack opening displacements change as the specimen length decreases which support the increase in the normalized stress intensity factors for the point and distributed loads and the decrease for the fixed grip for short specimen lengths.

The normalized transverse relative displacement, $\Delta u_t/(\sigma_0 h/E)$, is shown in Figures 22a,b and Table 5. The transverse displacement, Δu_t, is defined as,

$$\Delta u_t = |\Delta u_1| + |\Delta u_2| \qquad (37)$$

where Δu_1 and Δu_2 are the displacements shown in Figure 21a,b,c. The normalized transverse relative displacements

for the fixed grip condition are smaller than for the distributed and point load conditions because $\Delta u_2 = 0$ for the fixed grip conditions.

The normal stress distribution in front of the crack tip, $\sigma_{yy}(x,0)$, for various h/w values is provided in Figures 23a,b,c and Tables 6a,b,c. For the point and distributed load conditions, the normal stress distribution in front of the crack tip changes very little as h/w decreases from 100 to 1.5, however the distribution changes significantly as h/w decreases from 1.5 to 0.1. Significant changes in the stress distribution occur for the fixed grip condition for each h/w value in Table 6c. For specimens of long length (h/w = 100), there are compressive stresses near the edge of the specimen (near x/w = 1.0).

The fixed grip-displacement controlled problem was studied further because of its complexity. The finite element results were compared to the two limiting analytic solutions: (1) the tearing of an infinitely wide strip [16] for a very short specimen, Figure 24, and (2) the semi-infinite strip with a fixed end [20] for a very long specimen, Figure 25.

The tearing of an infinitely wide strip problem is shown in Figure 24. An external load is applied through rigid clamps held at $\epsilon_{yy} = \epsilon_o$ when the material begins to fracture. There are three distinguishable zones in the strip, zone I, an unloaded region where the strain energy density (W) equals zero, zone II, where W is unknown, and zone III, where W = constant, $\epsilon_{yy} = \epsilon_o$, $\epsilon_{xx} = \epsilon_{xy} = 0$. The stress intensity factor is given by [16]

$$K_I^V = \epsilon_o E (h/(1-\nu^2))^{1/2} \qquad (38)$$

The strain ϵ_o is given by,

$$\epsilon_o = \frac{V_o}{h} \qquad (39)$$

where V_o is the displacement at the fixed grip end and E is Young's Modulus. Substituting equation (39) into equation (38), the stress intensity factor can be expressed as

$$K_1^V = \frac{E\, v_o}{[h(1-\nu^2)]^{1/2}} \quad . \qquad (40)$$

A comparison between the normalized stress intensity factors for the single edge cracked test specimen under fixed grip conditions, and the infinitely wide strip with a fixed end, is provided in Figures 26a,b and Table 7. The stress intensity factors are normalized by the right hand side of equation (40), which means that the normalized stress intensity factor for the infinitely wide strip, K_1^V, has a constant value of one for all h/w values. The normalized stress intensity values for the single edge cracked specimen are less than five percent different from the infinitely wide strip for h/w values less than five. The results for the specimen diverge from the infinitely wide strip solution for large h/w values because of the long specimen length.

The normal and shear stress distribution along the fixed end of the single edge cracked specimen is shown in Figures 27 and Table 8 for various h/w values. For the

short specimen (h/w = .1) in Figure 27a, the unloaded region (zone I) can be seen near x/w = 0.

The normal stress at the fixed grip end, $\sigma_{yy}(x,h)$, (Figure 27a and Table 8) and the normal stress in front of the crack tip, $\sigma_{yy}(x,0)$, (Figure 23c and Table 6c) are not constant near x/w = 1 (zone III) which means that the strain energy density is not constant throughout zone III. This supports the differences in the normalized stress intensity factors between the specimen and the infinitely wide strip in Figure 26a,b and Table 7.

The semi-infinite strip solution with a fixed end by Gupta [20], shown in Figure 25, was used to study the stresses around the fixed grip. The solution shows that the shear and normal stresses are singular at the corners of the fixed end. The stress intensity factors at the corners are defined by,

$$K_1 = \lim_{r \to 0} (2)^{1/2} \cdot r^{\alpha} \sigma_{yy}(r,h)$$

$$K_2 = \lim_{r \to 0} (2)^{1/2} \cdot r^{\alpha} \sigma_{xy}(r,h) \qquad (41)$$

where r is a variable starting at the corners of the fixed

edge shown in Figure 25. The characteristic equation to determine α is given by

$$2\kappa\cos\pi\alpha = \kappa^2 + 1 - 4(\alpha - 1)^2 \qquad (42)$$

where $\kappa = 3-4\nu$ (plane strain)

$\kappa = (3 - \nu)/(1+ \nu)$ (plane stress).

The exponent of the stress singularity, α, depends on Poisson's ratio. The results of [20] also show that the stress intensity factor K_1 depends on K_2 and the ratio K_2/K_1 is given by

$$\frac{K_2}{K_1} = - \frac{(\kappa + 1)\sin\pi\alpha}{[(\kappa-1)(\cos\pi\alpha +1) - 2(\kappa+1)(\alpha-1) + 4(\alpha-1)^2]} \qquad (43)$$

For the plane stress conditions and $\nu = .33$, $\alpha = .2539$ from equation (42) and $K_2/K_1 = -.255$ from equation (43).

The finite element results for the single edge cracked specimen (h/w = 100) were compared to Gupta's results. The stresses on the fixed edge of the specimen,

shown in Figure 27e, compare well with the results from [20], except at the corners where the stress singularities exist. The finite elements did not provide an accurate representation of the normal and shear stress singularities near x/w = 0 and x/w = 1, as shown in Figures 27a,b,c,d,e , since the stress variation in the elements is linear. The actual stress distribution should follow the dashed curve. The shear stress in Figure 27e is an odd function in X, as it was in [20].

From equations (41), the stress intensity factor ratio can be expressed as,

$$\frac{K_2}{K_1} = \lim_{r \to 0} \frac{\sigma_{xy}(r,h)}{\sigma_{yy}(r,h)} \qquad (44)$$

The limit in equation (44) was approximated from the r = 0 value of the finite element stress ratios shown in Figure 28 and Table 9. For side A, K_2/K_1 = -.2154 and for side B, K_2/K_1 = .2107 which are 15.5 and 17.4 percent different from the analytical value.

3.4 A Comparison of Single Edge Cracked Bend Specimens

A comparison of the following types of single edge cracked bending specimens is made: (1) pure bending applied through a linear stress distribution normal to the edge (Figure 29a), (2) four point bending (Figure 29b), and three point bending (Figure 29c). Due to symmetry, only one half of the problem was analyzed.

The boundary conditions for the pure bend specimen are (Figure 30a):

1. $\sigma_{xx}(w,y) = \sigma_{xy}(w,y) = 0,$
2. $\sigma_{xx}(0,y) = \sigma_{xy}(0,y) = 0,$
3. $\sigma_{xy}(x,0) = 0, \quad 0 < x < w,$
   $\sigma_{yy}(x,0) = 0, \quad 0 < x < a,$
   $v(x,0) = 0, \quad a < x < w,$
4. $\sigma_{yy}(x,h) = \sigma_0, \quad \sigma_{xy}(x,h) = 0,$

where σ_0 is a linear stress distribution normal to the edge.

The boundary conditions for the four point bend

specimen are (Figure 30b):

1. $\sigma_{xy}(w,y) = 0, \quad 0 < y < h,$

   $\sigma_{xx}(w,y) = -P\delta(y-h),$

2. $\sigma_{xy}(0,y) = 0, \quad 0 < y < (h+d),$

   $\sigma_{xx}(0,y) = P\delta(y-h-d),$

3. $\sigma_{xy}(x,0) = 0, \quad 0 < x < w,$

   $\sigma_{yy}(X,0) = 0, \quad 0 < x < a,$

   $v(x,0) = 0, \quad a < x < w,$

4. $\sigma_{yy}(x,L) = \sigma_{xy}(x,L) = 0.$

In the finite element analysis, the boundary condition $\sigma_{xx}(w,y) = -P\delta(y-h)$ was replaced by $u(w,h) = 0$ to prevent rigid body displacement.

For the three point bend specimen, the boundary conditions are (Figure 30c):

1. $\sigma_{xy}(w,y) = 0, \quad 0 < y < L,$

   $\sigma_{xx}(w,y) = -P\delta(y-0),$

2. $\sigma_{xy}(0,y) = 0, \quad 0 < y < h,$

   $\sigma_{xx}(0,y) = P\delta(y-h),$

3. $\sigma_{xy}(x,0) = 0, \quad 0 < x < w,$

   $\sigma_{yy}(x,0) = 0, \quad 0 < x < a,$

   $v(x,0) = 0, \quad a < x < w,$

4. $\sigma_{yy}(x,L) = \sigma_{xy}(x,L) = 0.$

The boundary condition $\sigma_{xx}(w,y) = -P\delta(y-0)$ was replaced by $u(w,0) = v(w,0) = 0$ in the finite element analysis to prevent rigid body displacement.

The nominal bending stress for the three and four point bend specimens is calculated from

$$\sigma_o = M_o c/I = 6M_o/w^2 \qquad (40)$$

where c=w/2, I is the area moment of inertia about the z-axis, and $M_o = p \cdot h$ for the three point and $M_o = p \cdot d$ for the four point specimen.

This problem utilized the same meshes and geometry in the applied load boundary condition comparison, Figure 19. The ASTM [19] dimensions for the bending specimens are a/w = .5 and h/w = 2.

The normalized stress intensity factor, $K_1/\sigma_o(\pi a)^{1/2}$, is shown for various half-length to width ratios (h/w) in Figure 31a,b and Table 10 for the bending specimens. The normalized stress intensity factors for the four point bend and pure bend specimen are approximately the same for $h/w \geq .8$, however the three point bend specimen is significantly different from the other specimens until $h/w \geq 5$. The normalized stress intensity factor of 1.518 for the pure bending specimen is 1.5 percent different

from the theoretical value of 1.496 computed from [16], and the value of 1.424 for the three point bend specimen (for h/w = 2) is 0.9 percent different from the theoretical value of 1.411 computed from [16].

Another study was performed on the four point bend specimen to determine the effects of changing the distance between the point load and the roller pin, d (Figure 29b). A specimen with h/w = 10, a/w =.5, was used. The position of the point load P was kept constant at the coordinates (0,9w) while the position of the pin was varied. The results in Table 11 show that changing d had no effect on the normalized stress intensity factor.

Deformed plots of the bending specimens are shown in Figure 32a,b,c. The uniform bend and three point bend specimens show more rotation than the four point bend specimen.

Finally the normal stress distribution in front of the crack tip, $\sigma_{yy}(x,0)$, is provided in Figures 33a,b,c and Tables 12a,b,c for the bend specimens. The normal stress distributions for the pure bend specimen and the four point bend specimen are very similar, while the three point bend specimen has slightly different results. As h/w decreases, the normal stress distribution for the pure

bend and four point specimens changes very little, however the distribution changes significantly for the three point bend specimen. There are large compressive stresses in the three point bend specimen near x/w = 1.0 (near the pin) for h/w = .5.

4. CONCLUSION:

Accurate values of the Mode I stress intensity factor were computed using the collapsed quarter point quadrilateral elements, however the mesh around the crack tip must be carefully prepared which can be tedious. These elements used with the direct method provide a relatively easy way to compute stress intensity factors for complex geometries and loading conditions where handbook solutions do not exist. Also, the crack opening displacements from the finite element analysis yield more accurate stress intensity values than the stresses in front of the crack tip.

The single edge cracked specimen under the fixed grip, displacement controlled loading condition had significantly different normalized stress intensity factors than the point and distributed loading conditions for half-length to width ratios (h/w) less than twenty. The normalized stress intensity factors for the point and distributed loading conditions were exactly the same after $h/w \geq 1.25$. The type of applied loading condition effects the stress intensity factor around the crack tip for this specimen.

The normalized stress intensity factor for the three point bend specimen was significantly different from the pure bend and four point bend specimen for $h/w < 5$. The normalized stress intensity factors for the pure bend and four point bend specimens were approximately the same except for very short specimens. The four point bend configuration produces a closer approximation to a pure bending load than the three point bend configuration.

T A B L E S

Theta, θ, (degrees)	$\sigma_{\theta\theta}/\sigma_c$
0.00	3.99
3.75	3.95
7.50	3.86
11.25	3.69
15.00	3.49
18.75	3.22
22.50	2.92
26.25	2.59
30.00	2.22
33.75	1.86
37.50	1.47
41.25	1.11
45.00	.77
48.75	.44
52.50	.12
56.25	-.20
60.00	-.46
63.75	-.70
67.50	-.89
71.25	-1.05
75.00	-1.16
78.75	-1.25
82.50	-1.30
86.25	-1.33
90.00	-1.34

Table 1. Tangential stress ratio, $\sigma_{\theta\theta}/\sigma_c$, at nodal points about the boundary of the large central hole.

Theta, θ, (degrees)	$\sigma_{\theta\theta}/\sigma_o$
-90	-.11
-81	-.11
-72	-.11
-63	-.05
-54	.10
-45	.28
-36	.55
-27	.86
-18	1.18
-9	1.51
0	1.76
9	1.84
18	1.79
27	1.60
36	1.26
45	.97
54	.63
63	.17
72	-.15
81	-.38
90	-.44

Table 2. Tangential stress ratio, $\sigma_{\theta\theta}/\sigma_o$, at nodal points about the boundary of the small holes.

Crack Length, a(in)	K_1/σ_o	$K_1/\sigma_o(\pi a)^{1/2}$
.01	.704	3.973
.02	.949	3.784
.04	1.226	3.458
.06	1.405	3.235
.08	1.546	3.083
.10	1.671	2.981
.125	1.823	2.910
.15	1.979	2.883
.20	2.342	2.954
.25	2.846	3.211
.30	3.703	3.814
.325	4.510	4.464
.35	6.298	6.006

Table 3. Normalized stress intensity factor vs. crack length.

$K_1/\sigma_o(\pi a)^{1/2}$

h/w	Point Load	Distributed Load	Fixed Grip
.1	5.137	14.871	.455
.2	3.635	6.254	.645
.3	3.013	4.097	.778
.4	2.775	3.344	.873
.5	2.720	3.035	.959
.6	2.733	2.914	1.037
.8	2.788	2.846	1.171
1.0	2.823	2.836	1.287
1.25	2.836	2.836	1.415
1.5	2.839	2.836	1.524
3	-	-	1.940
5	-	-	2.208
10	-	-	2.470
15	-	-	2.581
20	-	-	2.637
30	-	-	2.702
40	-	-	2.733
100	2.836	2.836	2.793

Table 4. Normalized stress intensity factors vs. half-length to width ratio (h/w) for the single edge cracked specimen under various applied loading conditions.

$\Delta u_T / (\sigma_o h/E)$

h/w	Point Load	Distributed Load	Fixed Grip
.1	10.5862	54.9415	.8345
.2	5.3400	15.1480	.7984
.3	4.1126	7.9745	.7555
.4	3.9190	5.8678	.7318
.5	4.0403	5.1455	.7414
.6	4.2541	4.9094	.7701
.8	4.6752	4.8923	.8554
1.0	4.9538	5.0019	.9548
1.25	5.1296	5.1191	1.0780
1.5	5.2134	5.2001	1.1915
3	-	-	1.6671
5	-	-	1.9968
10	-	-	2.3332
15	-	-	2.4734
20	-	-	2.5468
30	-	-	2.6283
40	-	-	2.6695
100	5.5984	5.5984	2.7477

Table 5. Normalized transverse relative displacement ($\Delta u_T / \sigma_o h/E$) vs half-length to width ratio (h/w) for the single edge cracked test specimen under various loading conditions.

Point Load

$\sigma_{yy}(x,0)/\sigma_o$

x/w	h/w = 100	h/w = 1.5
.5	54.133	54.184
.5125	12.116	12.124
.55	8.842	8.847
.575	4.372	4.371
.600	3.506	3.505
.625	2.920	2.917
.65	2.423	2.420
.675	2.012	2.009
.700	1.639	1.635
.725	1.313	1.309
.750	.977	.974
.8125	.229	.227
.875	-.581	-.581
.9375	-1.500	-1.497
1.0	-2.731	-2.726

Table 6a. Normal stress in front of the crack tip, $\sigma_{yy}(x,0)$, for the single edge cracked specimen under a point load.

Point Load
$\sigma_{yy}(x,0)/\sigma_o$

x/w	h/w = .1
.5	138.294
.50625	31.251
.525	22.511
.5375	9.290
.550	5.841
.5625	3.365
.5750	1.593
.5875	.280
.600	-.504
.625	-1.230
.650	-1.252
.675	-.970
.700	-.690
.725	-.421
.750	-.257
.775	-.131
.800	-.067
.825	-.026
.850	-.008
.875	.001
.900	.003
.925	.004
.950	.003
.975	.003
1.0	.004

Table 6a (continued).

Distributed Load

$\sigma_{yy}(x,0)/\sigma_o$

x/w	h/w = 100	h/w = 1.5
.5	54.133	54.134
.5125	12.116	12.116
.55	8.842	8.842
.575	4.372	4.372
.600	3.506	3.506
.625	2.920	2.920
.65	2.423	2.423
.675	2.012	2.012
.700	1.639	1.638
.725	1.313	1.313
.750	.977	.977
.8125	.229	.229
.875	-.581	-.581
.9375	-1.50	-1.500
1.0	-2.731	-2.731

Table 6b. Normal stress in front of the crack tip, $\sigma_{yy}(x,0)$, for the single edge cracked specimen under a uniformly distributed load.

Distributed Load

$\sigma_{yy}(x,0)/\sigma_o$

x/w	h/w = .1
.5	426.646
.50625	66.295
.525	38.586
.5375	.705
.550	-5.909
.5625	-8.981
.5750	-10.511
.5875	-10.575
.600	-10.104
.625	-7.606
.650	-5.155
.675	-2.772
.700	-1.334
.725	-.208
.750	.374
.775	.751
.800	.913
.825	.999
.850	1.025
.875	1.030
.900	1.025
.925	1.018
.950	1.013
.975	1.009
1.0	1.010

Table 6b (continued).

Fixed Grip

$\sigma_{yy}(x,0)/\sigma_o$

x/w	h/w = 100	h/w = 1.5
.5	53.324	28.778
.5125	11.945	6.770
.55	8.722	5.066
.575	4.322	2.807
.600	3.472	2.419
.625	2.896	2.175
.65	2.409	1.975
.675	2.006	1.821
.700	1.640	1.683
.725	1.321	1.571
.750	.992	1.458
.8125	.260	1.213
.875	-.532	.945
.9375	-1.432	.625
1.0	-2.639	.160

Table 6c. Normal stress in front of the crack tip, $\sigma_{yy}(x,0)$, for the single edge cracked specimen under fixed grip-displacement controlled conditions.

Fixed Grip

$\sigma_{yy}(x,0)/\sigma_o$

x/w	h/w = .1
.5	11.566
.50625	3.309
.525	2.684
.5375	1.973
.550	1.923
.5625	1.920
.5750	1.920
.5875	1.932
.600	1.941
.625	1.956
.650	1.966
.675	1.970
.700	1.972
.725	1.971
.750	1.972
.775	1.969
.800	1.969
.825	1.965
.850	1.963
.875	1.958
.900	1.952
.925	1.913
.950	1.847
.975	1.708
1.0	1.408

Table 6c (continued).

h	Singled Edged Cracked Specimen (Fixed Grip) K_1 / $Ev_o/[h(1-\nu^2)]^{1/2}$	Infinitely Wide Strip With A Fixed End K_1 / $Ev_o/[h(1-\nu^2)]^{1/2}$
.1	.9653	1.0
.2	.9787	↓
.3	.9802	↓
.4	.9699	↓
.5	.9689	↓
.6	.9688	↓
.8	.9742	↓
1.0	.9834	↓
1.25	.9952	↓
1.5	1.0043	↓
3	1.0048	↓
5	.9535	↓
10	.8200	↓
15	.7234	↓
20	.6531	↓
30	.5571	↓
40	.4935	↓
100	.3257	1.0

Table 7. A comparison between the single edge cracked test specimen under fixed grip conditions and the infinitely wide strip solution with a fixed end.

h/w = .1

x/w	A	B	x/w	A	B
0.	.01	.00	.6	1.94	-.05
.025	.00	↓	.625	1.95	-.03
.050	↓	↓	.650	1.95	.00
.075	↓	↓	.675	1.95	.01
.100	↓	↓	.700	1.95	.02
.125	↓	↓	.725	1.94	.03
.150	↓	.00	.750	1.93	.05
.175	↓	-.01	.775	1.92	.07
.200	↓	↓	.800	1.91	.09
.225	↓	↓	.825	1.89	.11
.250	↓	↓	.850	1.87	.14
.275	↓	-.01	.875	1.85	.18
.300	↓	-.02	.900	1.84	.23
.325	↓	-.03	.925	1.75	.27
.350	.00	-.05	.950	1.72	.33
.375	.03	-.09	.975	2.05	.53
.400	.07	-.15	1.0	2.65	.79
.425	.20	-.25			
.450	.44	-.34			
.475	.84	-.39			
.500	1.27	-.40			
.525	1.61	-.30			
.550	1.84	-.19			
.575	1.92	-.12			

$A = \sigma_{yy}(x,h)/\sigma_o$

$B = \sigma_{xy}(x,h)/\sigma_o$

Table 8. Normal stress (σ_{yy}) and shear stress (σ_{xy}) along the fixed grip end of the single edge cracked specimen.

	h/w = .5		h/w = 1.5	
x/w	A	B	A	B
0.	.01	-.08	.44	-.18
.0625	-.01	-.11	.39	-.17
.125	.04	-.15	.37	-.15
.1875	.17	-.17	.45	-.14
.2500	.33	-.20	.54	-.13
.3125	.49	-.21	.63	-.12
.3750	.68	-.22	.73	-.10
.4375	.88	-.19	.83	-.08
.5000	1.07	-.15	.93	-.06
.5625	1.24	-.09	1.03	-.03
.6250	1.36	-.02	1.14	.00
.6875	1.48	.06	1.25	.04
.7500	1.57	.15	1.36	.08
.8125	1.58	.21	1.48	.14
.8750	1.66	.28	1.62	.22
.9375	2.12	.50	2.02	.37
1.0	2.95	.77	2.45	.52

$A = \sigma_{yy}(x,h)/\sigma_o$

$B = \sigma_{xy}(x,h)/\sigma_o$

Table 8. (cont.)

	h/w = 10.		h/w = 100.	
x/w	A	B	A	B
0.	1.022	-.244	1.26	-.27
.0625	.939	-.206	1.14	-.22
.1250	.859	-.166	1.02	-.17
.1875	.859	-.138	.99	-.14
.2500	.863	-.110	.97	-.11
.3125	.881	-.085	.96	-.08
.3750	.901	-.061	.95	-.05
.4375	.927	-.037	.95	-.03
.5000	.954	-.013	.95	.00
.5625	.985	.012	.96	.02
.6250	1.018	.038	.97	.05
.6875	1.057	.069	.98	.08
.7500	1.099	.101	.99	.10
.8125	1.159	.142	1.03	.14
.8750	1.223	.184	1.06	.18
.9375	1.386	.244	1.19	.23
1.0	1.552	.305	1.32	.28

$A = \sigma_{yy}(x,h)/\sigma_o$

$B = \sigma_{xy}(x,h)/\sigma_o$

Table 8. (cont.)

r/w	SIDE A A	SIDE B B
0.	.2154	.2107
.0625	.1956	.1908
.1250	.1705	.1656
.1875	.1408	.1364
.2500	.1093	.1053
.3125	.0817	.0781
.3750	.0536	.0502
.4375	.0276	.0243
.5000	.0017	.0017

A = $-\sigma_{xy}(r,h)/\sigma_{yy}(r,h)$ For Side A

B = $\sigma_{xy}(r,h)/\sigma_{yy}(r,h)$ For Side B

Table 9. Shear stress to normal stress ratio at the fixed grip end of the single edge cracked specimen (h/w = 100).

$$K_1 / \sigma_o (\pi a)^{1/2}$$

h/w	Pure Bending	4 Point Bending	3 Point Bending
.5	1.650	1.555	1.158
.6	1.570	1.546	1.217
.8	1.525	1.530	1.289
1.0	1.518	1.522	1.332
1.5	↓	1.518	1.392
2.0		1.517	1.424
5.0		1.517	1.480
10.0	1.518	1.517	1.499

Crack length to width ratio, a/w = .5

Table 10. A comparison of normalized stress intensity factors for single edge cracked bend specimens for various half-length to width (h/w) ratios.

d/w	Single Edge Cracked 4 Point Bend Specimen $K_1/\sigma_o(\pi a)^{1/2}$
.25	1.518
.5	1.517
1.0	1.518
1.5	↓
2.0	↓
7.0	1.518

Crack length to width ratio, a/w = .5

Specimen length to width ratio, h/w = 10

Table 11. Normalized stress intensity factor of the four point bend specimen for various distances between the point and the roller pin, d, (see Figure 29b).

Pure Bend Specimen

$\sigma_{yy}(x,0)/\sigma_o$

x/w	h/w=10	h/w=1.5	h/w = .5
.5	29.345	29.345	32.103
.5125	6.188	6.188	6.558
.55	4.371	4.371	4.558
.575	1.812	1.812	1.735
.6	1.259	1.259	1.129
.625	.863	.863	.707
.65	.518	.518	.351
.675	.222	.222	.056
.7	-.052	-.052	-.206
.725	-.300	-.300	-.438
.75	-.557	-.557	-.669
.8125	-1.140	-1.140	-1.176
.875	-1.766	-1.766	-1.726
.9375	-2.460	-2.460	-2.365
1.0	-3.345	-3.345	-3.277

Table 12a. Normal stress in front of the crack tip, $\sigma_{yy}(x,0)$, for the single edge cracked specimen under pure bending.

4 Point Bend Specimen

$\sigma_{yy}(x,0)/\sigma_o$

x/w	h/w=10	h/w=1.5	h/w= .5
.5	29.345	29.346	30.109
.5125	6.188	6.187	6.311
.55	4.371	4.371	4.444
.575	1.812	1.812	1.808
.6	1.259	1.259	1.236
.625	.863	.862	.827
.65	.518	.518	.472
.675	.222	.222	.168
.7	-.052	-.052	-.111
.725	-.300	-.300	-.359
.75	-.557	-.557	-.614
.8125	-1.140	-1.140	-1.180
.875	-1.766	-1.765	-1.767
.9375	-2.460	-2.460	-2.414
1.0	-3.345	-3.346	-3.257

Table 12b. Normal stress in front of the crack tip, $\sigma_{yy}(x,0)$, for the single edge cracked specimen under four point bending.

3 Point Bend Specimen

$\sigma_{yy}(x,0)/\sigma_o$

x/w	h/w=10	h/w=1.5	h/w= .5
.5	28.976	28.883	22.272
.5125	6.117	5.715	4.817
.55	4.324	4.055	3.449
.575	1.800	1.733	1.572
.6	1.256	1.240	1.191
.625	.886	.886	.918
.65	.528	.580	.684
.675	.239	.335	.543
.7	-.029	.103	.391
.725	-.285	-.201	-.024
.75	-.540	-.441	-.228
.8125	-1.073	-.691	.193
.875	-1.687	-1.240	-.190
.9375	-2.508	-2.780	-3.406
1.0	-3.610	-5.110	-8.605

Table 12c. Normal stress in front of the crack tip, $\sigma_{yy}(x,0)$, for the single edge cracked specimen under three point bending.

F I G U R E S

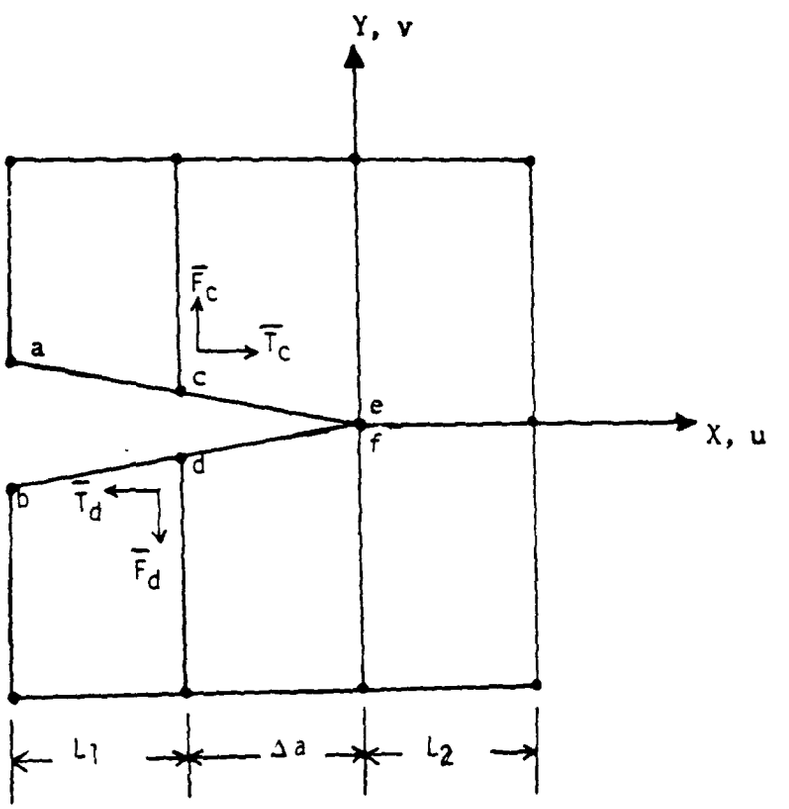

Figure 1. Finite element nodes near crack tip.

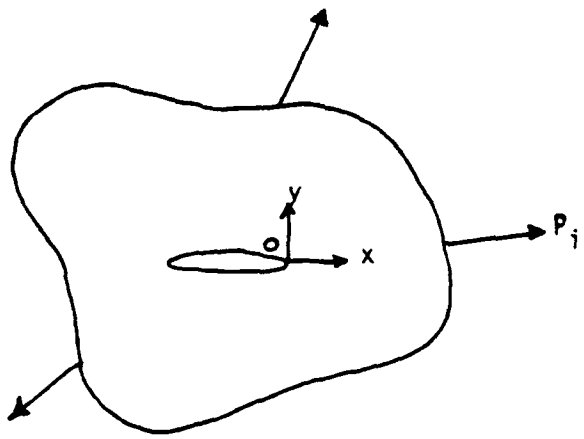

Figure 2a. A 2D solid with a flat crack,

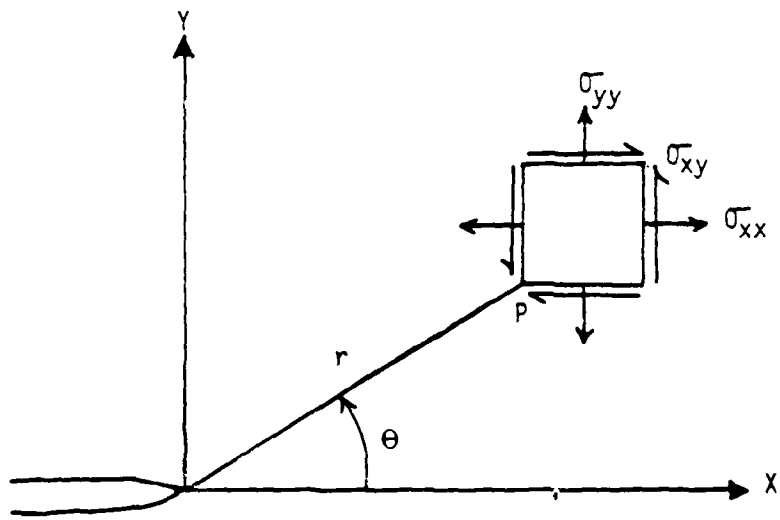

Figure 2b. Stress state around the crack tip.

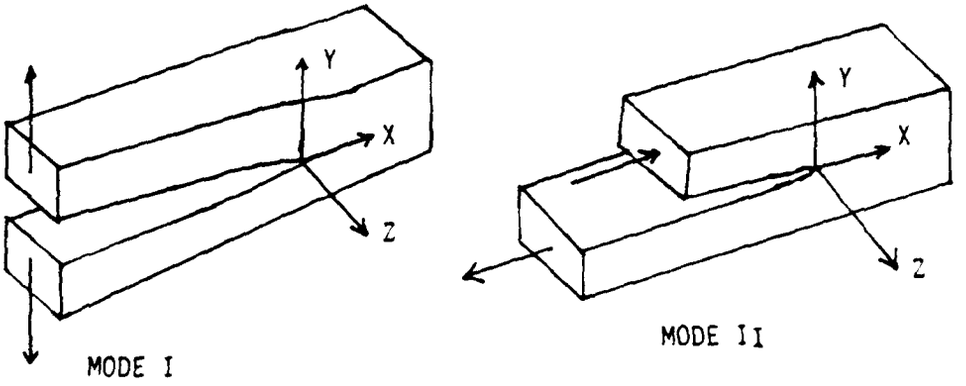

Figure 3. Loading modes for stress intensity factors.

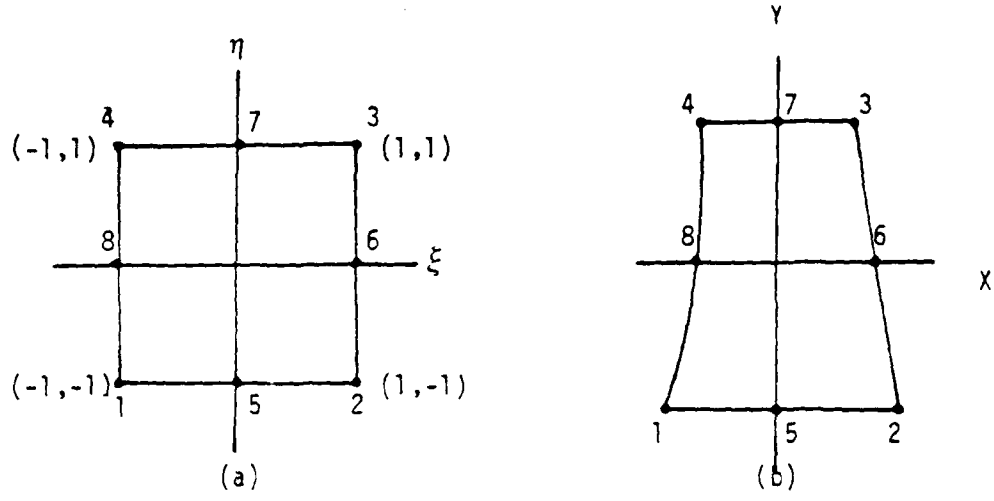

Figure 4. The isoparametric element in the: (a) local coordinate system and (b) Cartesian Coordinate System.

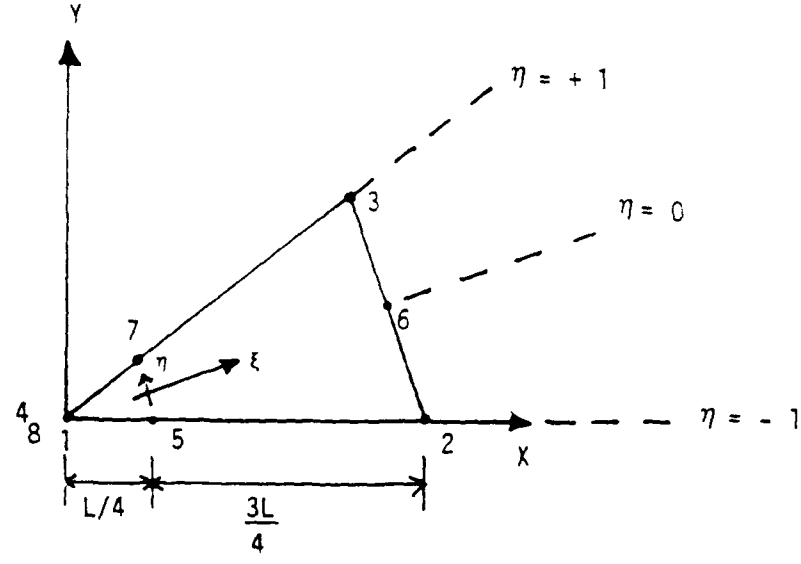

Figure 5. The collapsed quadrilateral element.

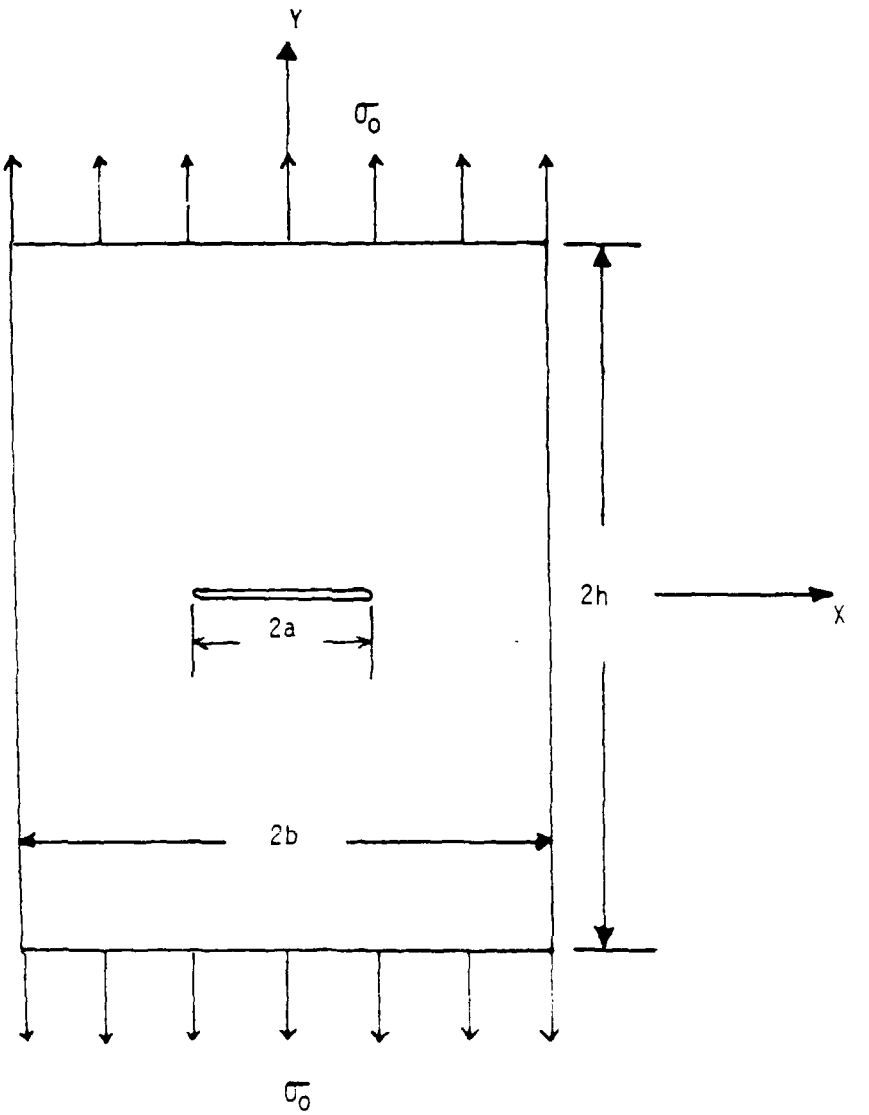

h = 1.5
b = .6875
a = .32

Figure 6. Geometry for the center cracked test specimen.

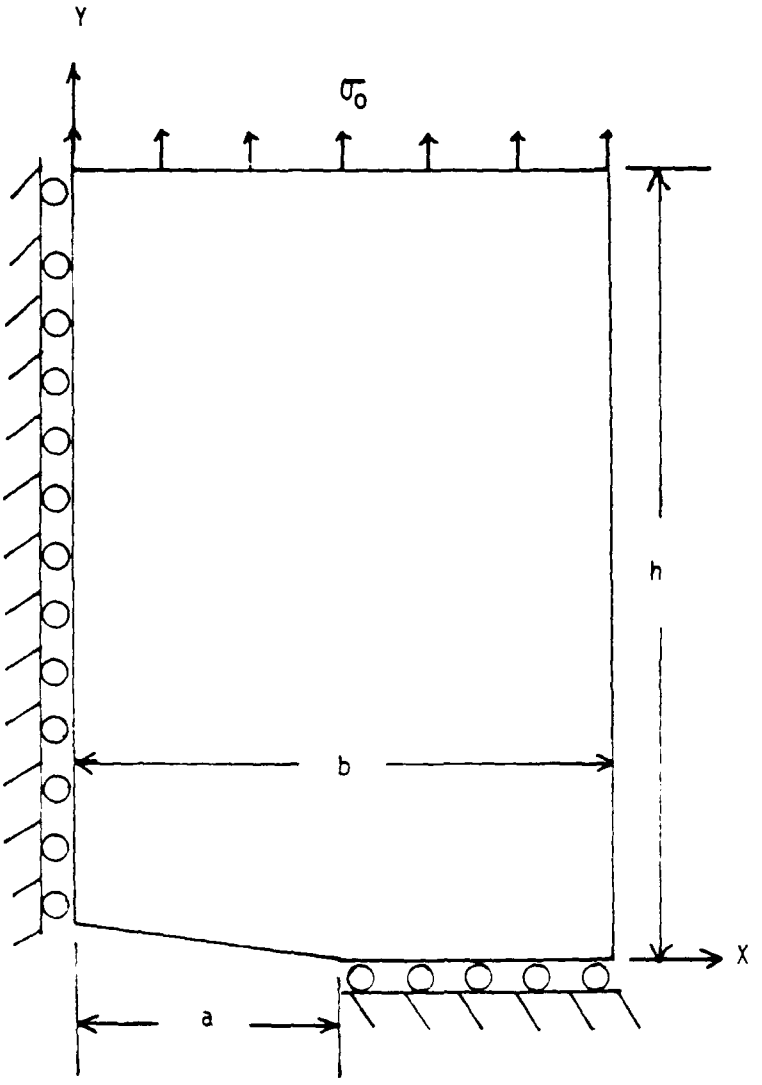

Figure 6a. Boundary conditions for the centrally cracked plate.

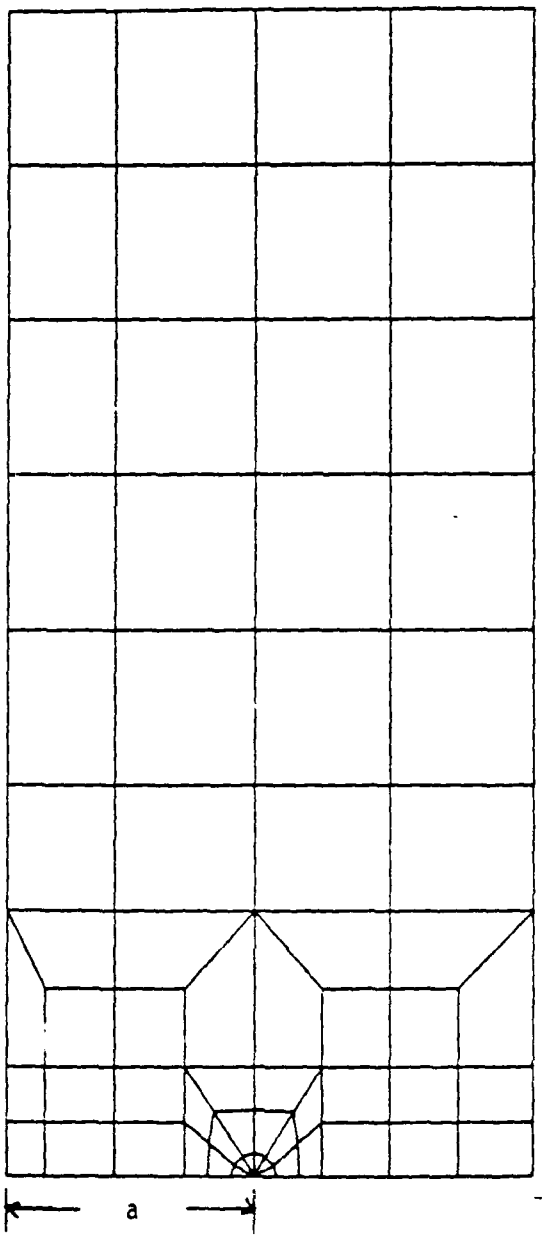

Figure 7. Finite element mesh for the center cracked test specimen.

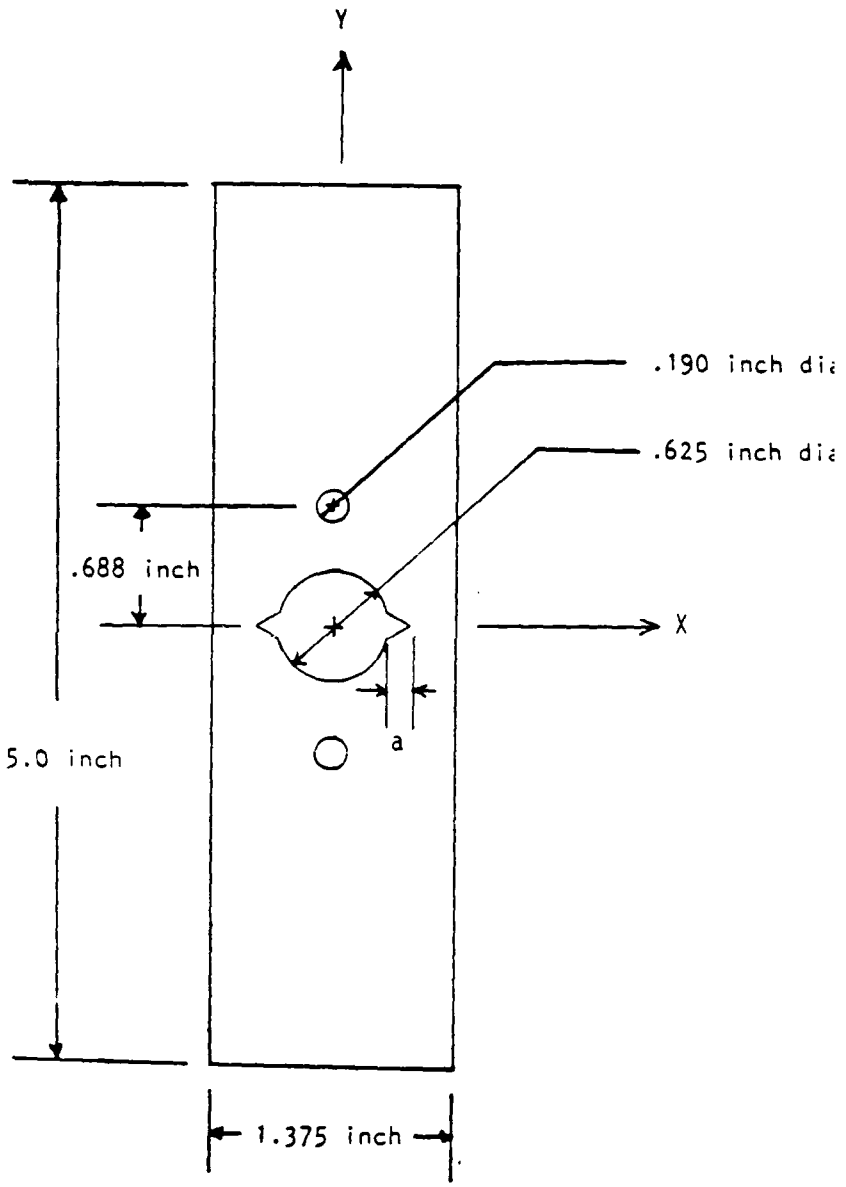

Figure 8. Fatigue test specimen geometry.

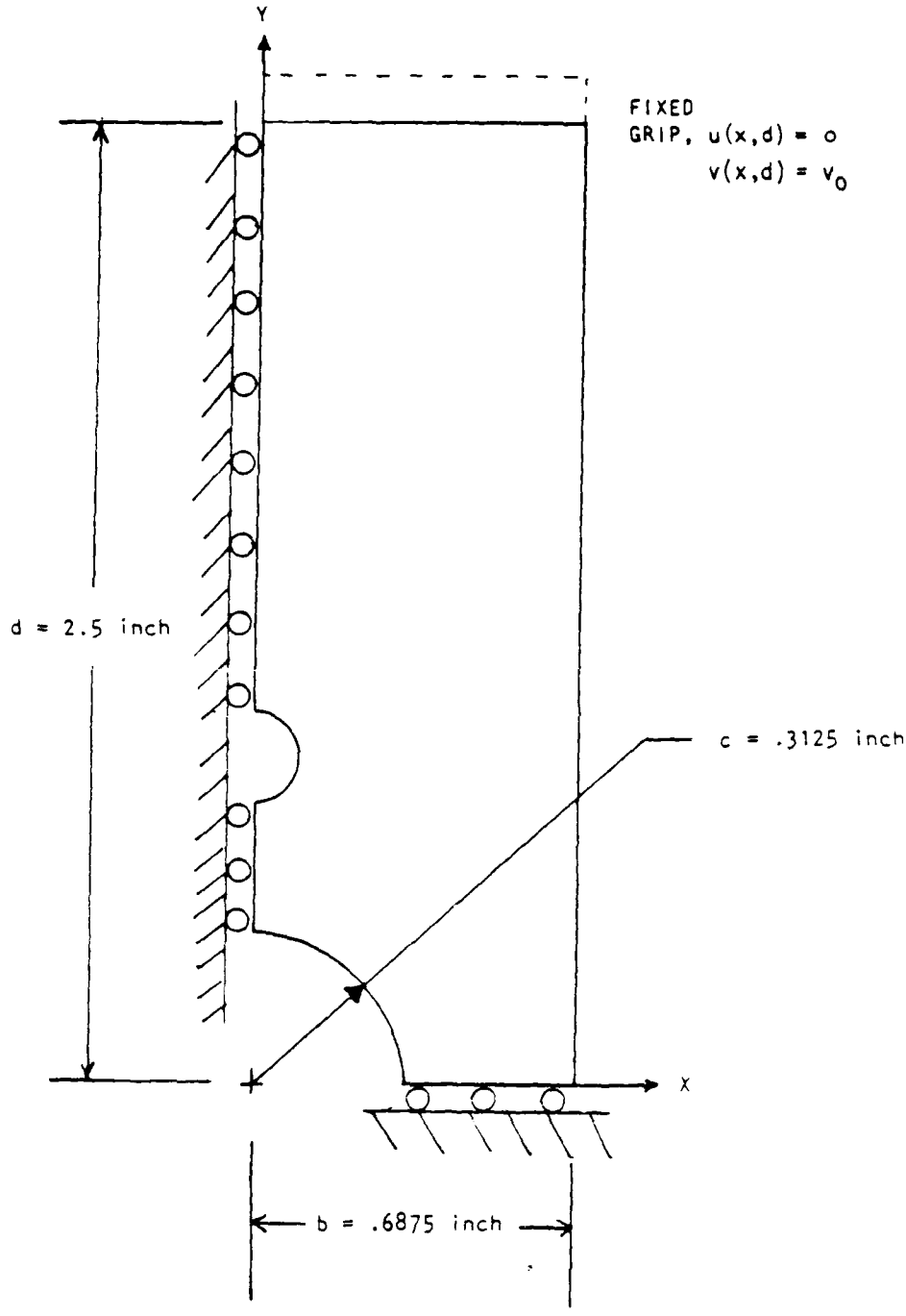

Figure 9. Applied loading and boundary conditions for the fatigue test specimen.

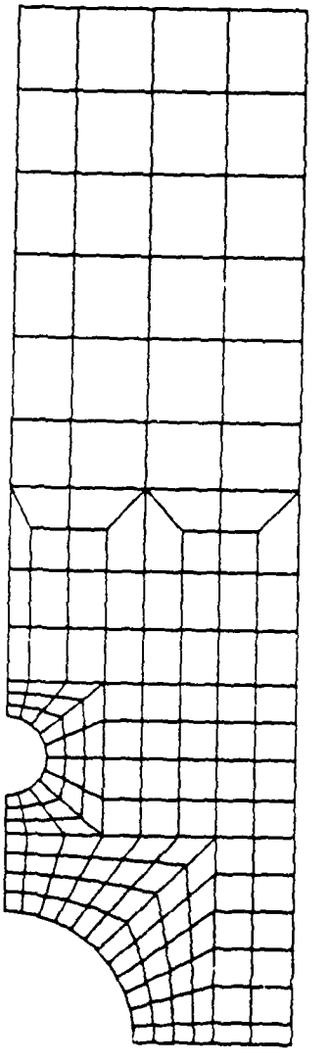

Figure 10. Finite element mesh of fatigue specimen without a crack.

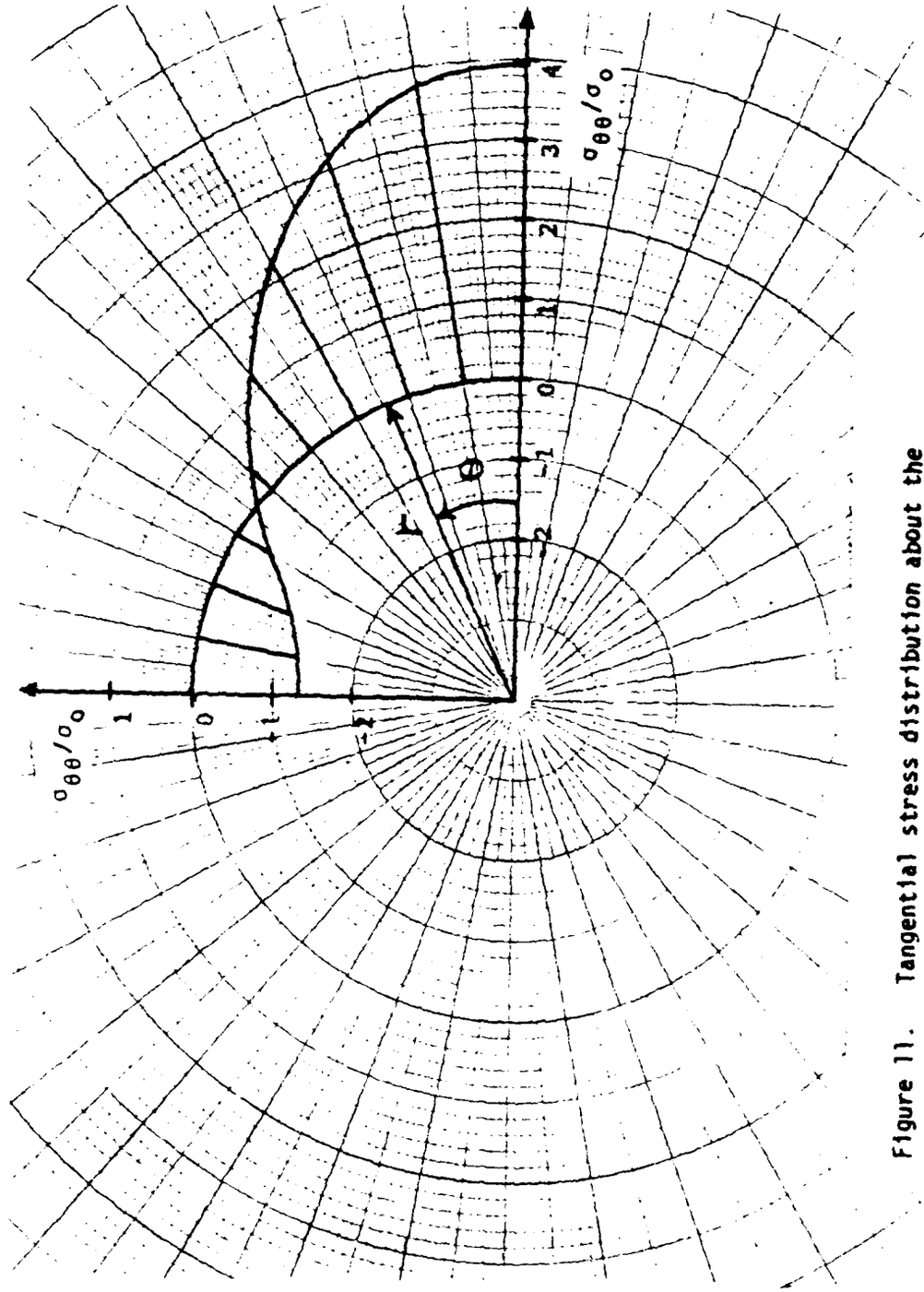

Figure 11. Tangential stress distribution about the boundary of the large central hole

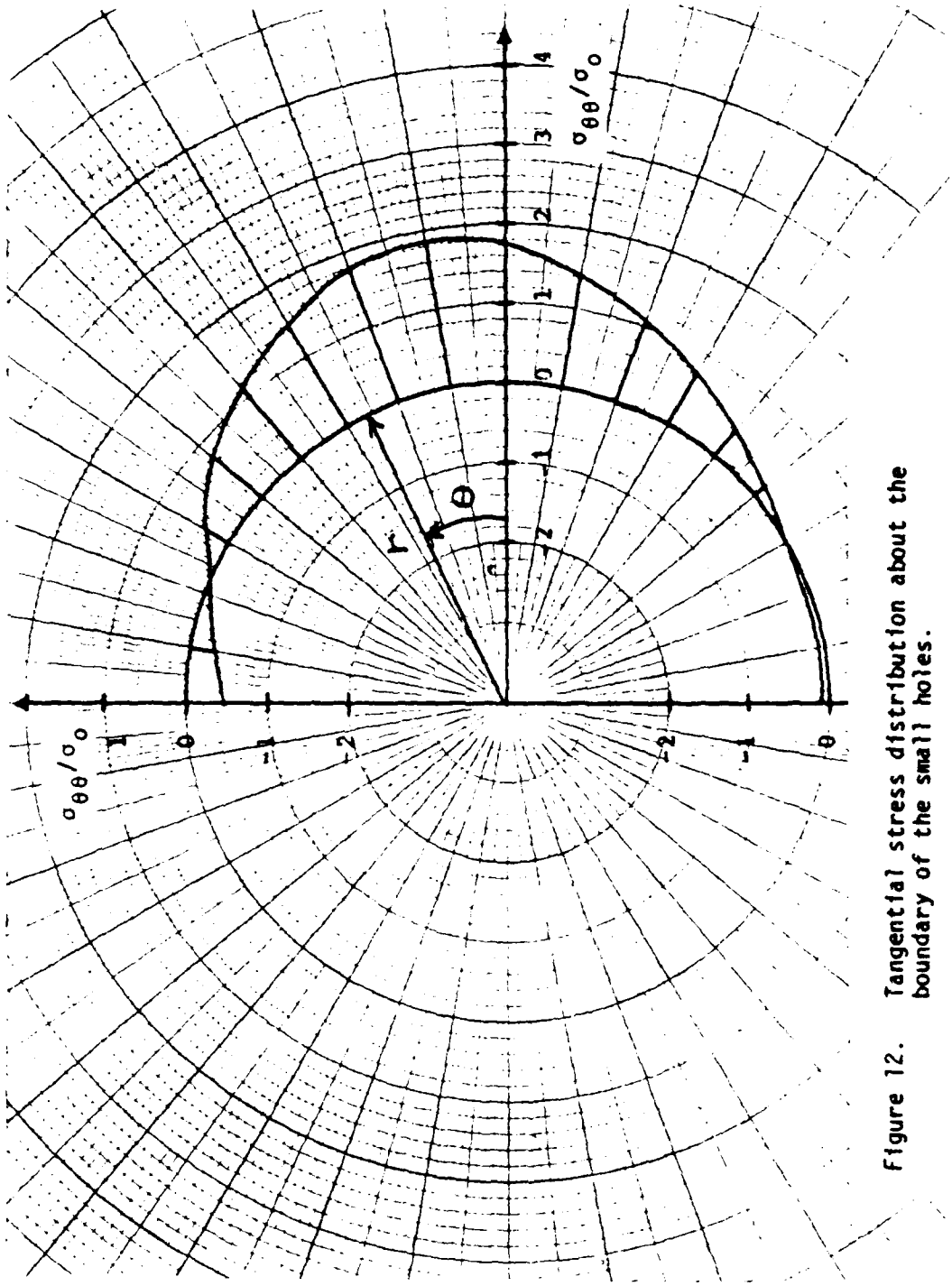

Figure 12. Tangential stress distribution about the boundary of the small holes.

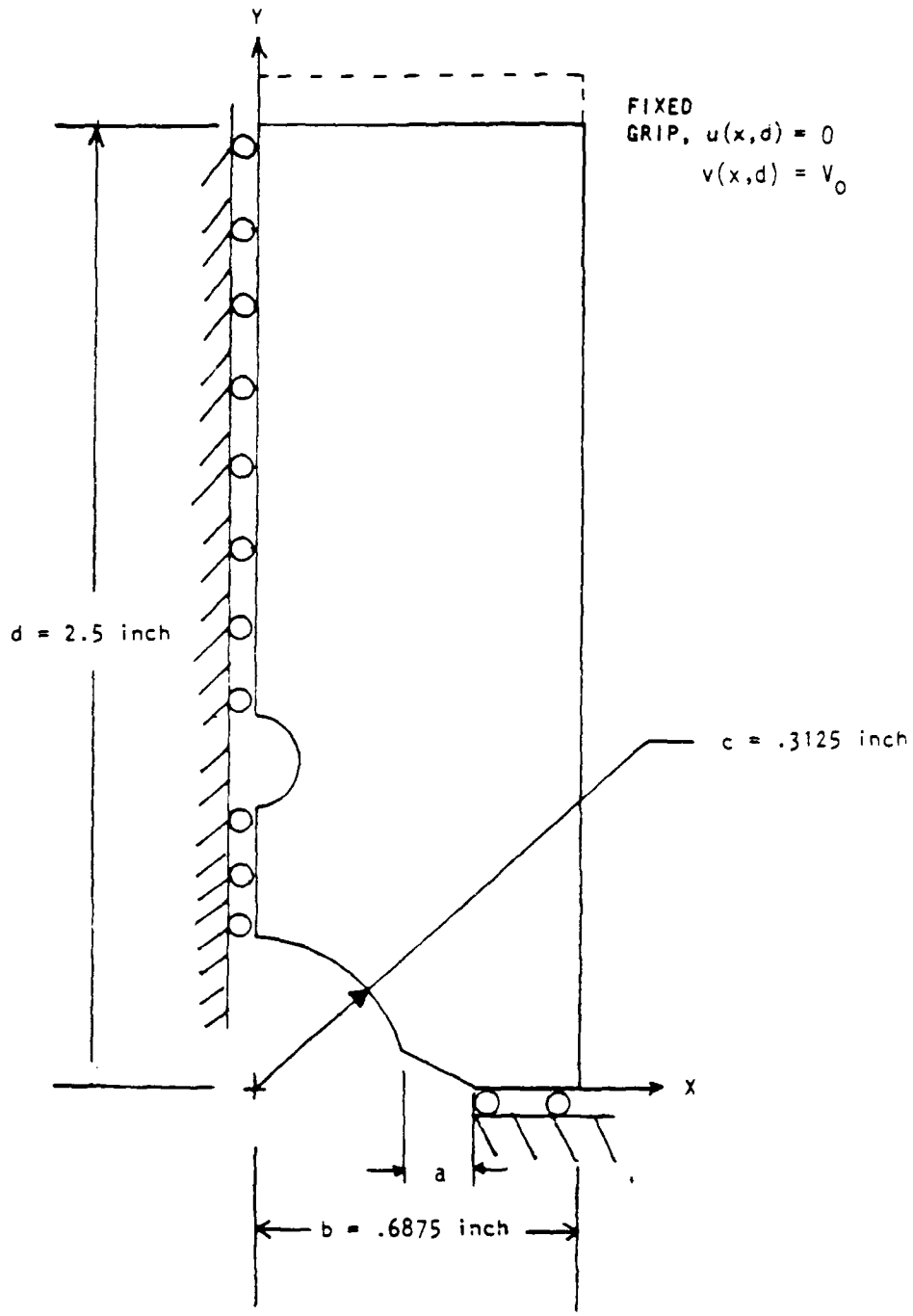

Figure 13. Boundary conditions for the cracked fatigue test specimen.

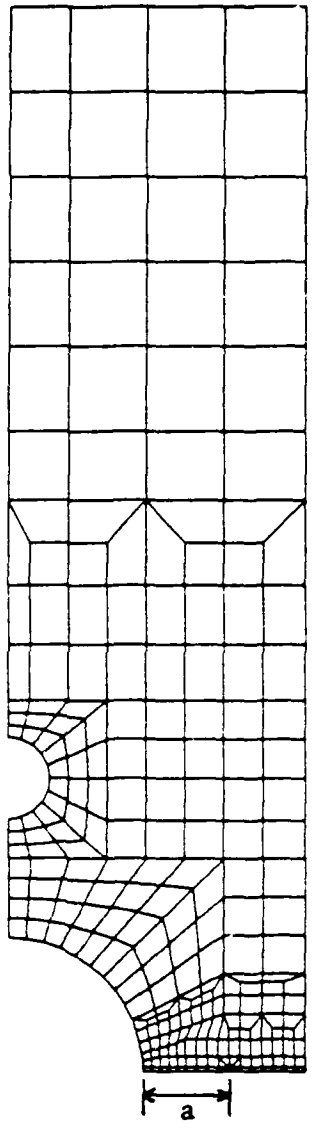

Figure 14a. Finite element mesh of the fatigue specimen with a crack.

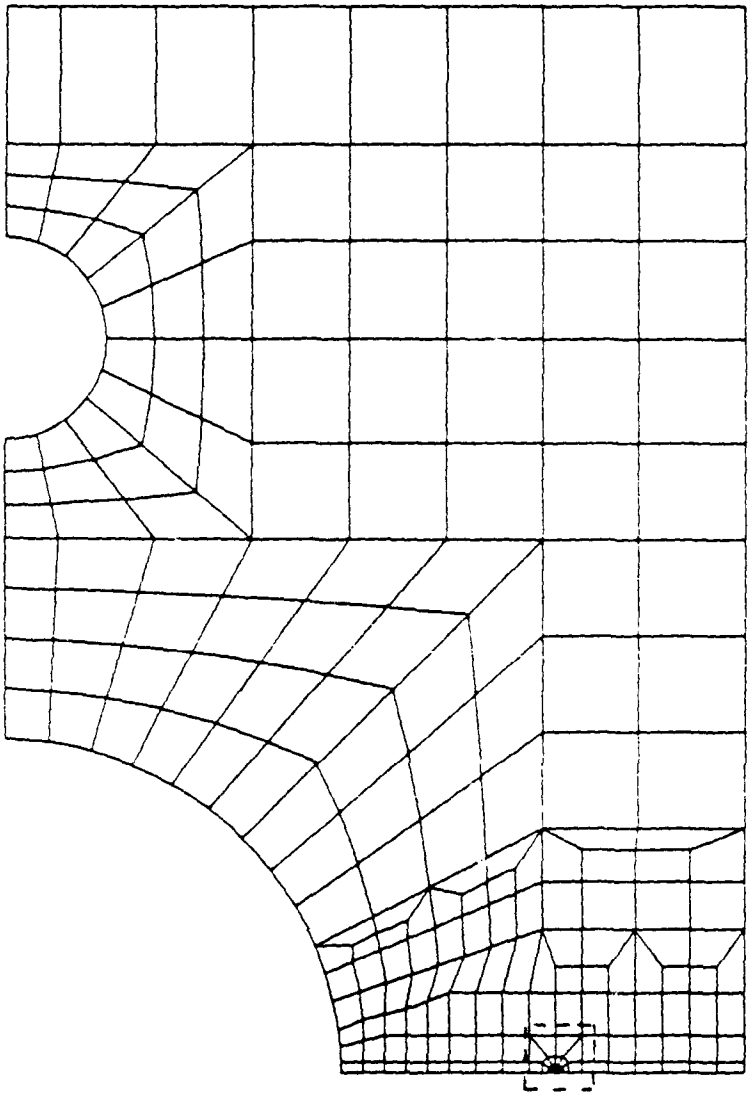

Figure 14b. Enlarged view of lower mesh region.

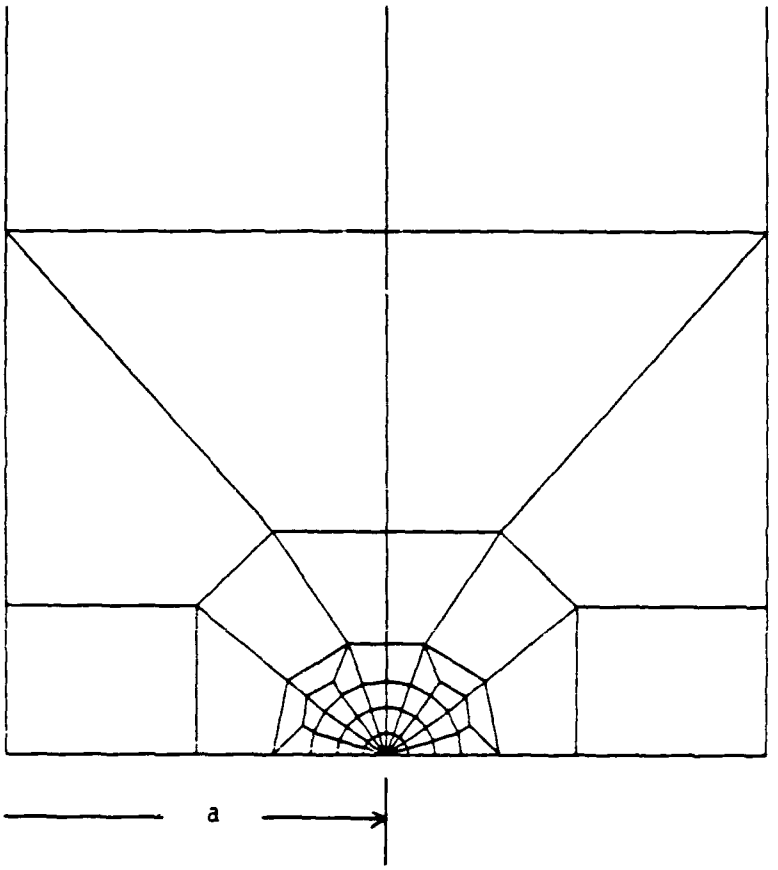

Figure 14c. Enlarged view of crack tip region (Region A).

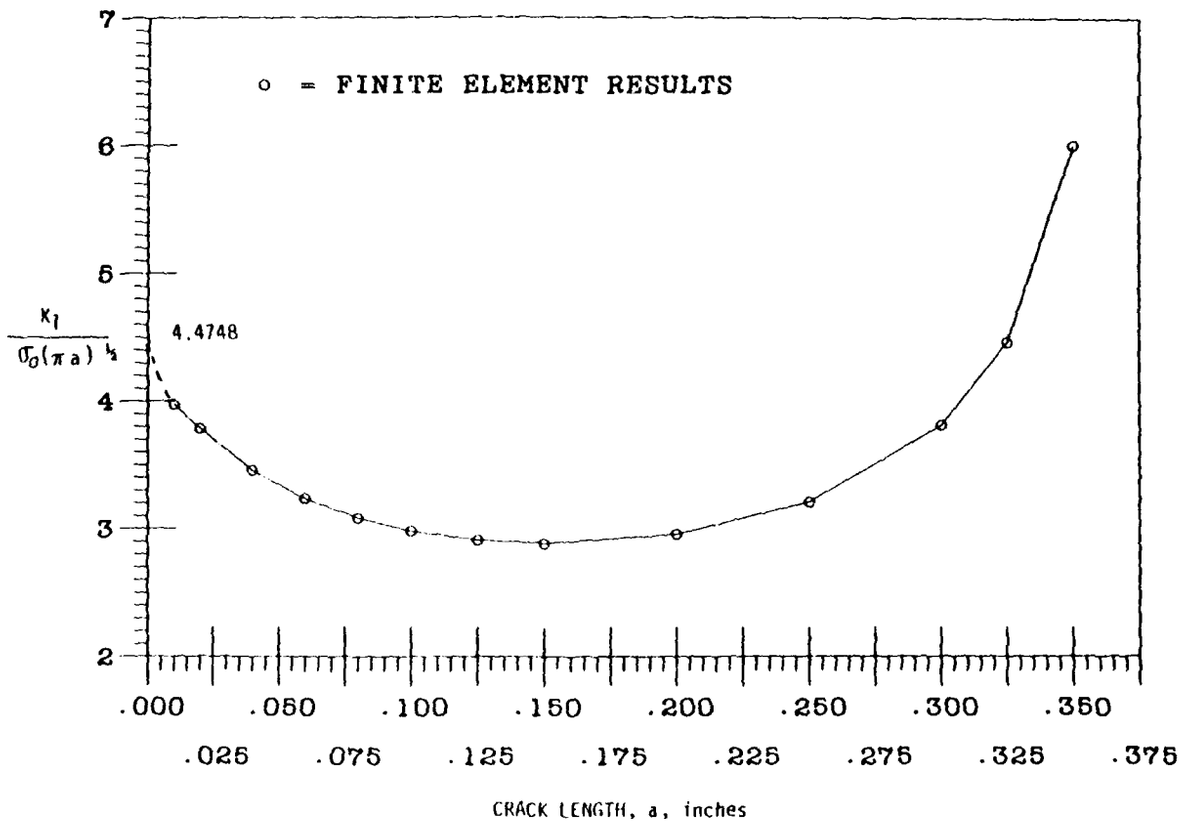

Figure 15. Normalized stress intensity factor vs. crack length for fatigue test specimen.

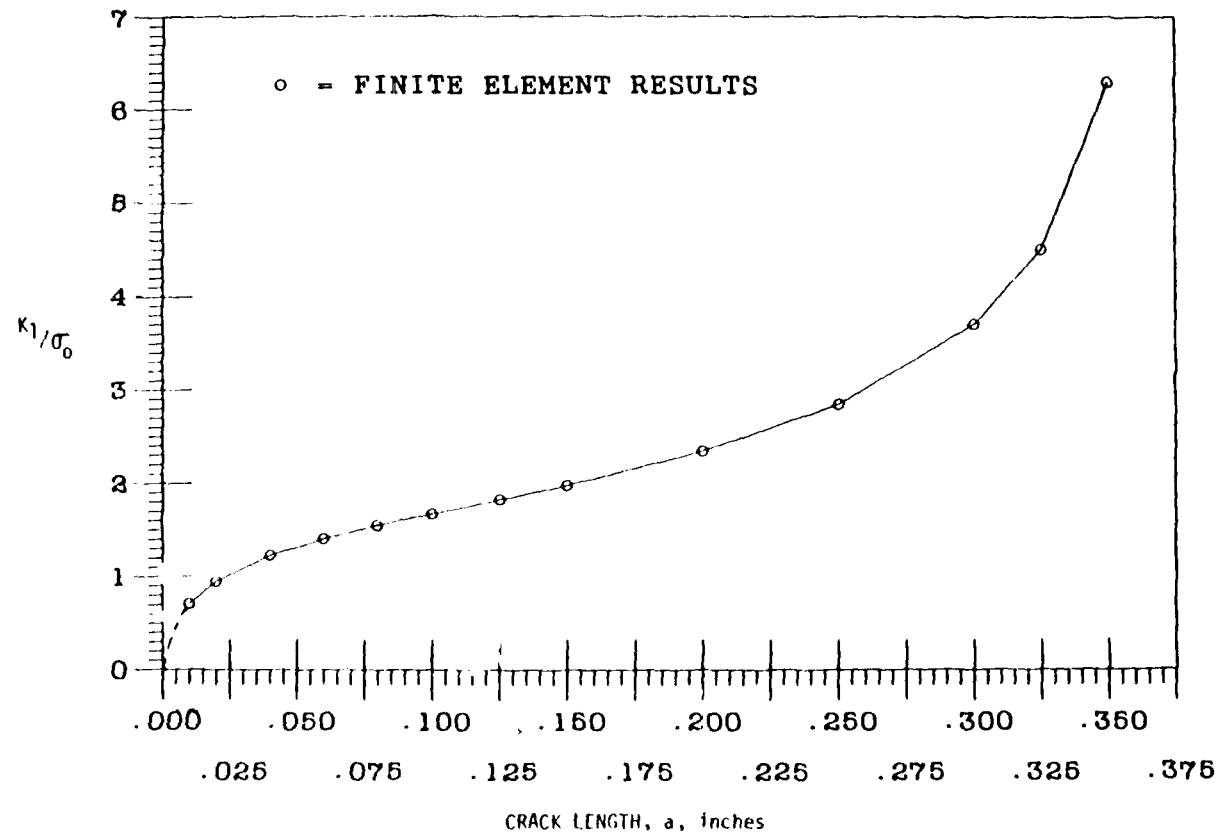

Figure 16. Stress intensity factor normalized with respect to σ_0 vs. crack length for fatigue test specimen.

AD-A198 895 FRACTURE MECHANICS ANALYSIS OF SOME FATIGUE AND FRACTURE TEST SPECIMENS U..(U) NAVAL AIR DEVELOPMENT CENTER WARMINSTER PA AIR VEHICLE AND CR.. G DELSERRO 2/2

UNCLASSIFIED 24 AUG 87 NADC-87145-60 F/G 11/6 NL

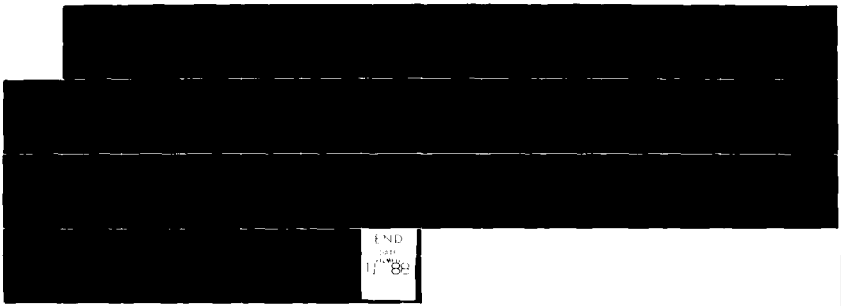

END
DATE
FILMED
11-88

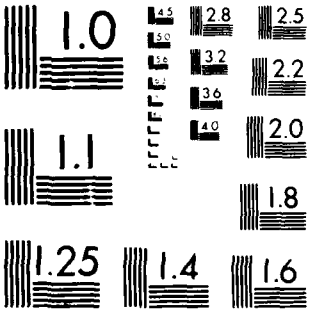

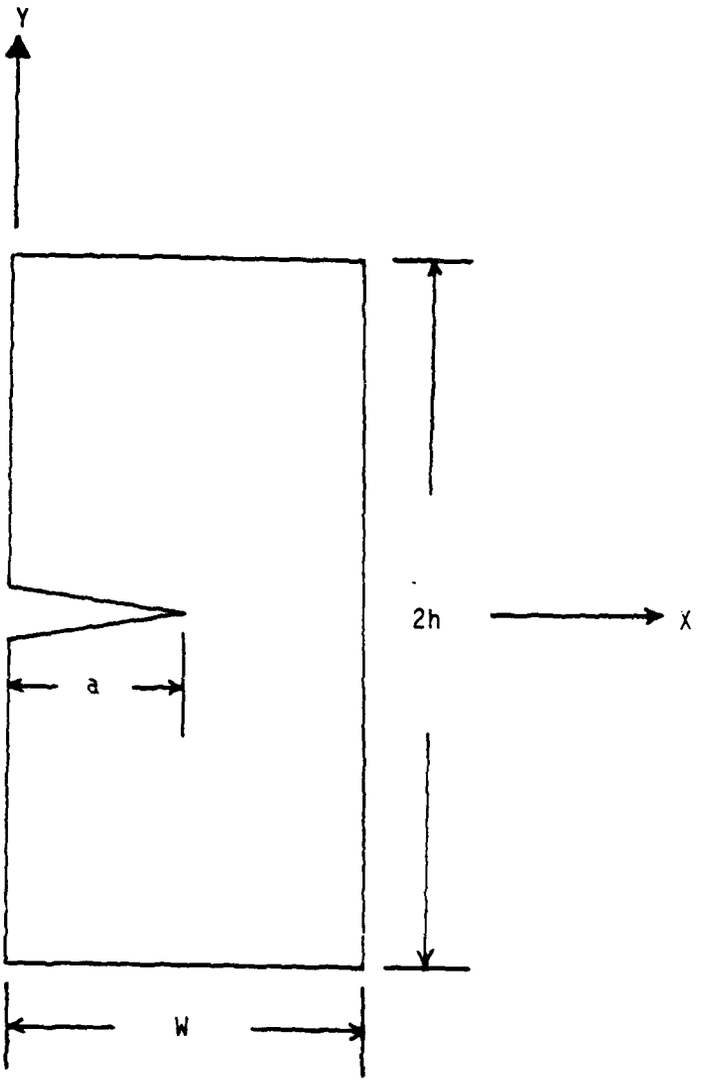

Figure 17. Single edge cracked test specimen, a/w = .5.

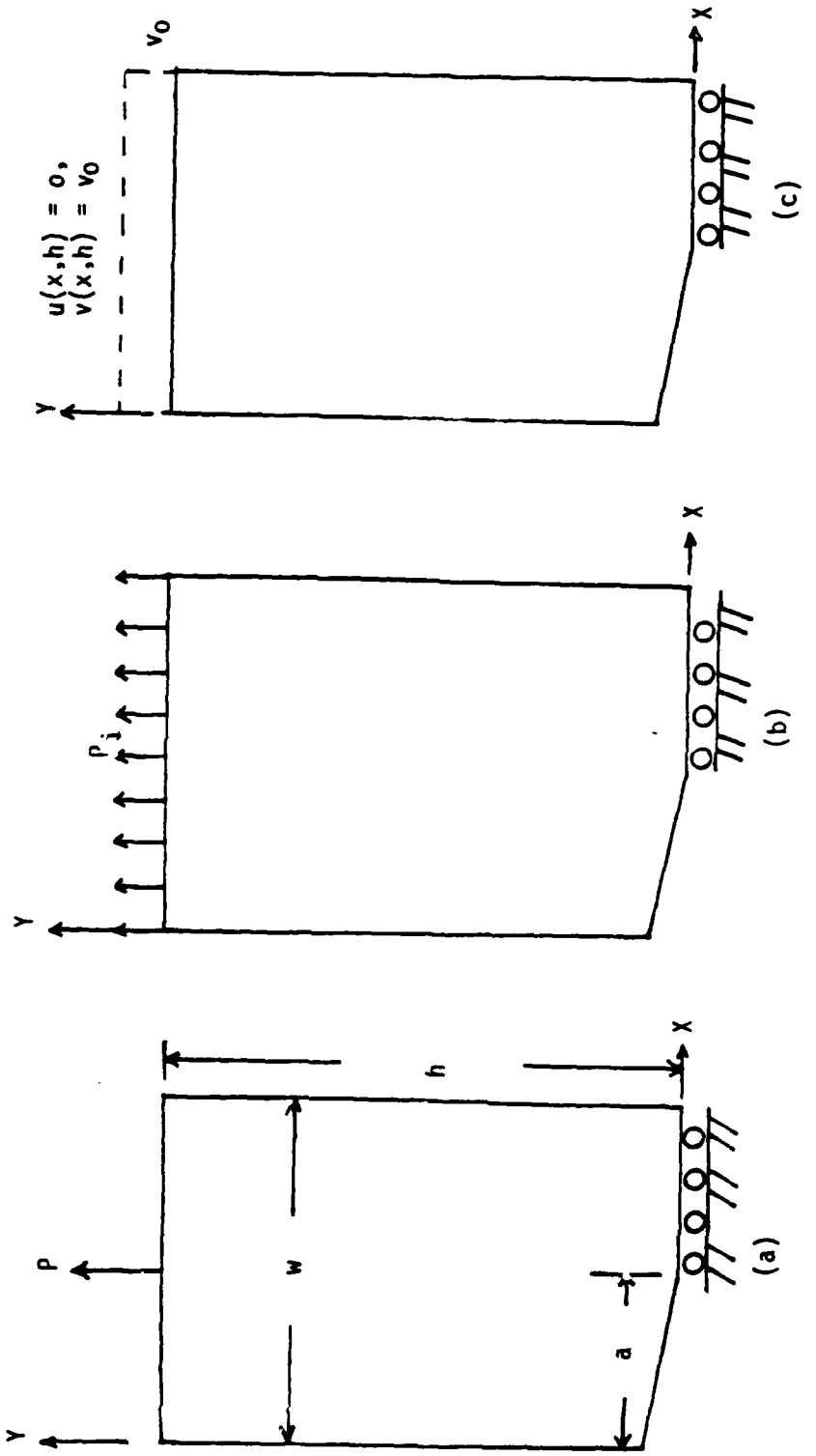

Figure 18. Boundary conditions for the single edge cracked specimen under: (a) a point load, (b) a uniformly distributed load, and (c) a displacement controlled, fixed grip condition.

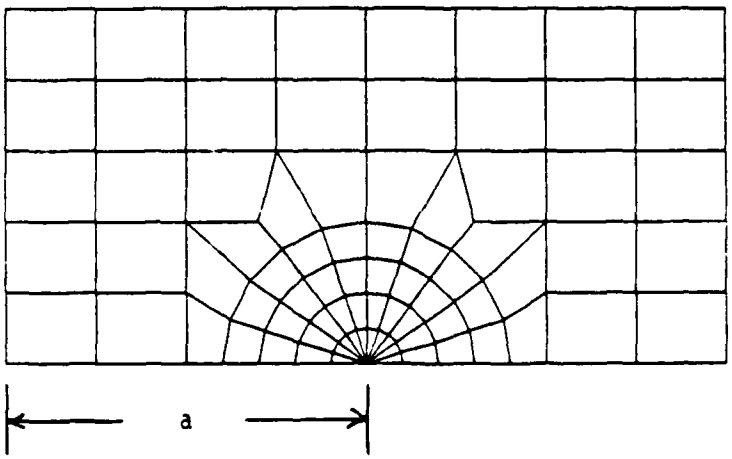

Figure 19a. Finite element mesh for the single edge cracked specimen, h/w = .5.

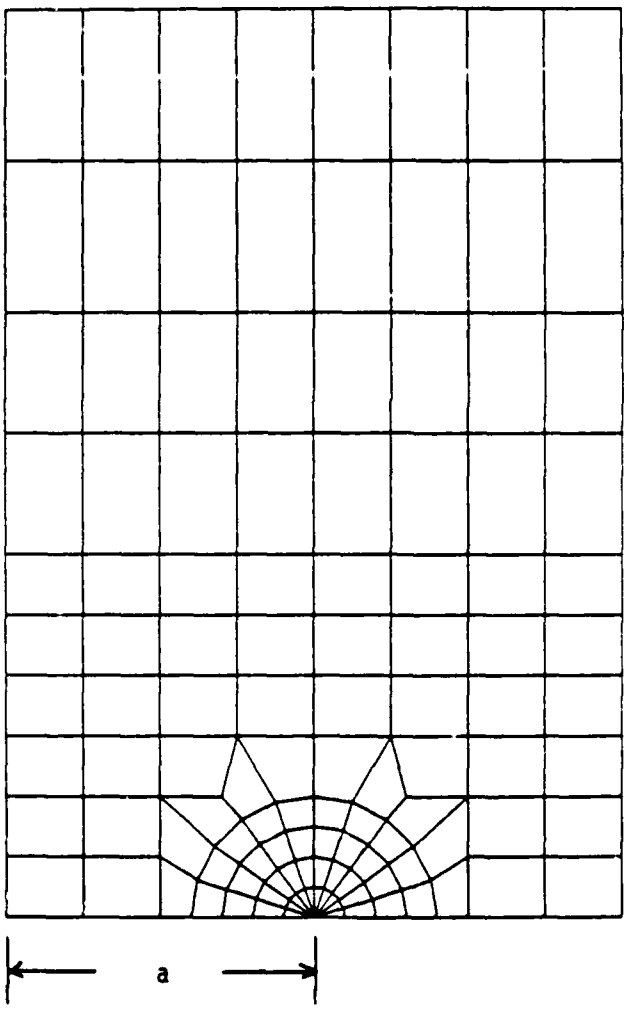

Figure 19b. Finite element mesh for the single edge cracked specimen, h/w = 1.5.

Figure 19c. Finite element mesh for the single edge cracked specimen, h/w = 20.

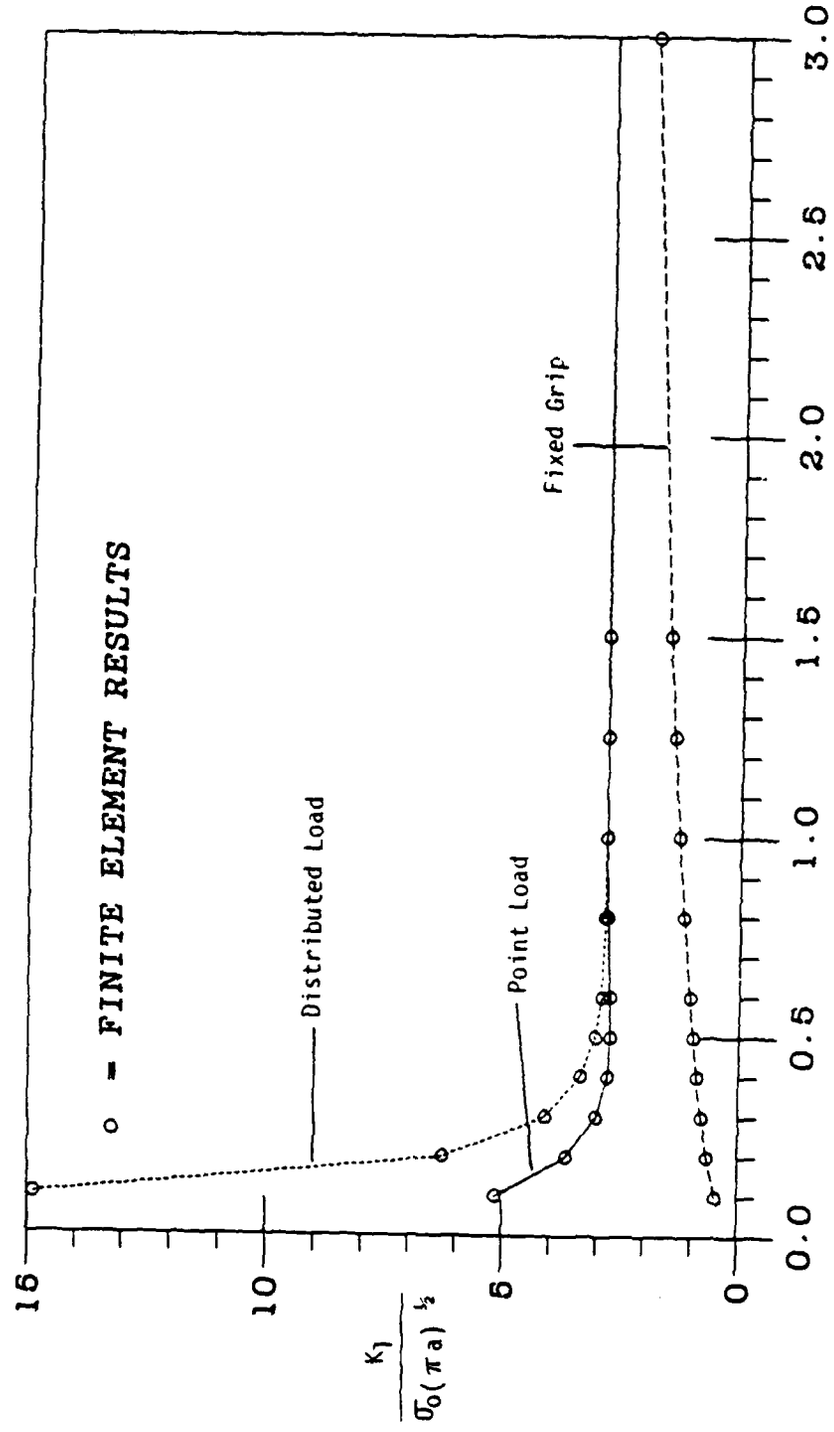

Figure 20a. Normalized stress intensity factor vs. half-length to width ratio (h/w) for the single edge cracked specimen under different applied loading conditions.

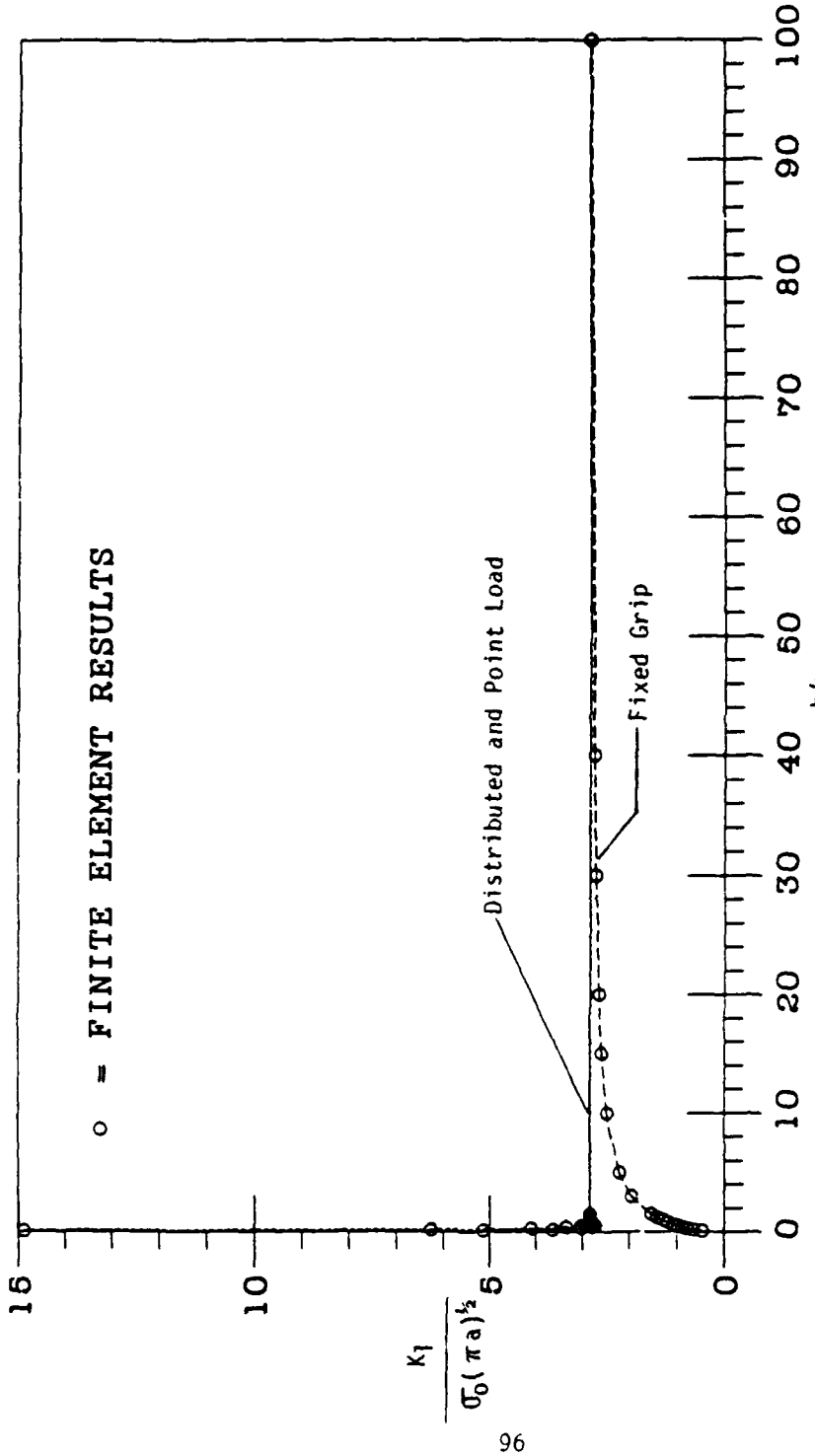

Figure 20b. Normalized stress intensity factor vs. half-length to width ratio (h/w) for the single edge cracked specimen under different applied loading conditions.

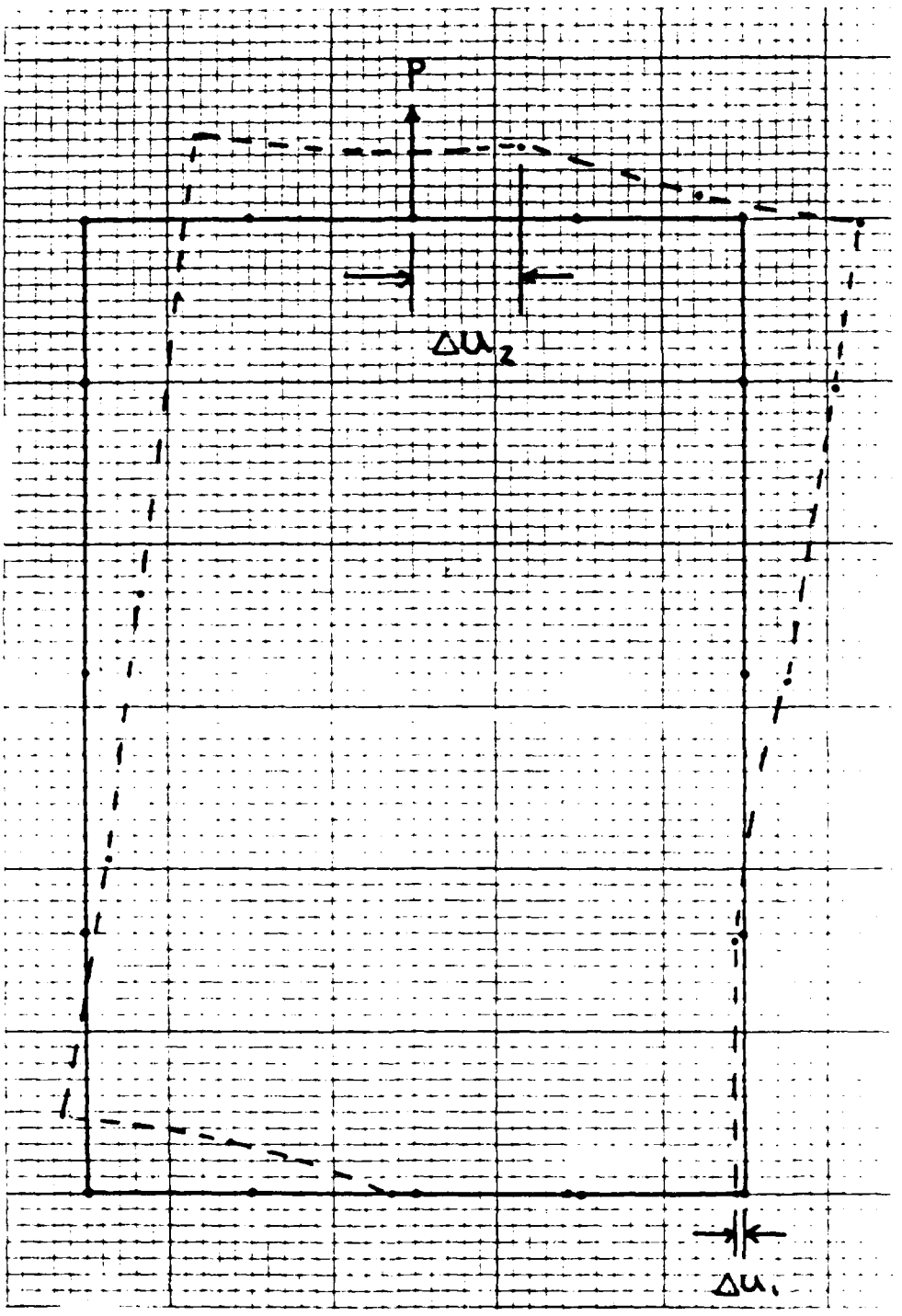

Figure 21a. Deformed plot of the point loaded single edge cracked specimen, h/w = 1.5.

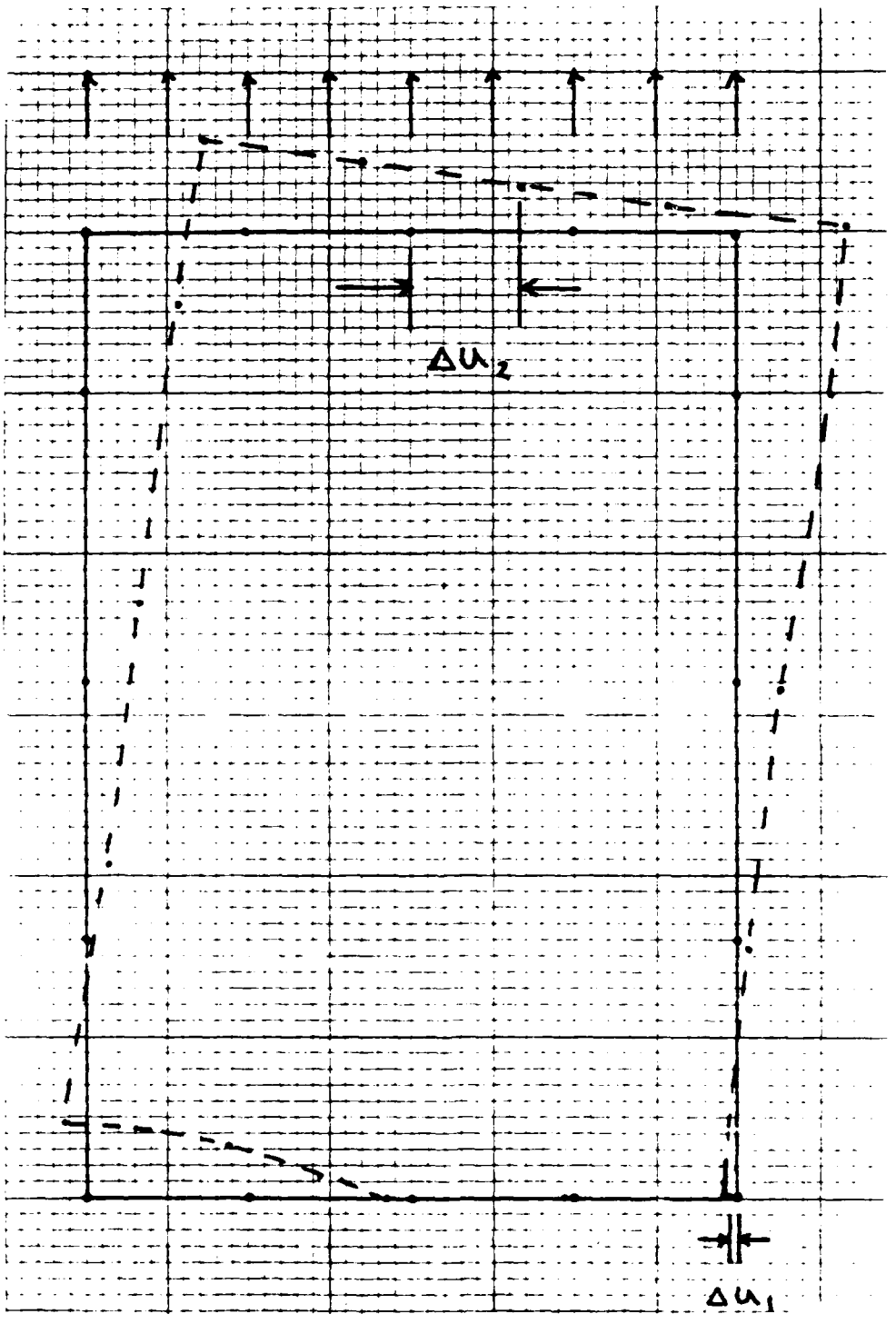

Figure 21b. Deformed plot of the uniformly distributed loaded single edge cracked specimen, h/w = 1.5.

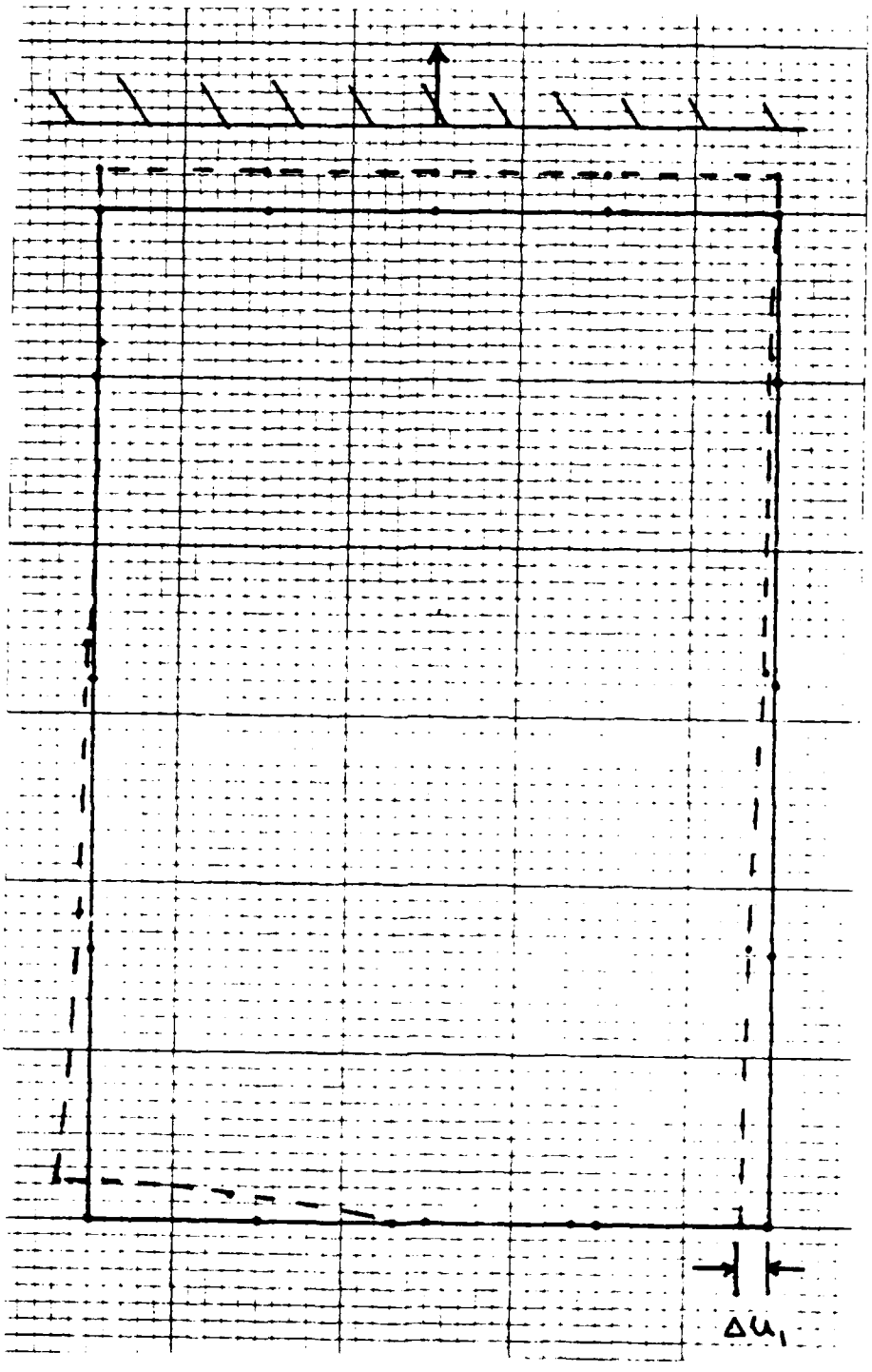

Figure 21c. Deformed plot of the single edge cracked specimen under displacement controlled – fixed grip conditions.

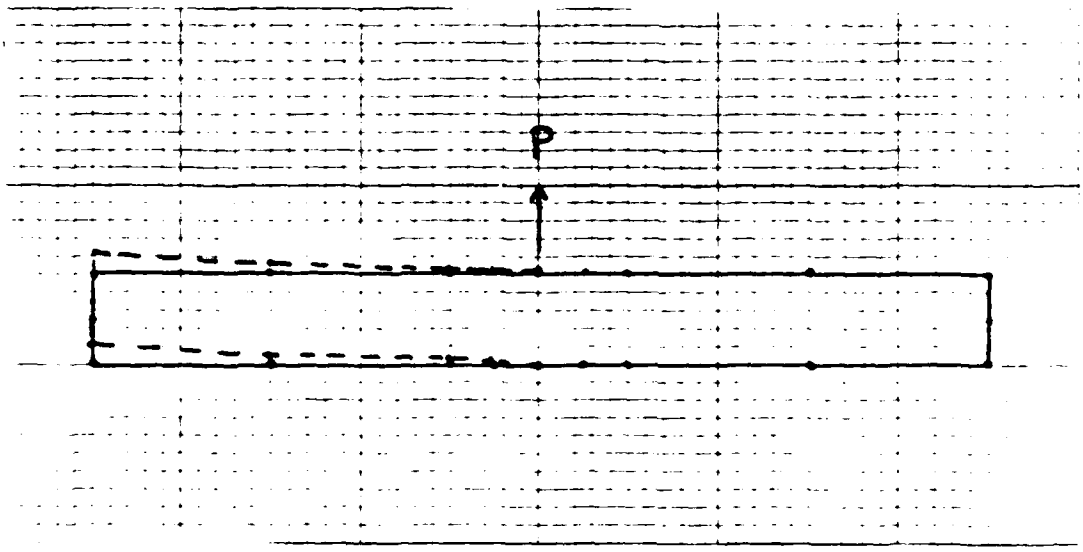

Figure 21d. Deformed plot of the point loaded single edge cracked specimen, h/w = .1.

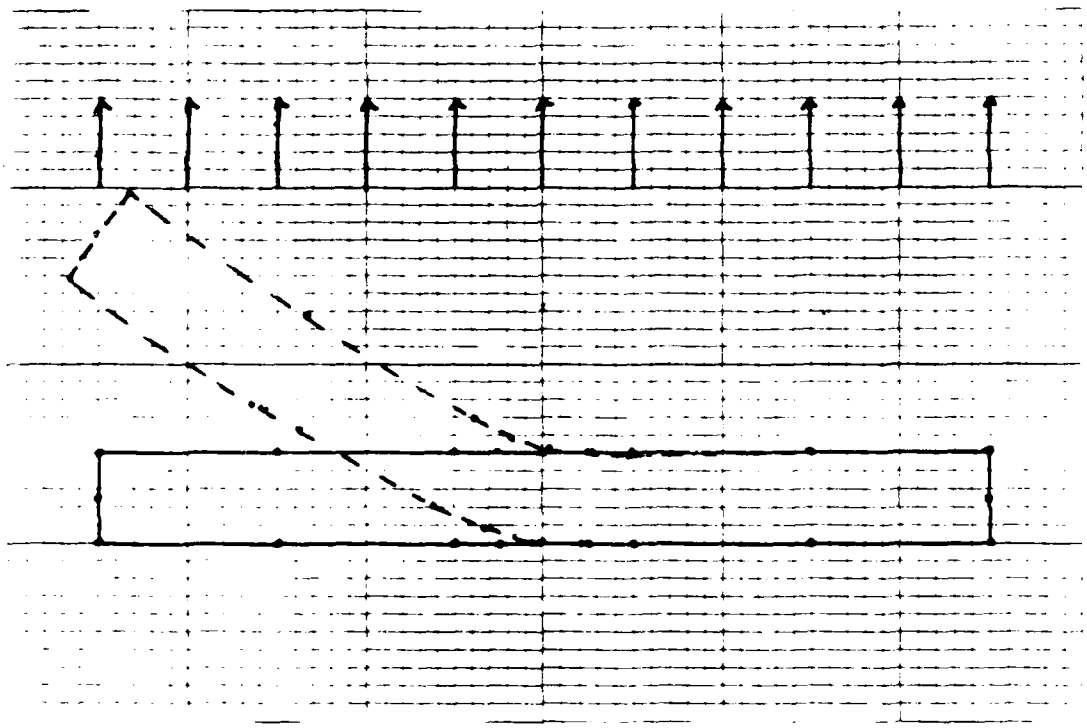

Figure 21e. Deformed plot of the uniformly distributed loaded single edge cracked specimen, h/w = .1.

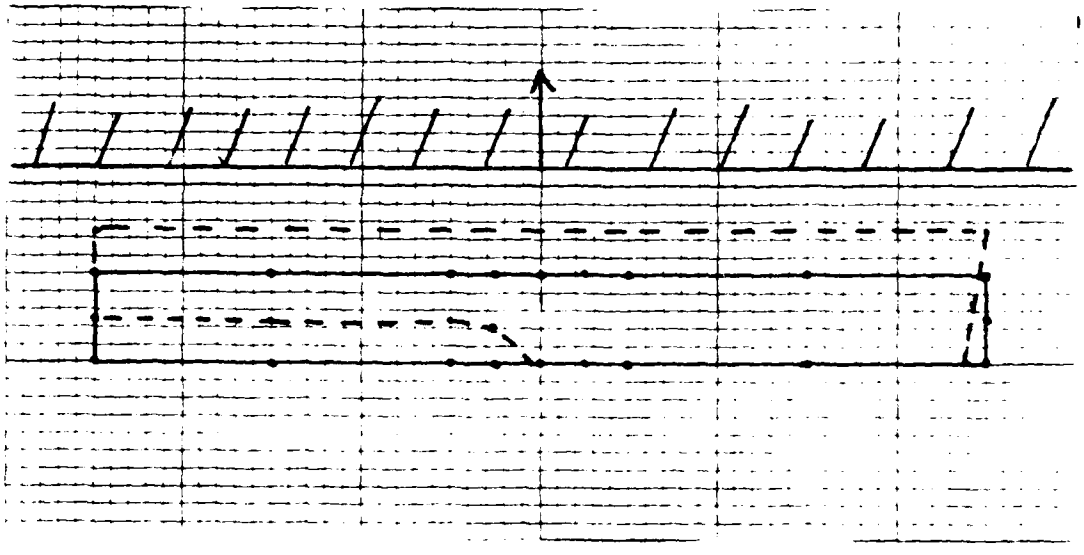

Figure 21f. Deformed plot of the single edge cracked specimen under displacement controlled - fixed grip conditions.

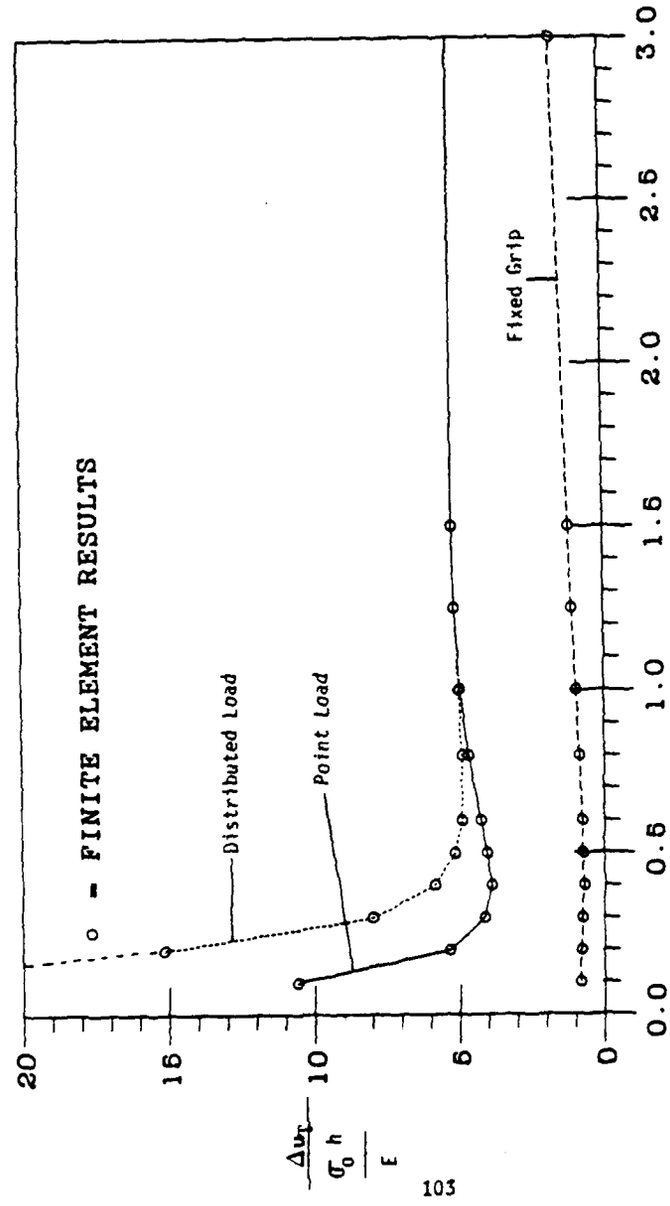

Figure 22a. Normalized transverse relative displacement ($\frac{\Delta u_T}{\sigma_0 h/E}$) vs half-length to width ration (h/w) for the single edge cracked specimen under various applied loading conditions.

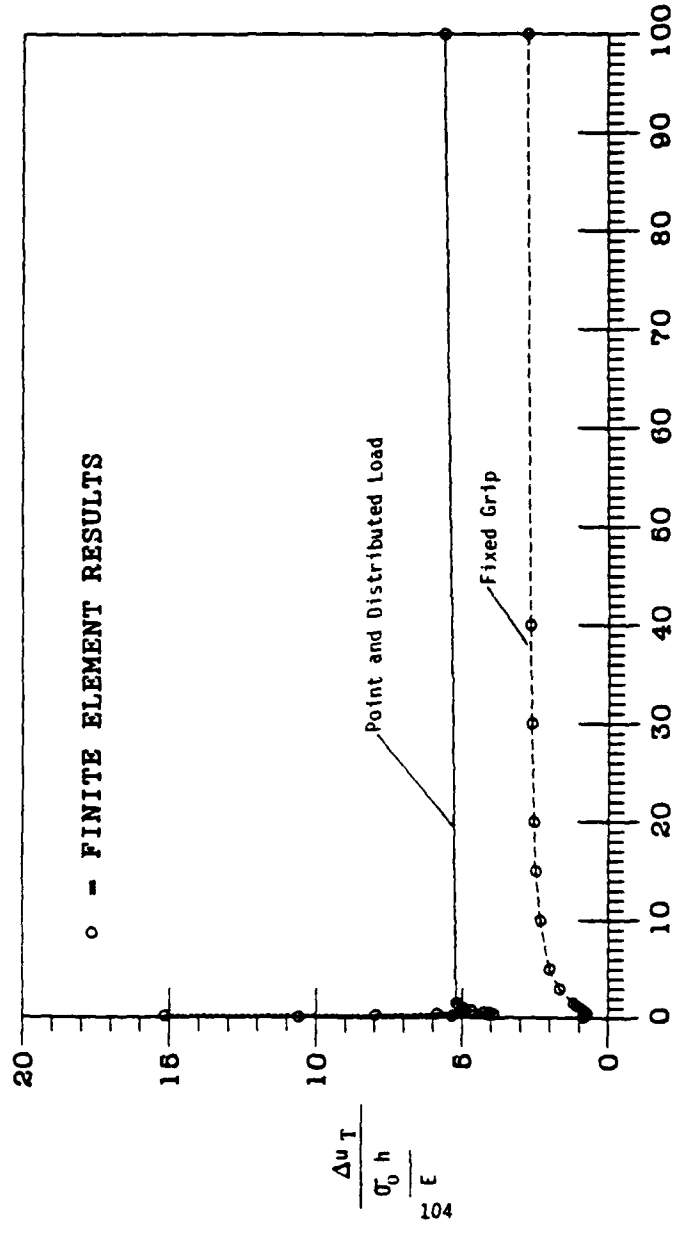

Figure 22b. Normalized transverse relative displacement ($\frac{\Delta u_T}{\sigma_0 \frac{h}{E}}$) vs half-length to width ration (h/w) for the single edge cracked specimen under various applied loading conditions.

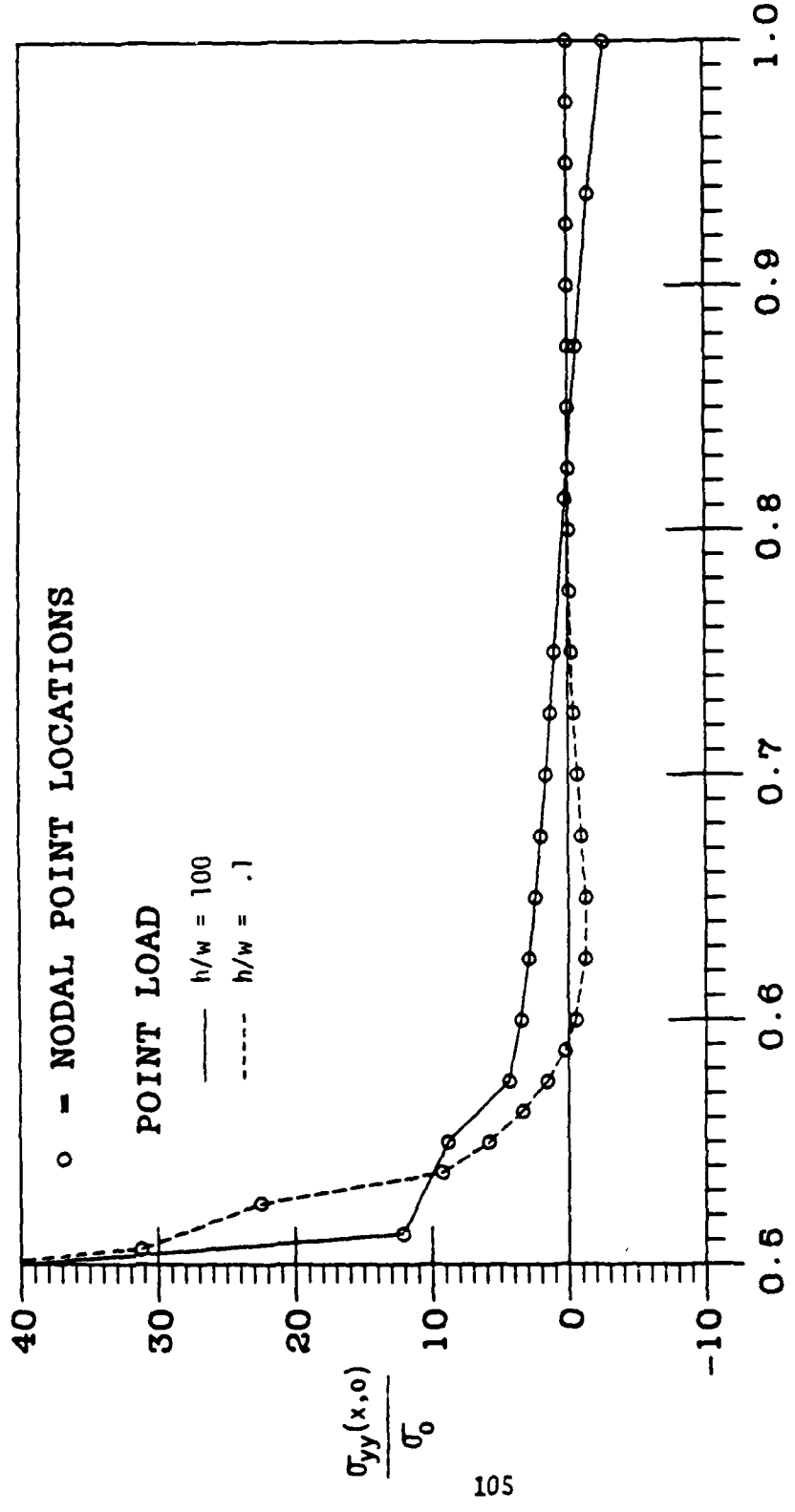

Figure 23a. Normal stress in front of the crack tip, $\sigma_{yy}(x,o)$, for the single edge cracked specimen under a point load.

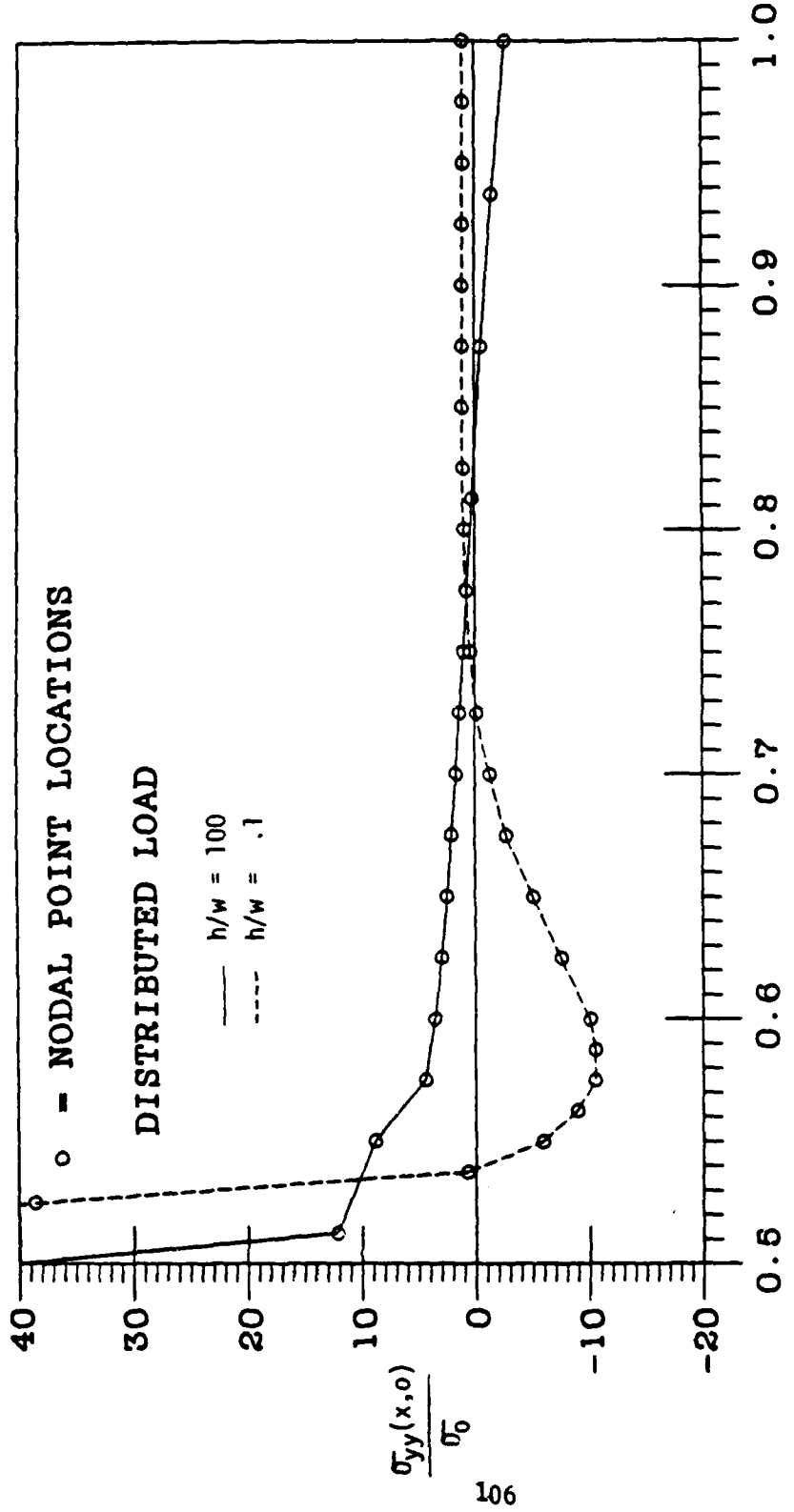

Figure 23b. Normal stress in front of the crack tip, $\sigma_{yy}(x,o)$, for the single edge cracked specimen under a uniformly distributed load.

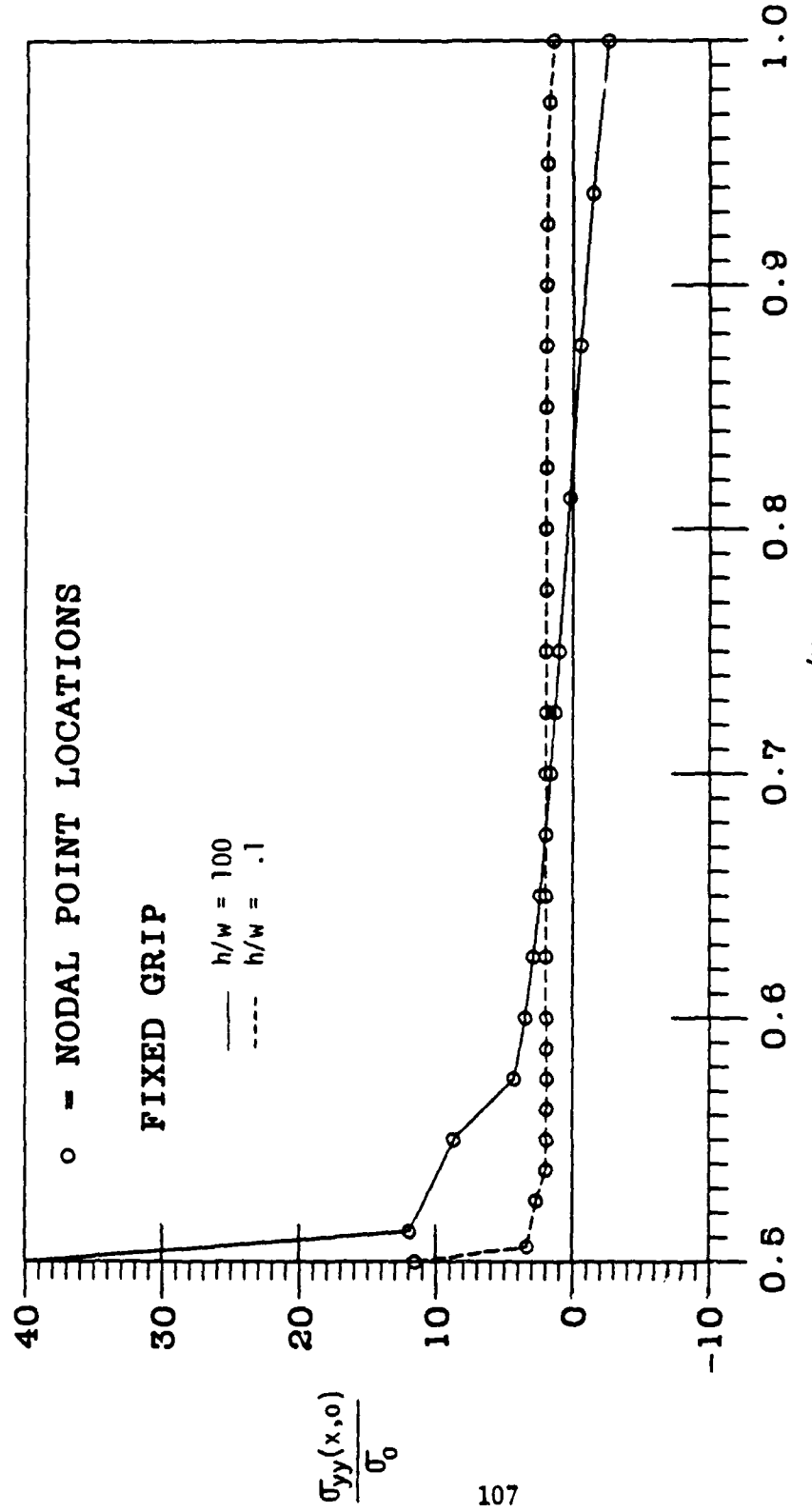

Figure 23c. Normal stress in front of the crack tip, $\sigma_{yy}(x,o)$, for the single edge cracked specimen under fixed grip - displacement controlled conditions.

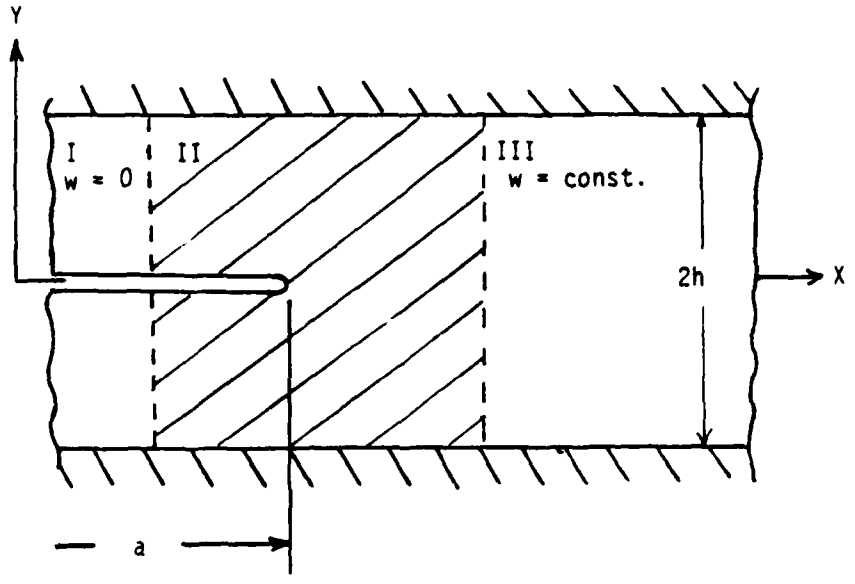

Figure 24. The tearing of an infinitely wide strip.

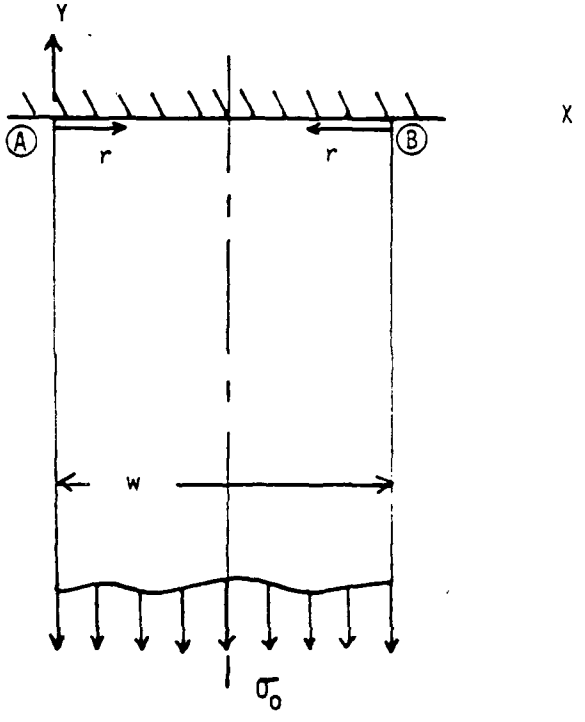

Figure 25. The semi-infinite strip with a fixed end.

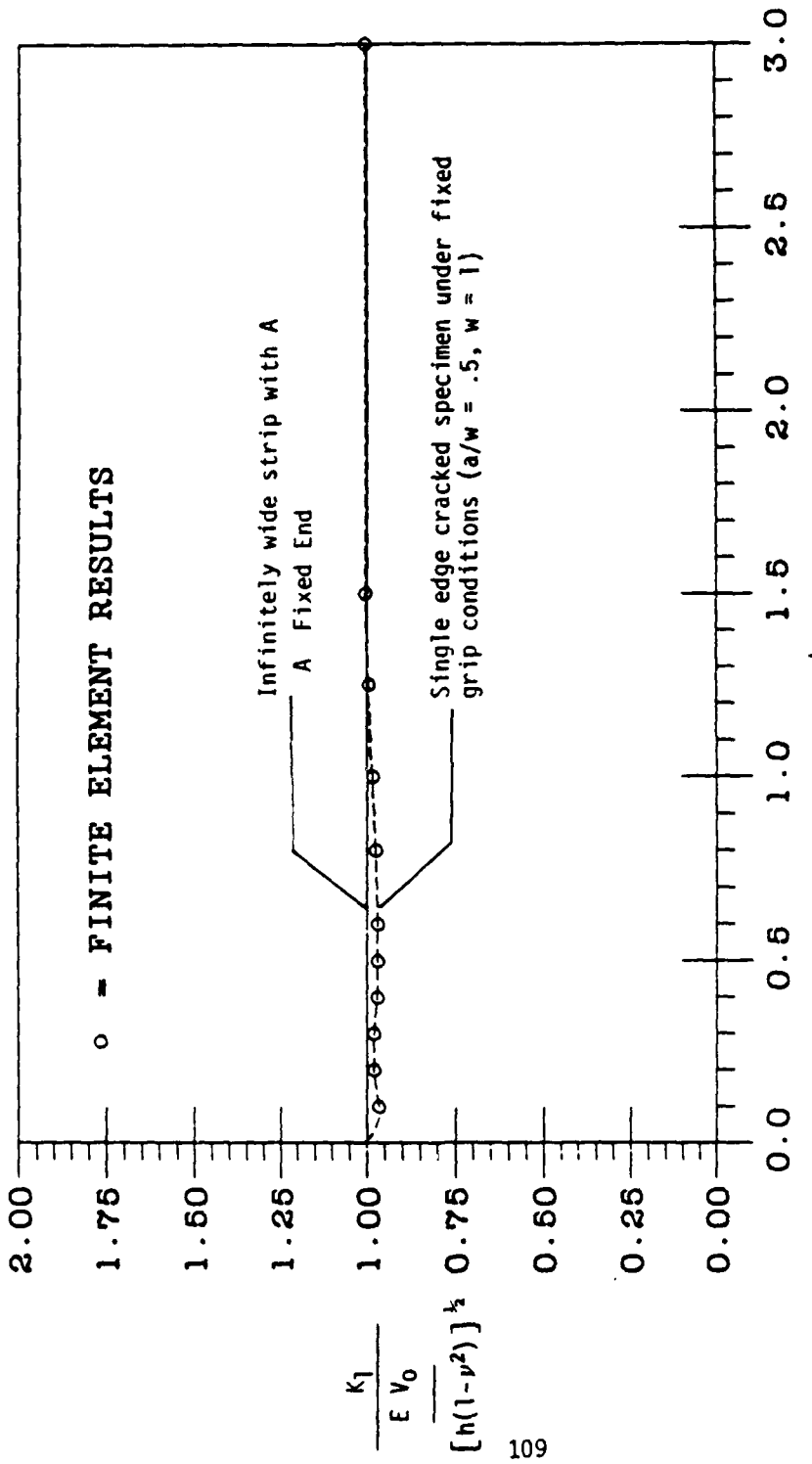

Figure 26a. A comparison between the single edge cracked specimen under fixed grip conditions and the infinitely wide strip with a fixed end.

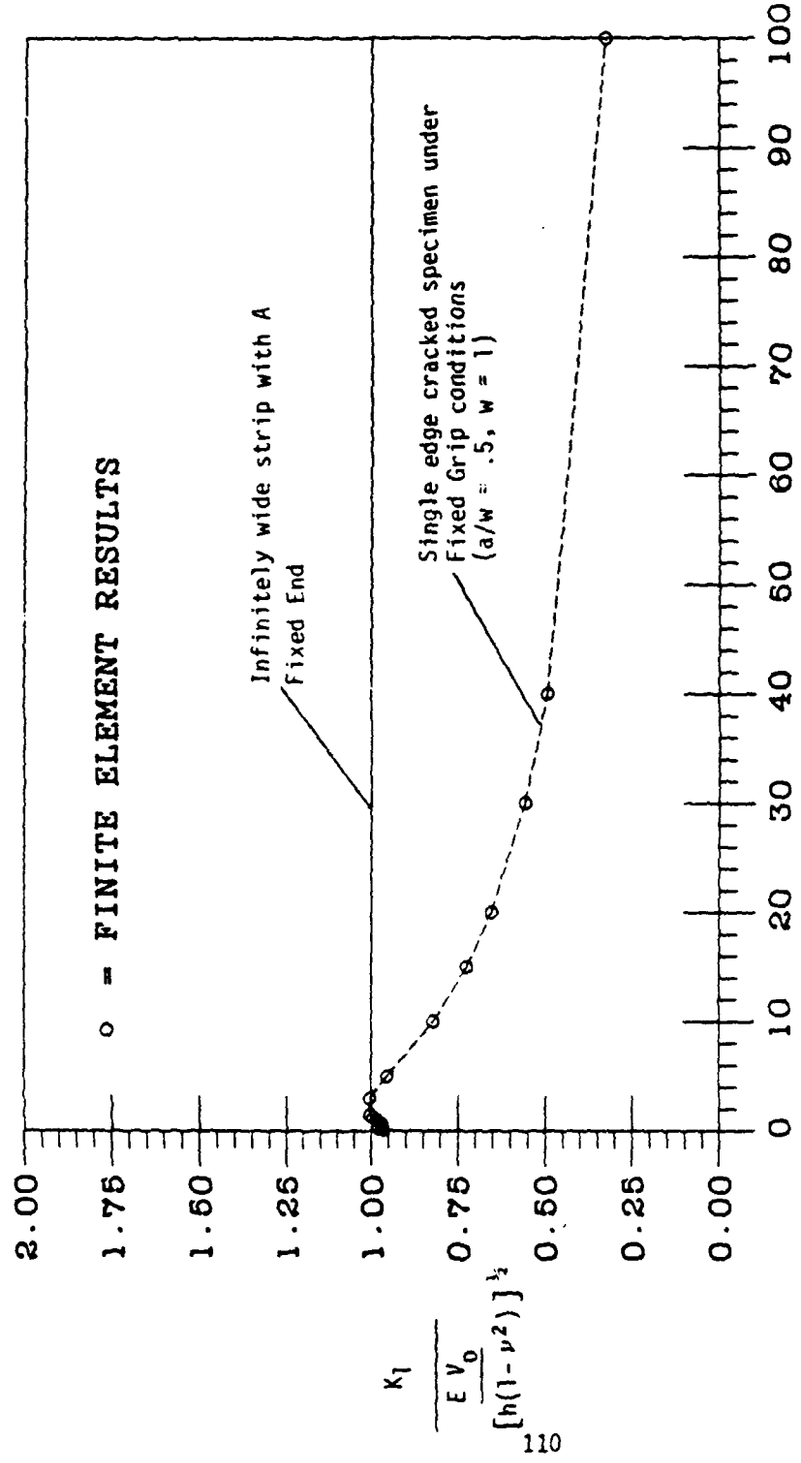

Figure 26b. A comparison between the single edge cracked specimen under fixed grip conditions and the infinitely wide strip with a fixed end.

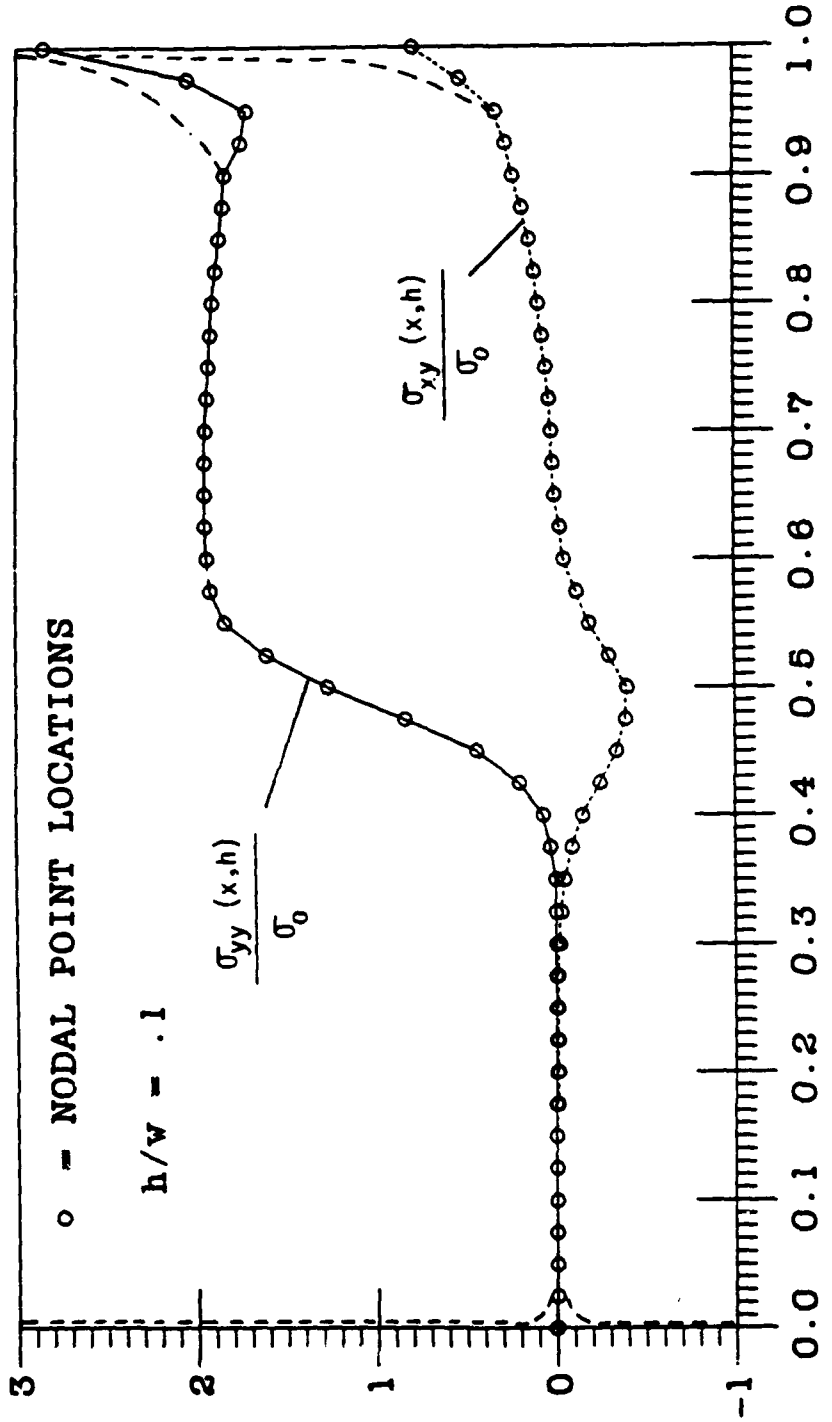

Figure 27a. Normal stress (σ_{yy}) and shear stress (σ_{xy}) along the fixed grip end of the single edge cracked specimen, h/w = .1.

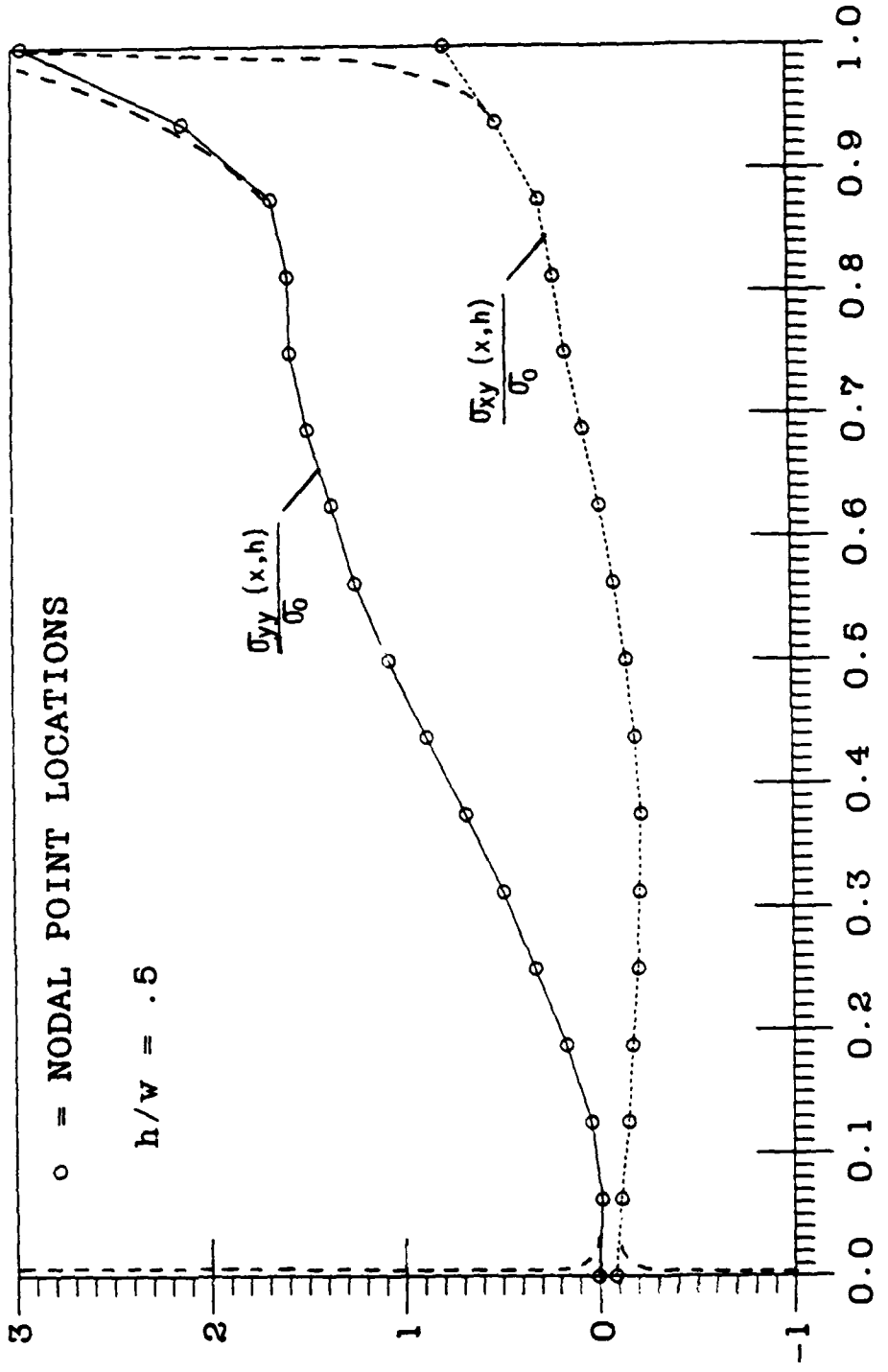

Figure 27b. Normal stress (σ_{yy}) and shear stress (σ_{xy}) along the fixed grip end of the single edge cracked specimen, h/w = .5.

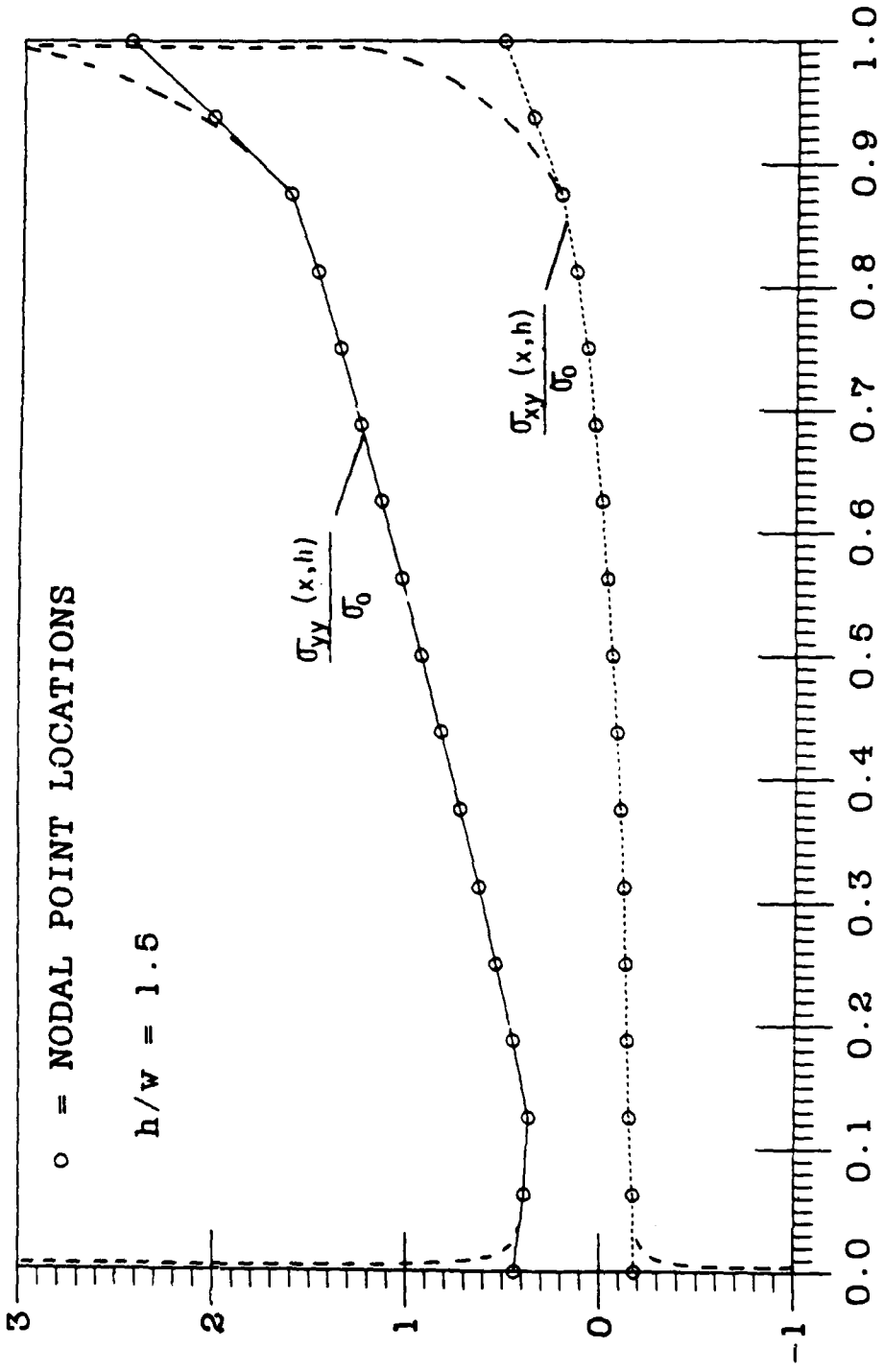

Figure 27c. Normal stress (σ_{yy}) and shear stress (σ_{xy}) along the fixed grip end of the single edge cracked specimen, h/w = 1.5.

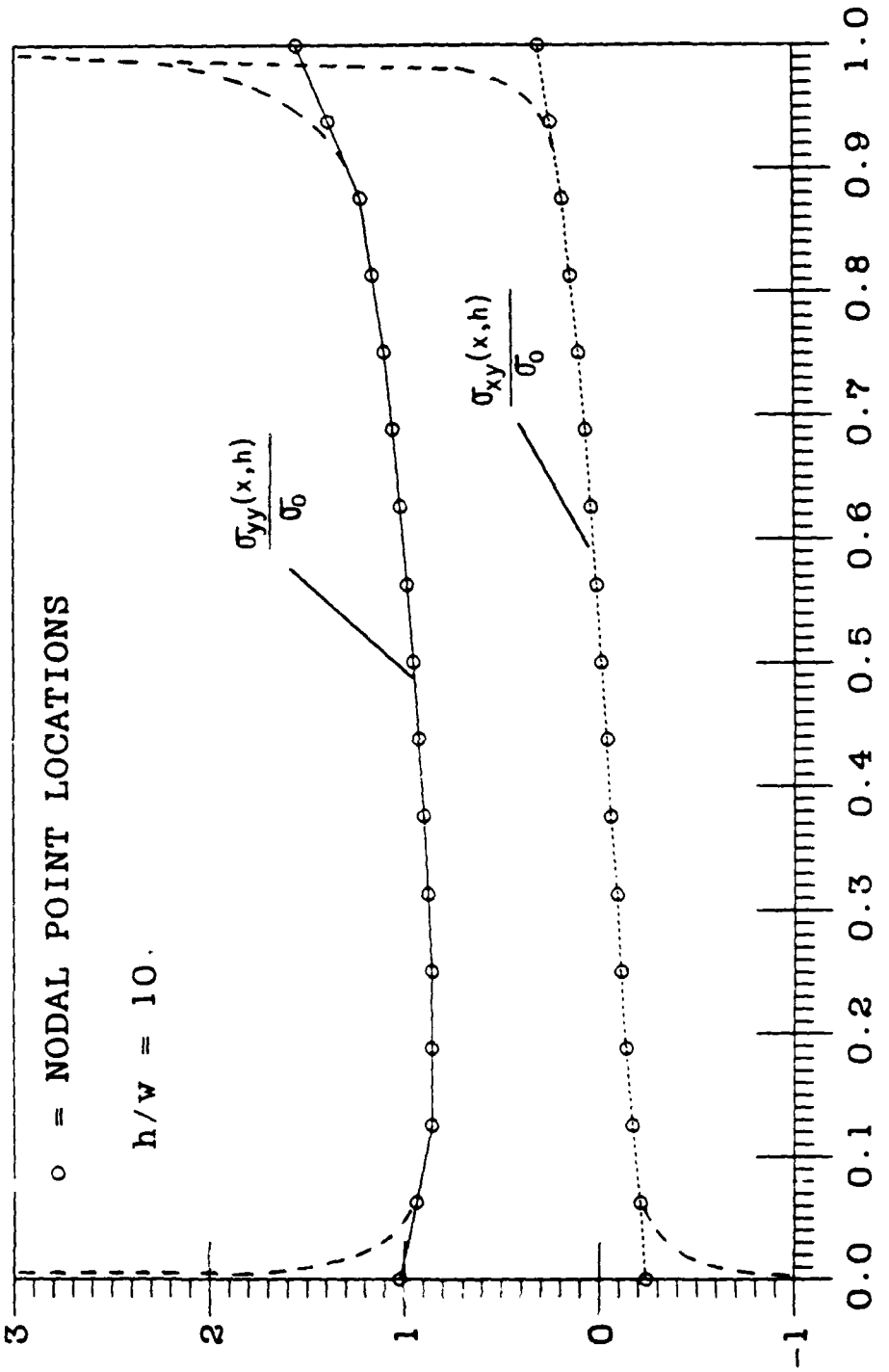

Figure 27d. Normal stress (σ_{yy}) and shear stress (σ_{xy}) along the fixed grip end of the single edge cracked specimen, h/w = 10.

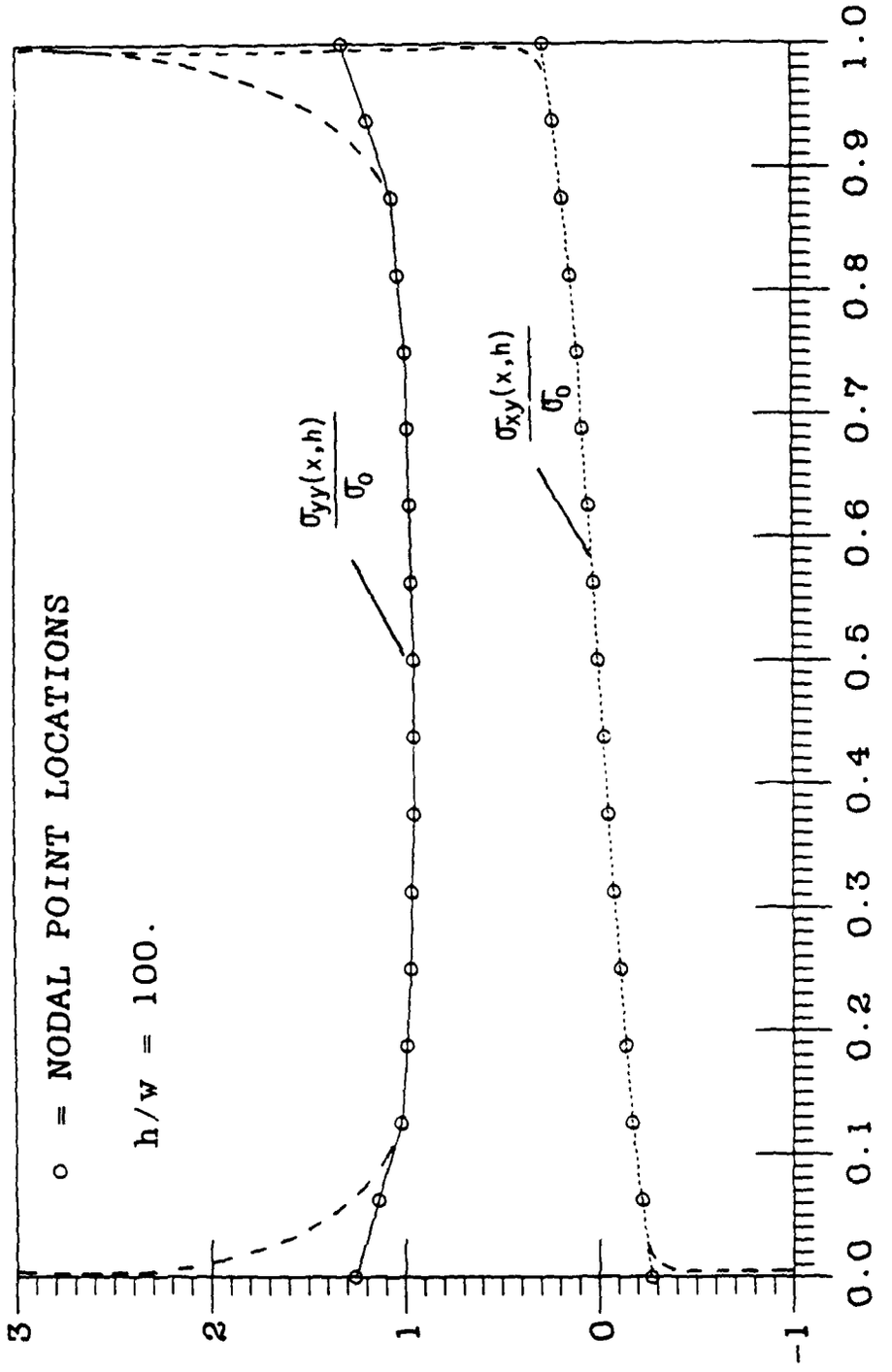

Figure 27e. Normal stress (σ_{yy}) and shear stress (σ_{xy}) along the fixed grip end of the single edge cracked specimen, h/w = 100.

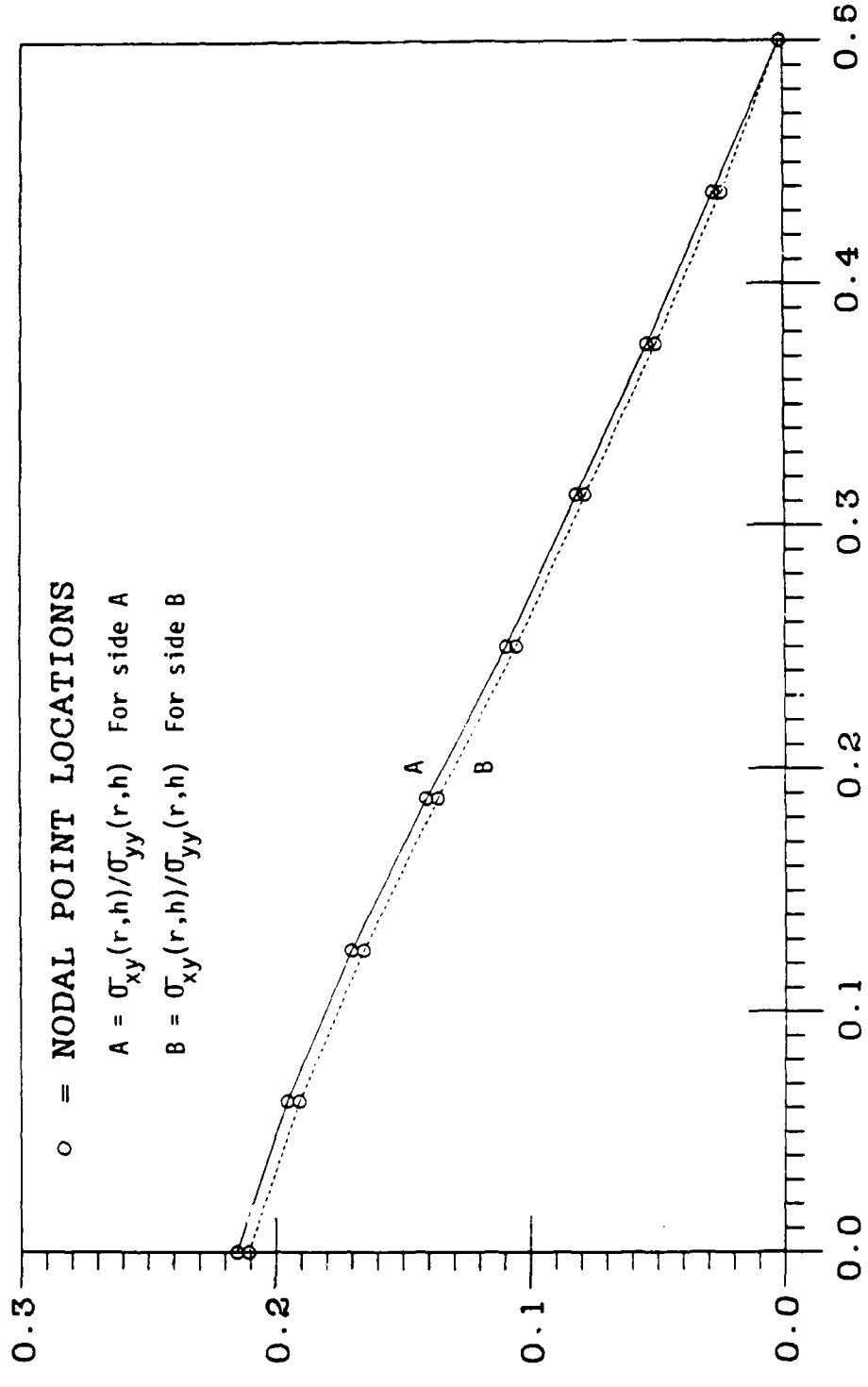

Figure 28. Shear stress to normal stress ratio at the fixed grip end of the single edge cracked specimen (h/w = 100).

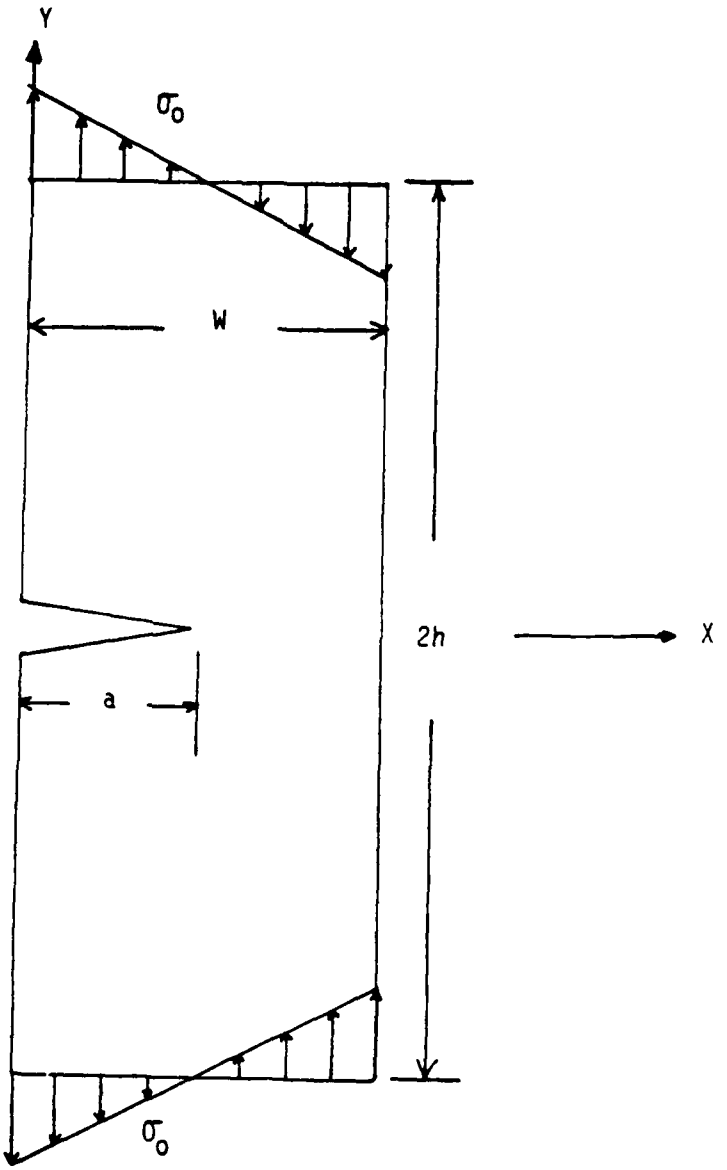

Figure 29a. Uniform bend specimen.

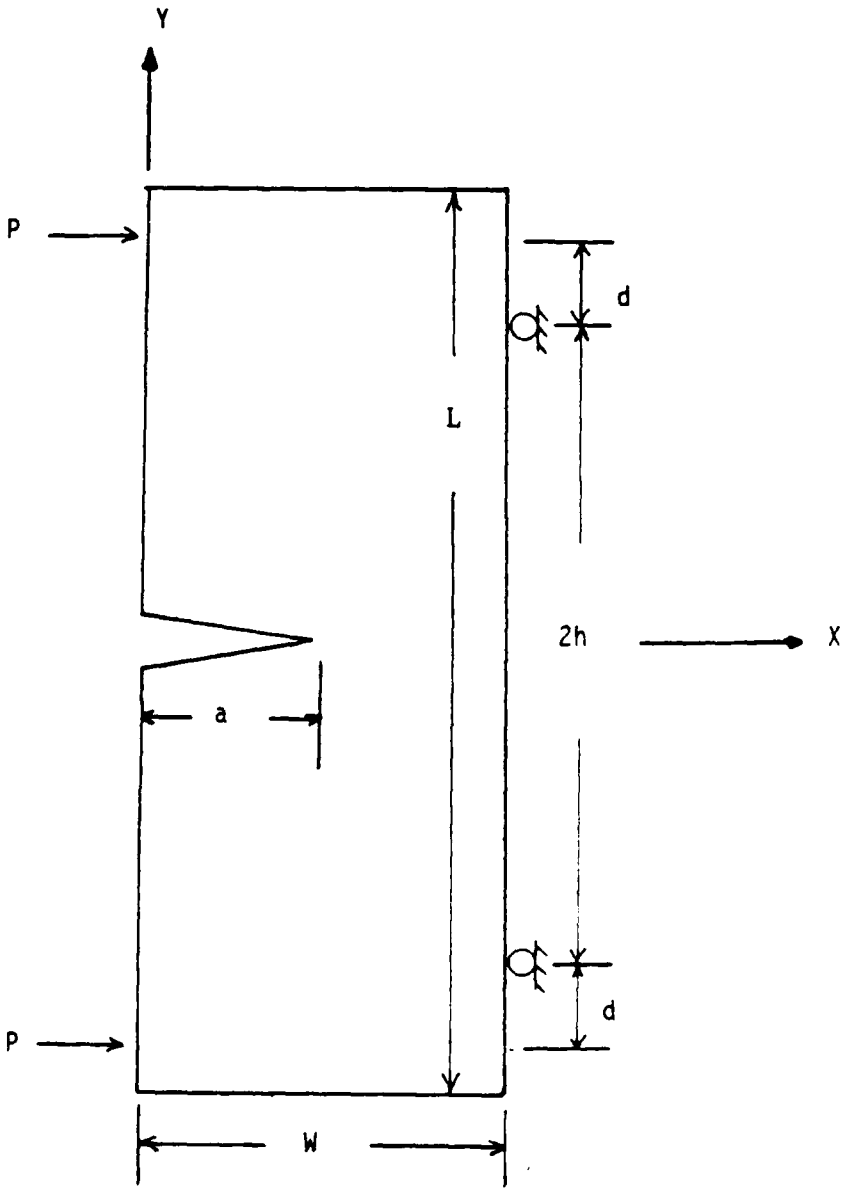

Figure 29b. Four point bend specimen.

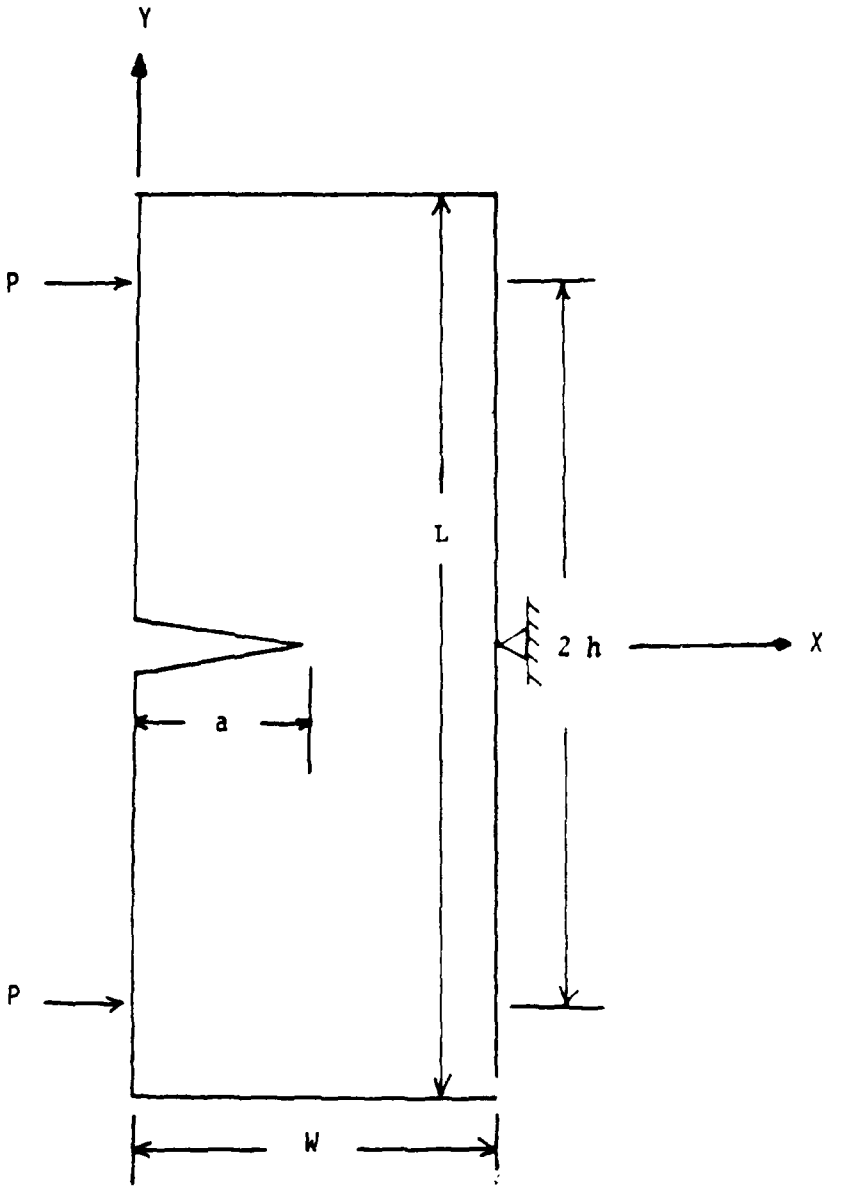

Figure 29c. Three point bend specimen.

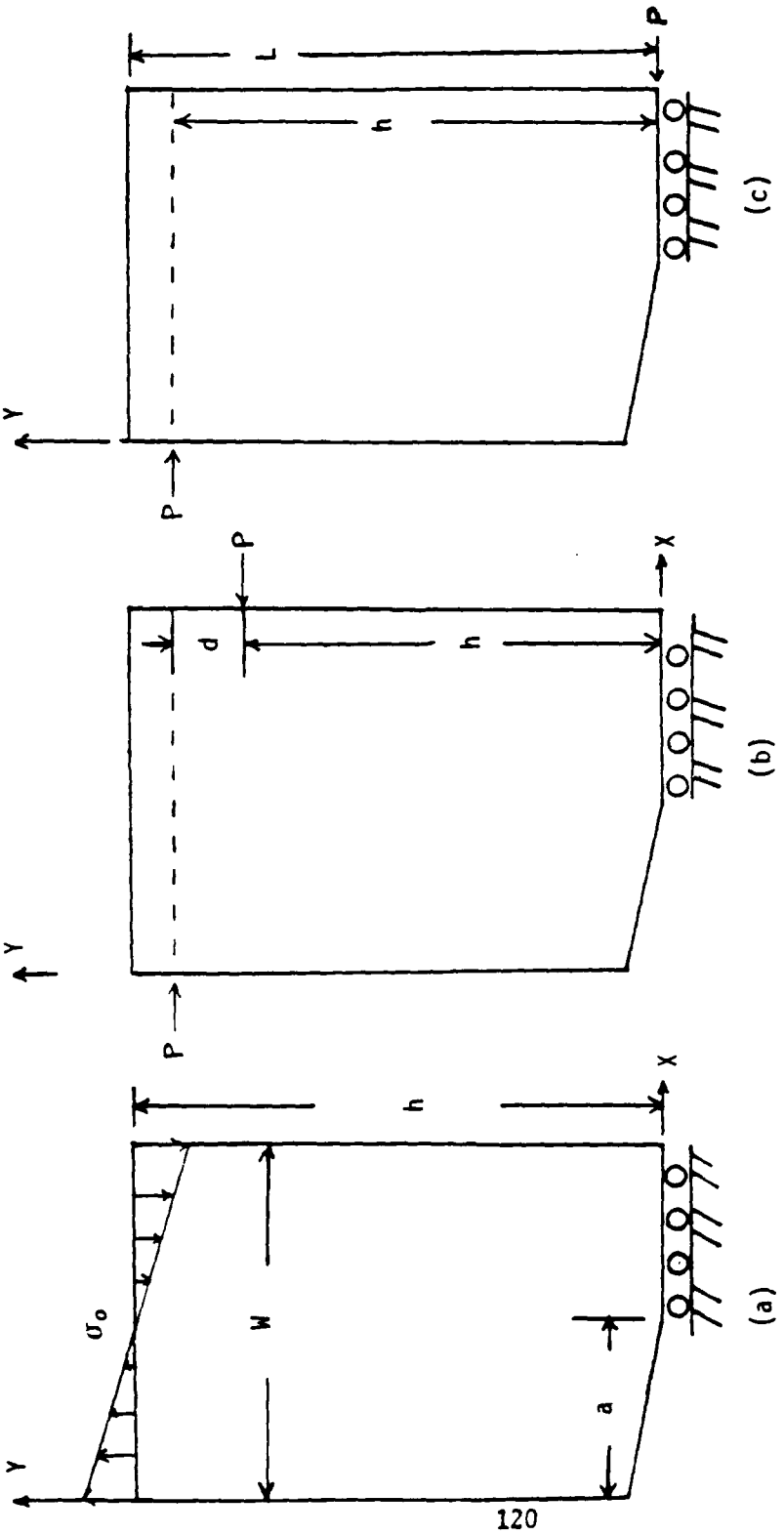

Figure 30. Boundary conditions for single edge cracked bend specimens: (a) uniform bend specimen, (b) four point bend specimen, and (c) three point bend specimen.

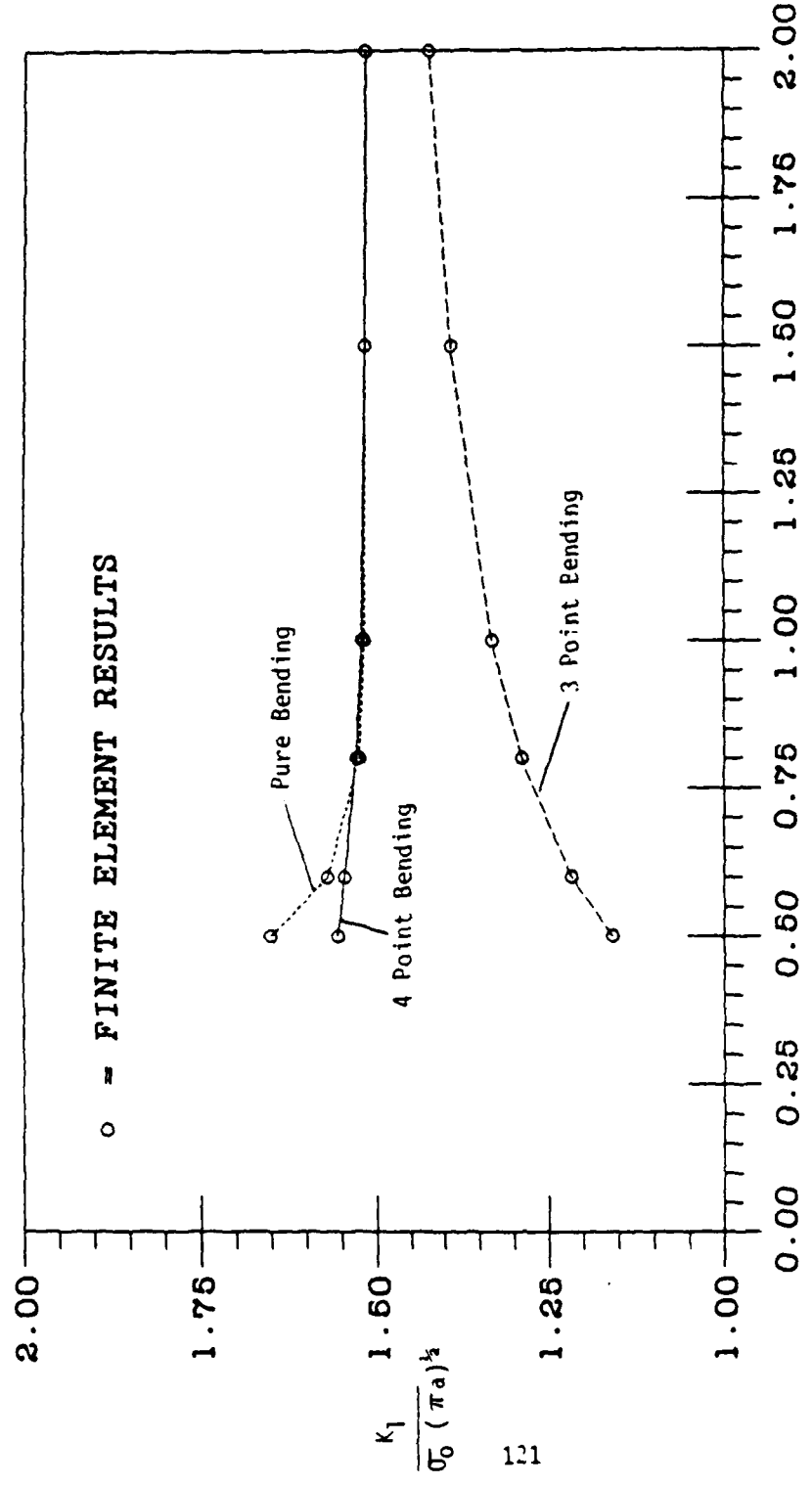

Figure 31a. Normalized stress intensity factor vs. half-length to width ratio (h/w) for single edge cracked bend specimens.

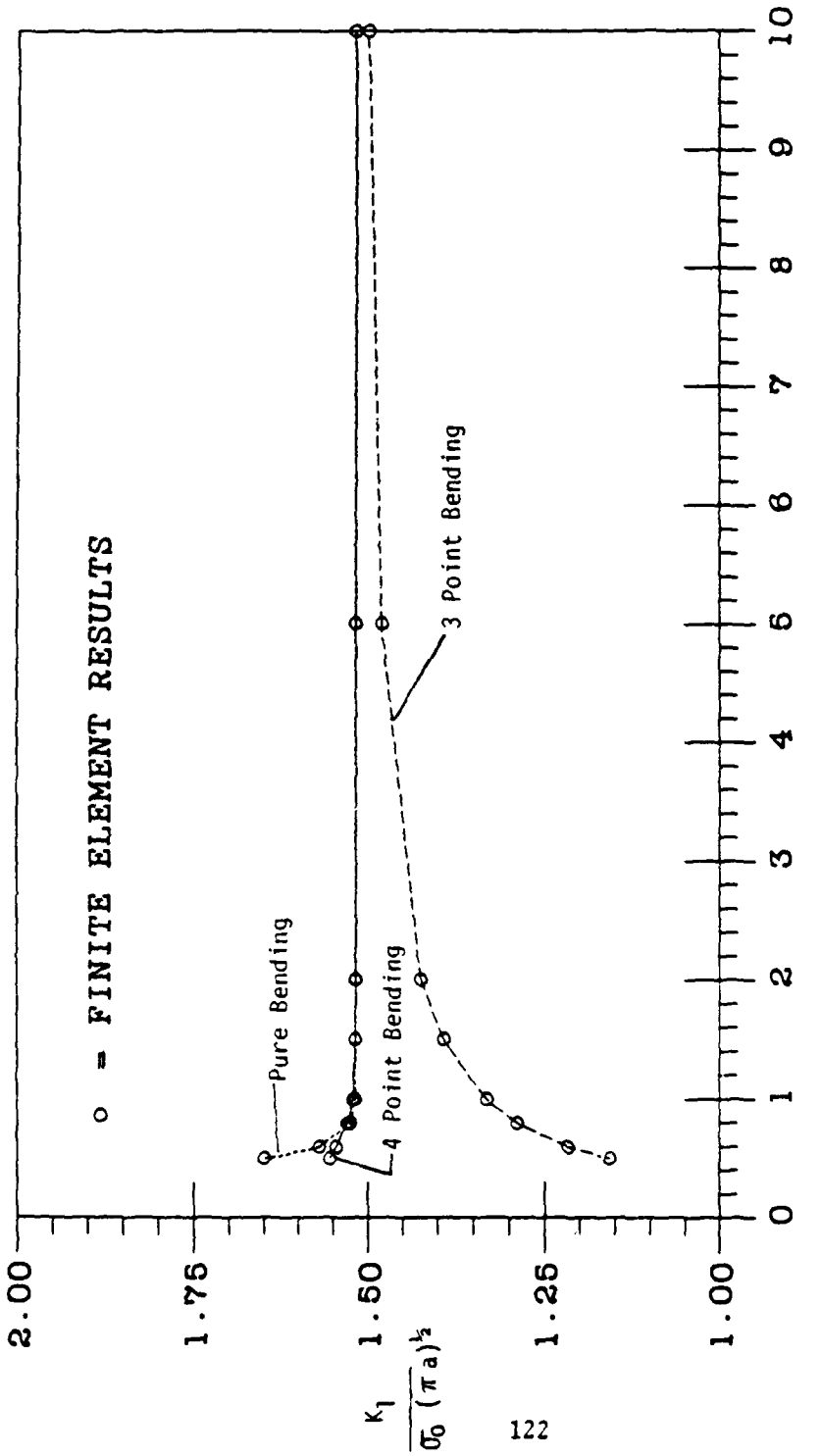

Figure 31b. Normalized stress intensity factor vs. half-length to width ratio (h/w) for single edge cracked bend specimens.

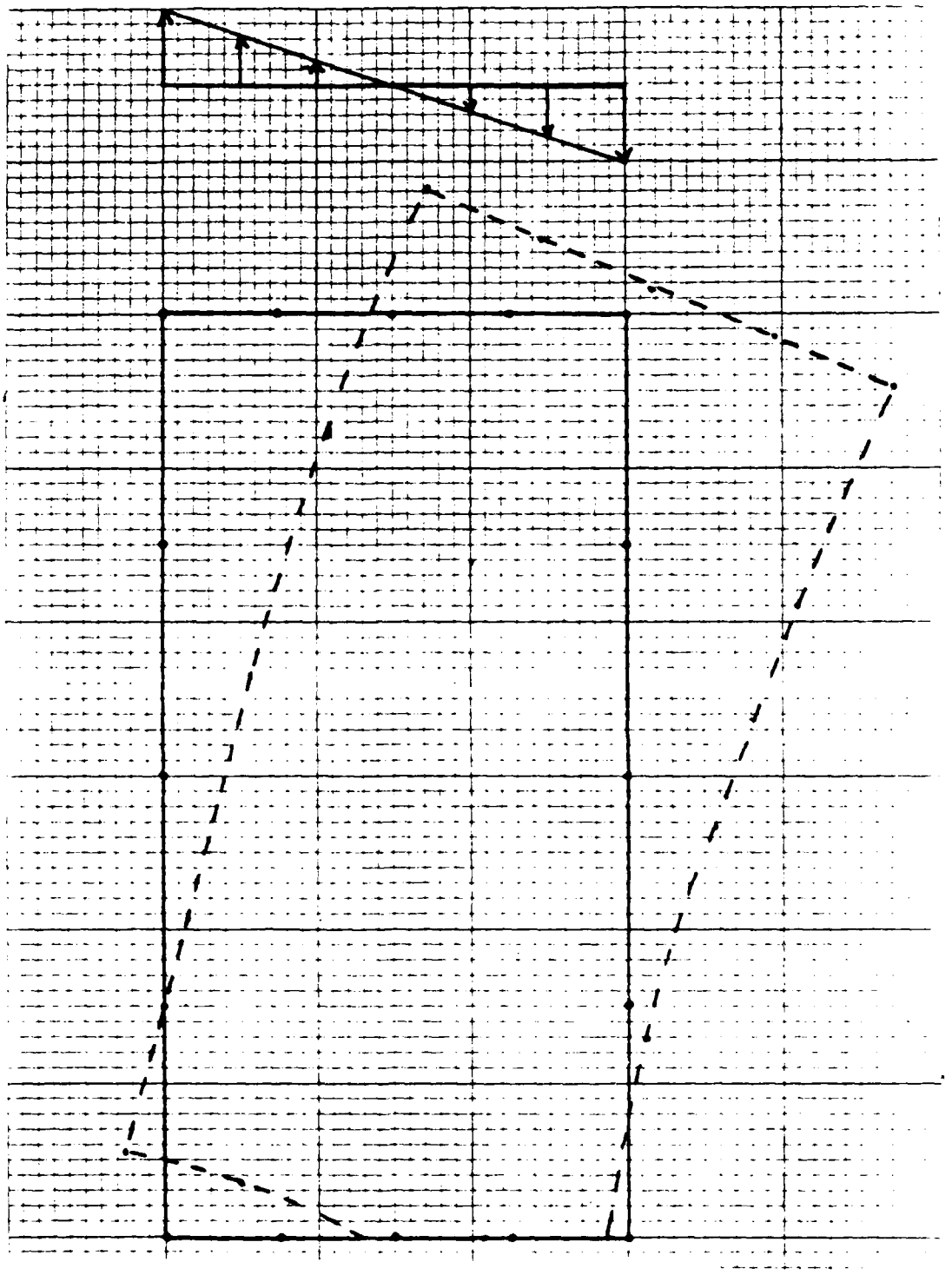

Figure 32a. Deformed plot of a single edge cracked specimen under a uniform bending load.

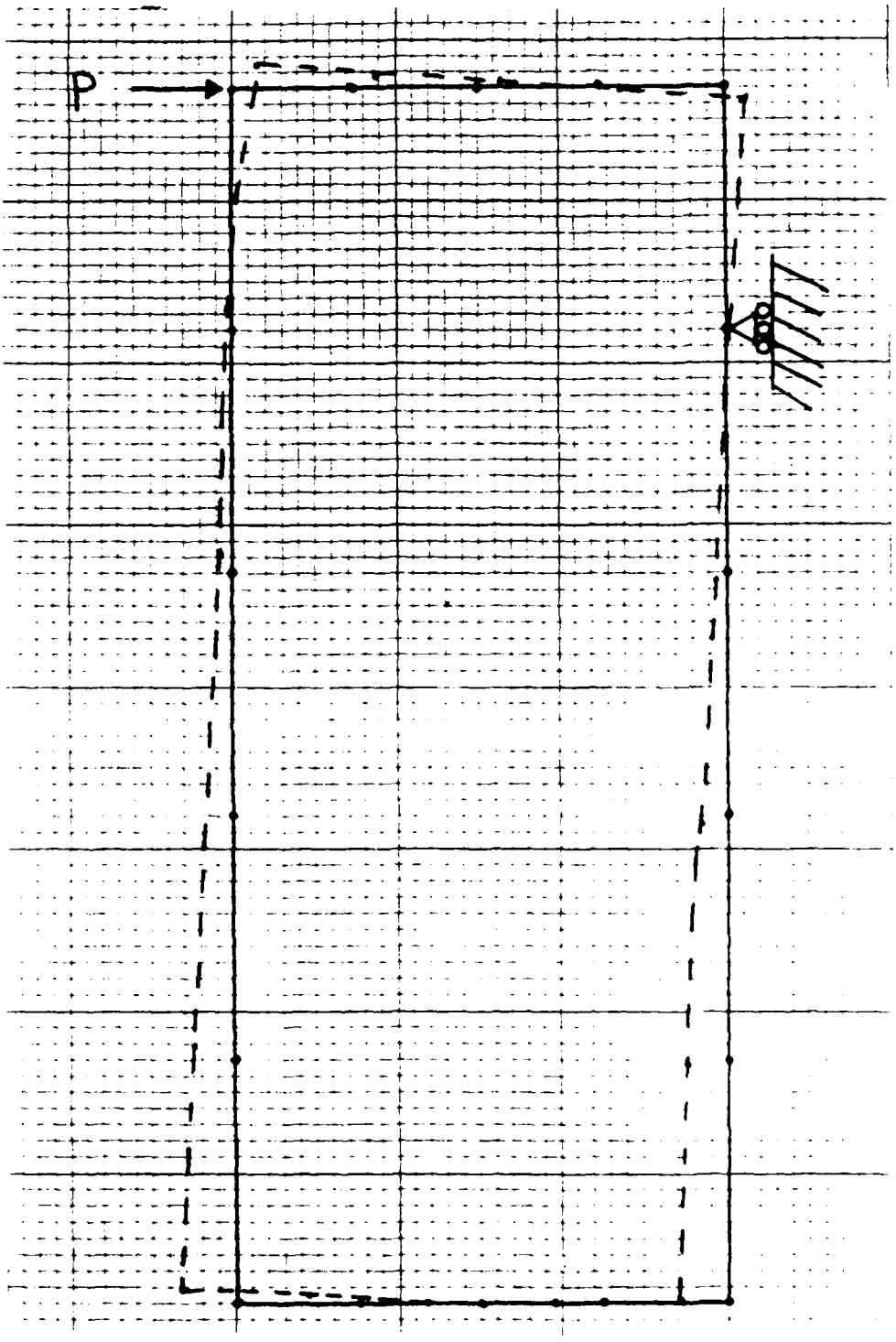

Figure 32b. Deformed plot of a single edge cracked specimen under four point bending.

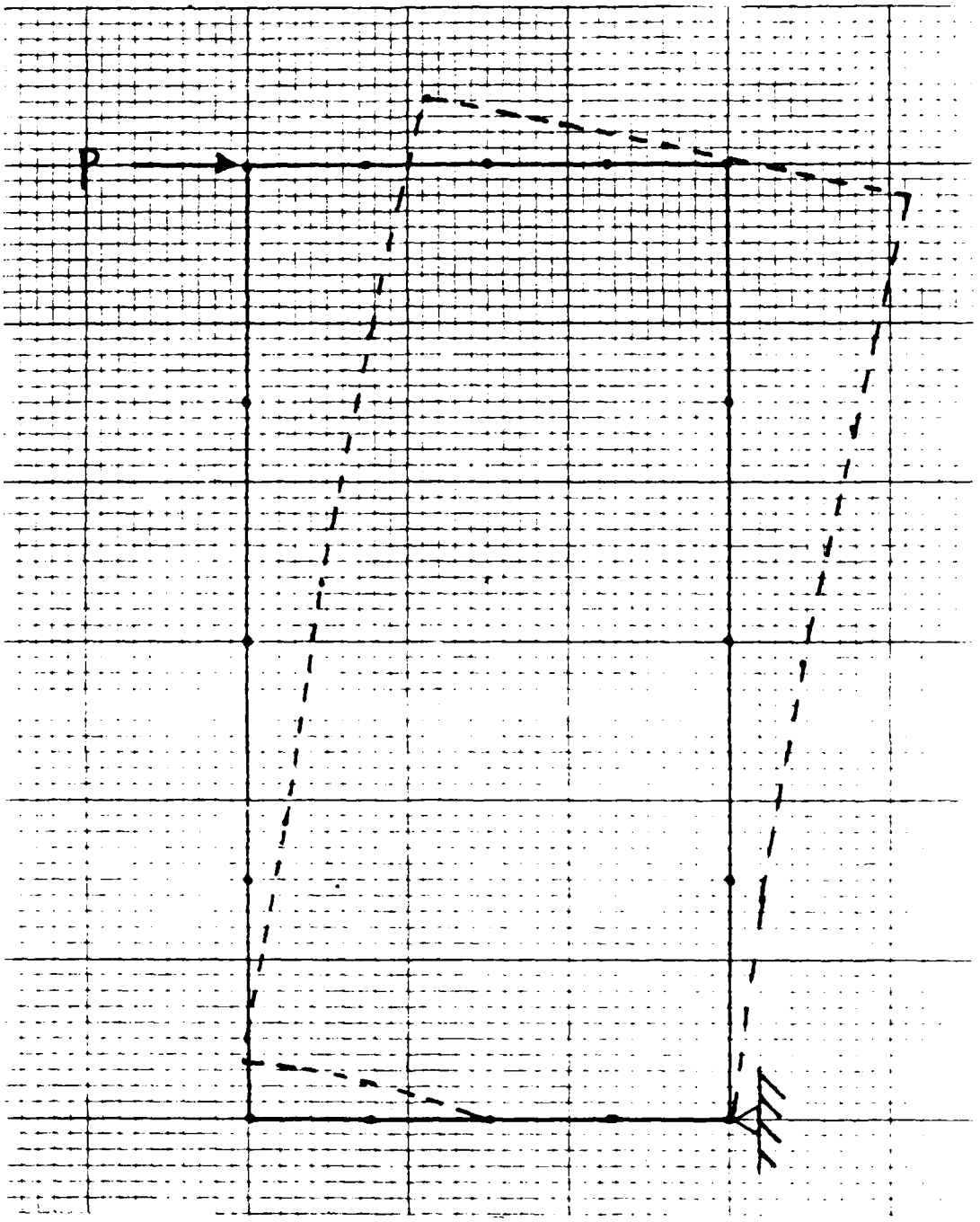

Figure 32c. Deformed plot of a single edge cracked specimen under three point bending.

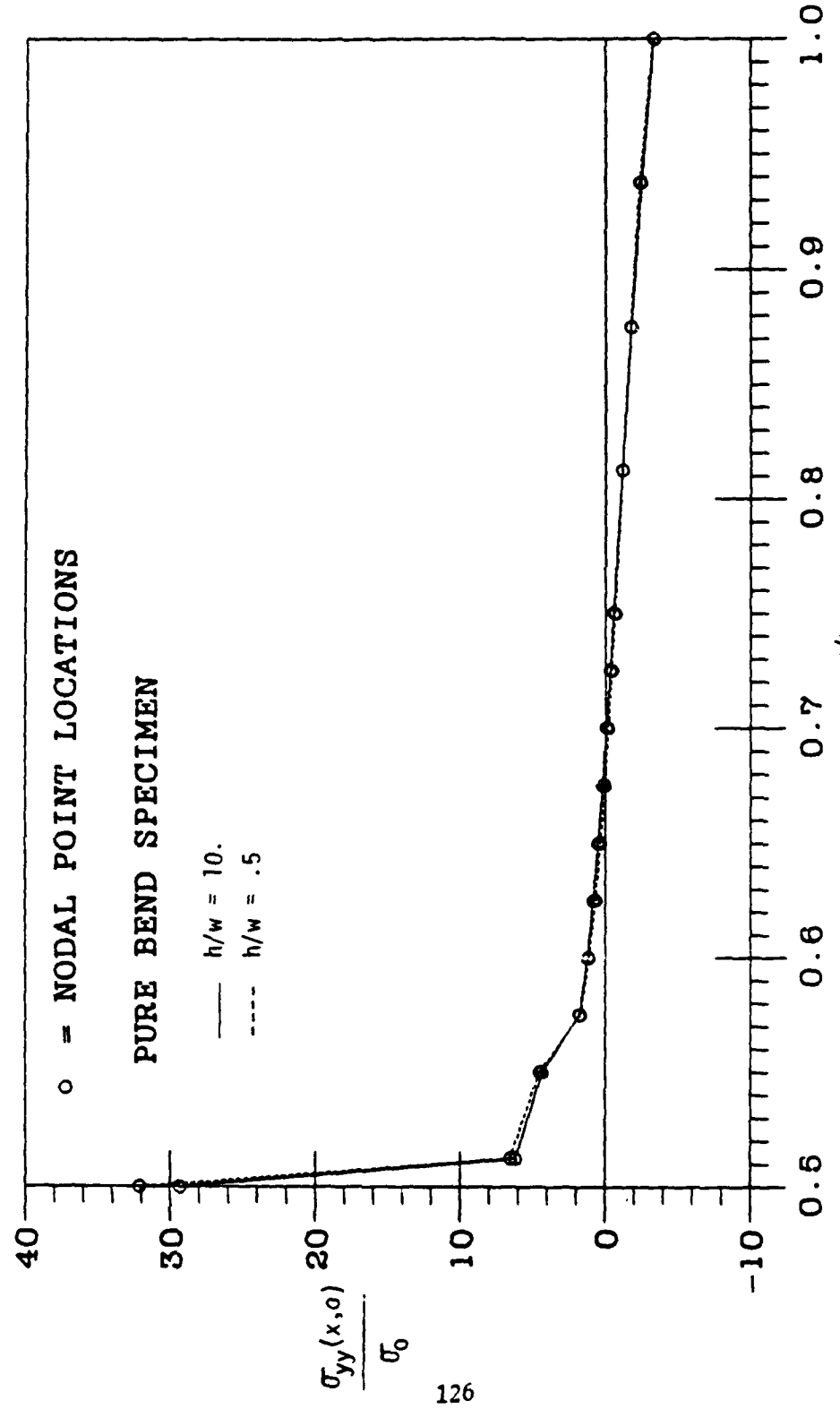

Figure 33a. Normal stress in front of the crack tip, $\sigma_{yy}(x,o)$, for the single edge cracked specimen under pure bending.

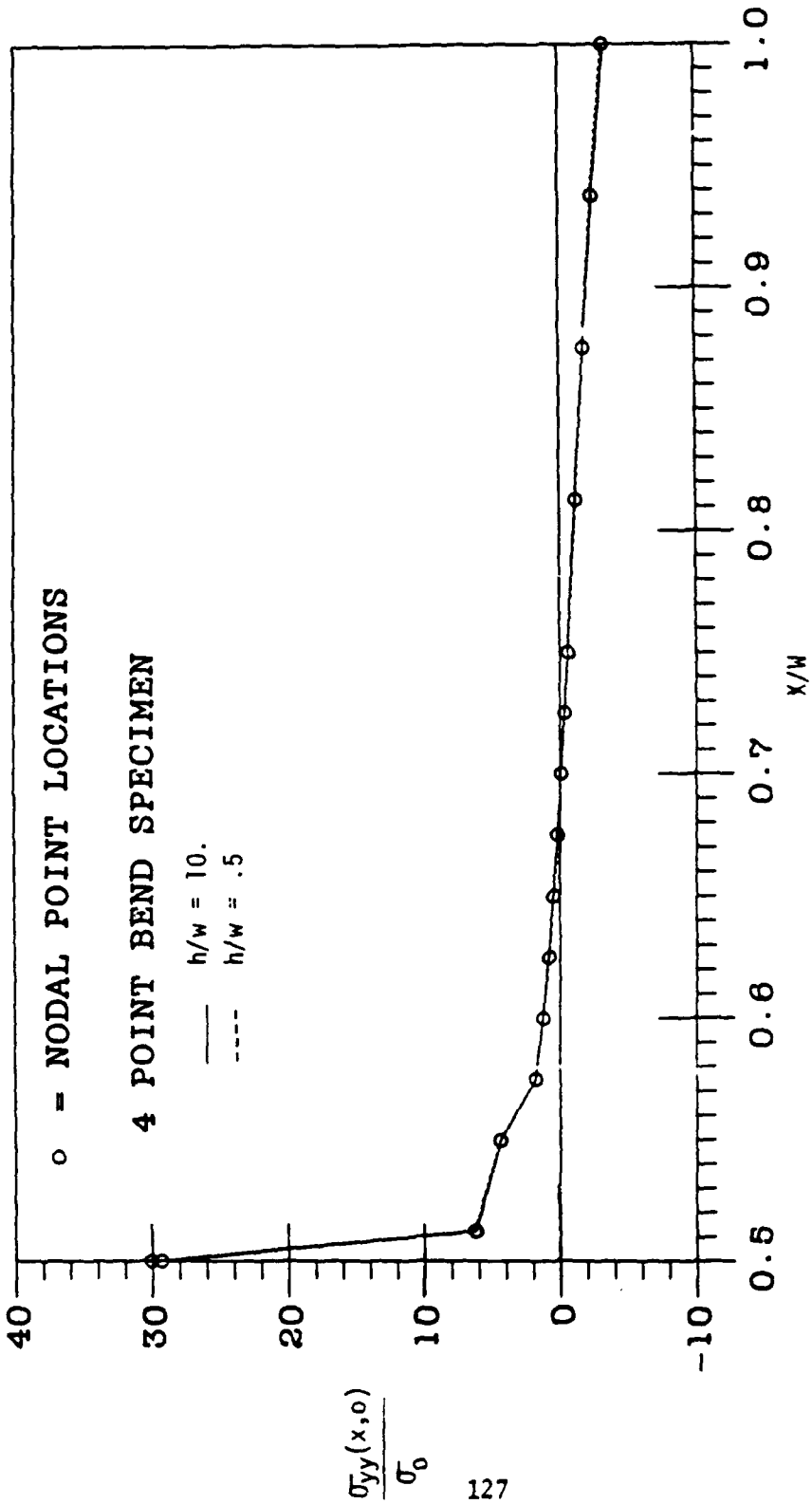

Figure 33b. Normal stress in front of the crack tip, $\sigma_{yy}(x,o)$, for the single edge cracked specimen under four point bending.

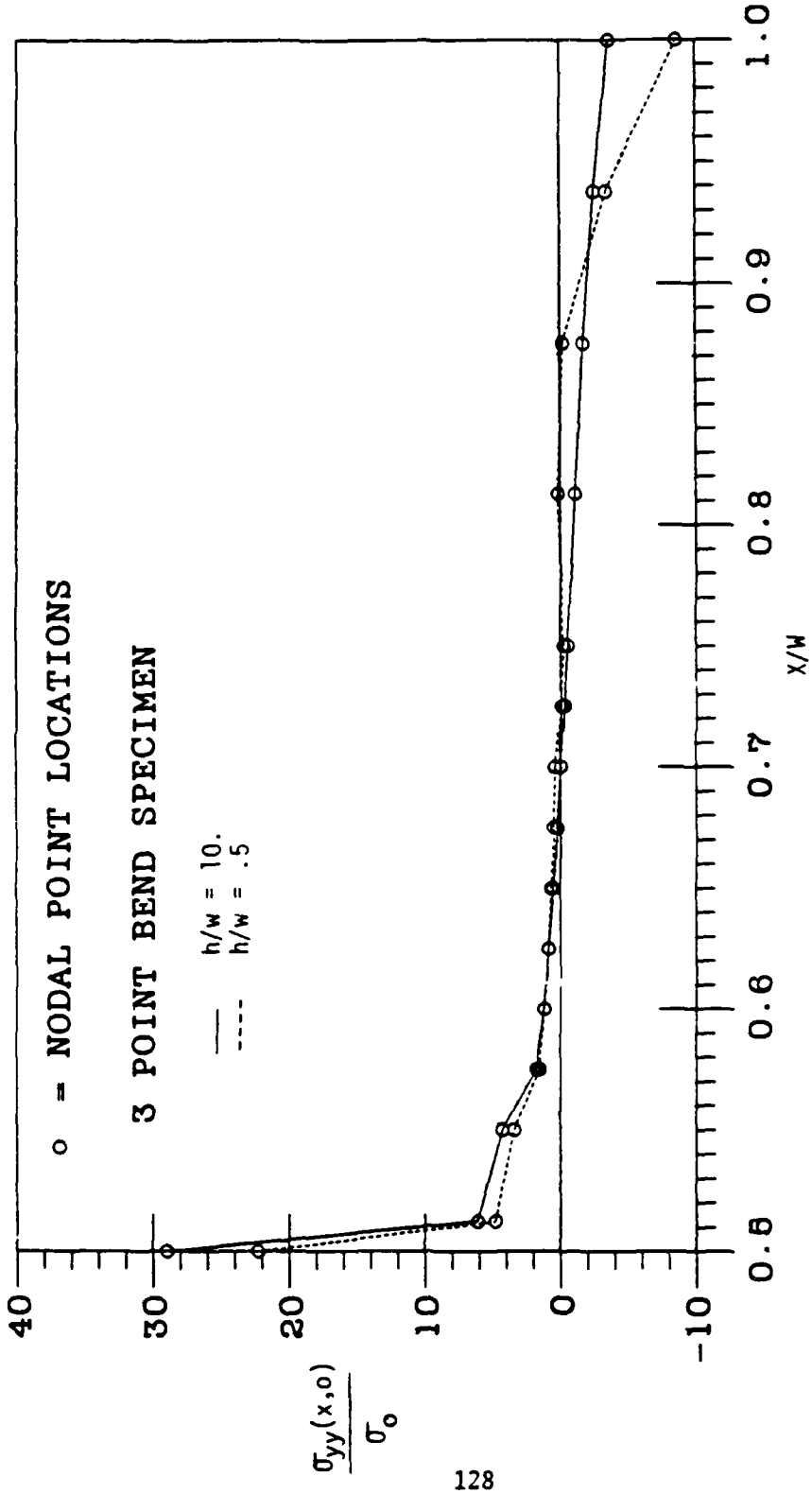

Figure 33c. Normal stress in front of the crack tip, $\sigma_{yy}(x,o)$, for the single edge cracked specimen under three point bending.

REFERENCES

1. S. K. Chan, I. S. Tuba and W. K. Wilson, "On The Finite Element Method In Linear Fracture Mechanics", Engng Fract. Mech., Vol. 2, 1970, pp. 1-17.

2. D. M. Tracey, "Finite Elements For Determination Of Crack Tip Elastic Stress Intensity Factors", Engng Fract. Mech., Vol. 3, 1971, pp. 255-265.

3. R. S. Barsoum, "On The Use Of Isoparametric Finite Elements In Linear Fracture Mechanics", Int. J. Numer. Methods Eng., Vol 10., 1976, pp. 25-37.

4. R. D. Henshall and K. G. Shaw, "Crack Tip Finite Elements Are Unnecessary", Int. J. Numer. Methods Eng., Vol. 9, 1975, pp. 495-507.

5. G. B. Sinclair and D. Mullen, "A Simple Yet Accurate Finite Element Procedure For Computing Stress Intensity Factors", Int. J. Numer. Methods Eng., Vol. 18, 1982, pp. 1587-1600.

6. D. M. Parks, "A Stiffness Derivative Finite Element Technique For Determination Of Crack Tip Stress Intensity Factors", Int. J. Fracture, Vol. 10, 1974, pp. 487-502.

7. R. M. Walsh Jr., and R. B. Pipes, "Strain Energy Release Rate Determination Of Stress Intensity Factors By Finite Element Methods", Engng Fract. Mech., Vol. 22, 1985, pp. 17-33.

8. H. Ishikawa, "A Finite Element Analysis Of Stress Intensity Factors For Combined Tensile And Shear Loads By Only A Virtual Crack Extension", Int. J. Fracture, Vol. 16, 1980, pp. R243-R246.

9. E. F. Rybicki and M. F. Kanninen, "A Finite Element Calculation Of Stress Intensity Factors By A Modified Crack Closure Integral", Engng Fract. Mech., Vol. 9, 1977, pp. 931-938.

10. P. Tong, T. H. H. Pian, and S. J. Lasry, "A Hybrid-Element Approach To Crack Problems In Plane Elasticity", Int. J. Numer. Methods Eng., Vol. 7, 1973, pp. 297-308.

11. E. Byskov, "The Calculation Of Stress Intensity Factors Using The Finite Element Method With Cracked Elements", Int. J. Fract. Mech., Vol. 6, 1970, pp. 159-167.

12. L. N. Gifford, Jr. and P. D. Hilton, "Stress Intensity Factors By Enriched Finite Elements", Engng Fract. Mech., Vol 10, 1978, pp. 485-496.

13. J. R. Rice, "A Path Independent Integral And The Approximate Analysis Of Strain Concentration By Notches And Cracks", J. Appl. Mech., Vol. 35, 1968, pp. 379-386.

14. G. R. Irwin, "Analysis Of Stresses And Strains Near The End Of A Crack Traversing A Plate", J. Appl. Mech., Vol. 24, 1957, pp. 361-364.

15. O. C. Zienkiewicz, "The Finite Element Method", 3rd edn., McGraw-Hill, New York, 1977.

16. F. Erdogan, "Mech 203 Notes, Fracture Mechanics", Lehigh University.

17. C. E. Freese and D. M. Tracey, "The Natural Isoparametric Triangle Versus Collapsed Quadlateral For Elastic Crack Analysis", Int. J. Fract., Vol. 12, 1976, pp. 767-770.

18. N. A. B. Yehia and M. S. Shephard, "On The Effect Of Quarter-Point Element Size On Fracture Criteria", Int. J. Numer. Methods Eng., Vol. 21, 1985, pp. 1911-1924.

19. W. F. Brown, Jr. and J. E. Srawley, "Plane Strain Crack Toughness Testing Of High Strength Metallic Materials", ASTM STP 410, 1969.

20. G. D. Gupta, "An Integral Equation Approach To The Semi-Infinite Strip Problem", J. Appl. Mech., 1973, pp. 1-7.

No. of Copies

LTV AEROSPACE & DEFENSE CO., Vought Missile & Advanced Program Division
P.O. Box 225907, Dalas, TX 75265-0003
(Attn: Dr. C. Dumisnil) 1
(Attn: Mr. T. Gray) 1

MCCONNELL DOUGLAS CORPORATION, St. Louis, MO 63166
(Attn: Mr. L. Impellizeri) 1
(Attn: Dr. R. Pinckert) 1

NORTHROP CORPORATION, One Northrop Avenue, Hawthorne, CA 90250
(Attn: Mr. Alan Liu) 1
(Attn: Dr. M. Ratwani) 1

ROCKWELL INTERNATIONAL, Columbus, OH 43216
(Attn: Mr. F. Kaufman) 1

ROCKWELL INTERNATIONAL, Los Angeles, CA 90009
(Attn: Mr. J. Chang) 1

ROCKWELL INTERNATIONAL SCIENCE CENTER, 1049 Camino Dos Rios
Thousand Oaks, CA 91360
(Attn: Dr. F. Morris) 1

ROHR CORPORATION, Riverside, CA 92503
(Attn: Dr. F. Riel) 1

SIKORSKY AIRCRAFT, Stratford, CT 06622 1

UNIVERSITY OF DAYTON RESEARCH INSTITUTE, 300 College Park Avenue, Dayton, OH 45469 1
(Attn: Dr. J. Gallagher) .....

UNIVERSITY OF ILLINOIS, College of Engineering, Dept. of Mechanics
and Industrial Eng., Urbana, IL 61801
(Attn: Prof. J.D. Morrow) 1
(Attn: D.F. Socie) 1

UNIVERSITY OF PENNSYLVANIA, Dept. of Mechanical Engineering and Applied Mechanics
111 Towne Bldg., D3, Philadephia, PA 19104
(Attn: Dr. Burgers) 1

No. of Copies

INFORMATION SERVICES

DEFENSE TECHNICAL INFORMATION CENTER (DTIC), Bldg. 5,
Cameron Station, Alexandria, VA 22314
(Attn: Administrator) 2

MCIC, Battelle Columbus Laboratories, 505 King Avenue
Columbus, OH 43201 1

NTIS, U.S. Department of Commerce, Springfield, VA 22151 2

ALCOA, ALCOA Labs, ALCOA Center, PA 15069
(Attn: Mr. J.G. Kaufman) 1

BATTELLE COLUMBUS LABS, 505 King Avenue, Columbus, OH 43201
(Attn: Dr. B. Leis) 1

BELL HELICOPTER, Textron Inc., P.O. Box 482, Ft. Worth, TX 76101
(Attn: M. Keith Stevenson) 1

BOEING VERTOL, P.O. Box 16858, Philadelphia, PA 19142
(Attn: Mr. W. Potthoff) 1

BOEING COMMERCIAL AIRPLANE CO., P.O. Box 3707, Seattle, WA 98124
(Attn: Mr. T. Porter) 1

DOUGLAS AIRCRAFT CO., 3855 Lakewood Blvd., Long Beach, CA 90846
(Attn: Mr. Luce, Mail Code 7-21) 1

DREXEL UNIVERSITY, Philadelphia, PA 19104
(Attn: Dr. Averbuch) 1

FAIRCHILD INDUSTRIES, Hagerstown, MD 21740
(Attn: Technical Library) 1

GENERAL DYNAMICS, Convair Division, San Diego, CA 92138
(Attn: Mr. G. Kruse) 1

GENERAL DYNAMICS CORPORATION, P.O. Box 748, Ft. Worth, TX 76101
(Attn: Dr. S. Manning) 1

GRUMMAN AEROSPACE CORPORATION, South Oyster Bay Road, Bethpage, L.I. NY 11714
(Attn: Dr. H. Armen) 1
(Attn: Dr. B. Leftheris) 1
(Attn: Dr. H. Eidenoff) 1

LEHIGH UNIVERSITY, Bethlehem, PA 18015
(Attn: Prof. G.C. Sih) 1
(Attn: Prof. R.P. Wei) 1
(Attn: Prof. F. Erdogan) 1

LOCKHEED-CALIFORNIA CO., 2555 N. Hollywood Way, Burbank, CA 91520
(Attn: Mr. E.K. Walker) 1

LOCKHEED-GEORGIA CO., Marietta, GA 30673
(Attn: Mr. T. Adams) 1

DISTRIBUTION LIST

Report No. NADC-87145-60

NAVY	*No. of Copies*
ONT, 800 N. Quincy Street, Arlington, VA 22217	
(Attn: Cdr. R. Fuller, OCNR-212)	1
NAVAIRSYSCOM, Washington, D.C. 20361	
(Attn: AIR-00D4)	2
(Attn: AIR-311B)	3
(Attn: AIR-530)	2
(Attn: AIR-5302)	1
(Attn: AIR-53021)	1
(Attn: AIR-530215)	1
NAVAIRTESTCEN, Patuxent River, MD 20670	
(Attn: Dr. J. Hoeg)	1
NAVAIRENGCEN, Lakehurst, NJ 08733	
(Attn: Mr. F. Sinartra)	1
(Attn: Mr. Neil Goodis)	1
NAVAIREWORKFAC, NAS, Alameda, CA 94501	1
NAVAIREWORKFAC, MCAS, Cherry Point, NC 28533	1
NAVAIREWORKFAC, NAS, Jacksonville, FL 32212	1
NAVAIREWORKFAC, NAS, Norfolk, VA 23511	
(Attn: Mr. Stokley)	1
NAVAIREWORKFAC, NAS, North Island, San Diego, CA 92135	1
NAVAIREWORKFAC, NAS, Pensacola, FL 32508	1
NAVAL WEAPONS CENTER, China Lake, CA 93555	1
NAVAVLOGCEN, Patuxent River, MD 20670	1
NAVPGSCHL, Monterey, CA 95940	1
NAVSEASYSCOM, Crystal Mall 4, Rm. 109, Washington, DC 20360	
(Attn: Mr. Vanderveldt)	1
NAVSHIPRANDCEN, Bethesda, MD 20034	1
NAVSHIPRANDCEN, Annapolis, MD 21402	1
NRL, Washington, DC 20375	
(Attn: T. Crooker)	1
NSWC, WHITE OAK LABORATORY, Silver Spring, MD 20910	1
ONR, Arlington, VA 22217	
(Attn: Dr. Y. Rajapakse, Code 474	1
NAVAIRDEVCEN, Warminster, PA 18974	10
(3 for Code 8131)	
)5 for Code 6042)	
(1 for Code 6043)	
(1 for Code 6041)	

DISTRIBUTION LIST (continued)

Report No. NADC-87145-60

	No. of Copies
FAA	
FAA, Washington, DC 20591	
(Attn: J.R. Soderquist)	1
FAA, Technology Center, Atlantic City, NJ 08405	
(Attn: Mr. D. Nesterok, ACT-330)	1
NASA	
NASA, Langley Research Center, Hampton, VA 23365	
(Attn: John Davidson)	1
NASA, Lewis Research Center, Cleveland, OH 44135	
(Attn: Technical Library)	1
NASA, George C. Marshall Space Flight Center, Huntsville, AL 35812	
(Attn: Technical Library)	1
USAF	
AFWAL, WPAFB, OH 45433	
(Attn: AFWAL/FIBE)	1
(Attn: FIBEC)	1
(Attn: FIBAA)	1
(Attn: AFWAL/FIB)	1
OGDEN ALC, Hill AFB, UT 84055	
(Attn: MANCC)	1
Oklahoma City ALC, Tinker AFV, OK 73145	
(Attn: MAQCP)	1
Sacramento ALC, McClellan AFV, CA 95652	
(Attn: MANE)	1
San Antonio ALC, Kelly AFB, TX 78241	
(Attn: MMETM)	1
Warner Robbins ALC, Robins AFB, GA 30198	
(Attn: MMSRD/Dr. T. Christian)	1
U.S. ARMY	
USARTL (AVRADCOM), Applied Technology Laboratory, Fort Eustis, VA 23604	
(Attn: H. Reddick)	1
U.S. Army Materials and Mechanics Reserach Center (DRXMR-PL)	
Watertown, MA 02171	1
U.S. Army Research Office, Durham, NC 27701	1
U.S. Army R&D Center, Fort Belvoir, VA 22060-5606	
(Attn: STRBE-VC/Lisa Ryan)	1